

Studying the Effects of Anti-prion Compounds on PrP Folding at the Single-molecule Level

by

Negar Rezajooei

A thesis submitted in partial fulfillment of the requirements for the degree of

Master of Science

Department of Physics
University of Alberta

© Negar Rezajooei, 2016

Abstract

Prion diseases, are associated with the misfolded form of the prion protein (PrP^{Sc}). The prion protein (PrP) has a unique means of transferring infectious diseases, based on a misfolded conformation. However, the mechanism of formation of PrP^{Sc} remains unclear owing to difficulties in defining the structure of PrP^{Sc} . Understanding the different folding pathways available to the protein and identifying those that lead to misfolding and aggregation, is possible through the use of single-molecule methods. However, finding these pathways is not easy due to the complexity in understanding the energy landscape. This thesis consists of two parts. In the first part, the sample preparation methods using different linking chemistries are explained. In the second part, the interaction between anti-prion ligands and PrP is investigated.

In order to compare the effects of species on folding and misfolding pathways, we used single molecule force spectroscopy with the high resolution optical tweezers to study mouse PrP (MoPrP). Mouse PrP molecules suspended between two polystyrene beads via double stranded DNA handles. The optical tweezers were used to apply tension in order to denature a single molecule of MoPrP. As a result, the structural changes of a single molecule were monitored via the end-to-end extension of the molecule. By moving the traps apart at a constant rate, the extension of the molecule increases monotonically until the protein unfolded causing a sudden increase in extension and concomitant drop in force. After Analyzing the data, the results showed shorter contour length changes compared with the expected value from NMR. However, the value of the contour length change matched the distance between one end of the molecule and either middle Cys(78) or Cys(113). We also confirmed internal labeling using an experiment which was performed with a fluorescent dye. In this experiment we used MoPrP without any external cysteine (Cys). The result showed that in-

ternal Cys of MoPrP got labeled with the fluorescent dye. The similar results were observed by repeated the measurements on the sample that was prepared using another attachment chemistry called click chemistry. The internal Cys labeling problem was fixed by replacing the reducing agent in our sample preparation method with a weaker reducing agent. Anti-prion ligands may offer a solution to prion diseases. Certain ligands that can interact with PrP, could potentially be considered as pharmacological chaperones. We also studied about the role of iron-tetrapyrrole, a potential pharmacological chaperone, on the folding pathway of Syrian hamster PrP (ShPrP). The results suggested that Iron(III) meso-tetra (N-methyl-4-pyridyl-prophine) (Fe-TMPyP) can bind to a single PrP molecule in two ways; either binding to the folded PrP monomer or to the unfolded PrP monomer. Fe-TMPyP can stabilize the native structure of single PrP molecules thermodynamically, kinetically, and mechanically by binding to the folded PrP. In addition, binding of Fe-TMPyP to the partially folded protein prevents the folding of the protein to the native state. Iron-tetrapyrrole bound to dimer PrP was also investigated using optical tweezers. Without tetrapyrrole, PrP-dimer always misfolded. In the presence of tetrapyrrole, the dimer sometimes shows natively folded states.

We also planned to measure Syrian PrP (ShPrP) with another anti-prion compound called pentosan polysulphate (PPS). To do the measurements we first needed to know the thermodynamics of interactions between protein and PPS. Measuring heat using isothermal titration calorimetry (ITC), is a way of finding this information before starting force extension measurements. We performed the ITC experiment with PPS compound and ShPrP without any external Cys. We get a result of affinity binding (K_d value) between $K_d = 0.05 \mu M$ to $K_d = 5 \mu M$, consistent with the surface plasmon resonance (SPR) data given the large error. In order to clarify the results, further experiments should be performed. As a future work, I want to do force extension measurements on the PPS bound to ShPrP and investigate the role of ligand on the folding pathway of ShPrP. In conclusion, single molecule methods give us opportunity to understand disease and biological function related to misfolded prion protein. The information derived from single molecule studies can be used to develop potential drugs which have anti-transmissible spongiform encephalopathies effects, such as sulfonated dyes, sulphated glycans, cyclic tetrapyrroles, quinacrine, and so on.

I dedicate this thesis to my parents. For their love, support and encouragement. Thank you for teaching me to believe in myself and to follow my dreams.

Acknowledgements

I would first like to express my sincere gratitude to my thesis advisor Dr. Michael Woodside of the Physics department at University of Alberta. He provided continuous support of my Master's studies and research with patience, motivation and immense knowledge. In addition, I want to give thanks for the opportunities I was given to work in well-equipped laboratories to follow my research.

Besides my advisor, I would like to thank the rest of my thesis committee: : Dr. Jack Tuszyński and Dr. Mark Freeman for their encouragement and insightful comments they provided at all levels of the research project. I would like to extend my thanks to Dr. Lindsay LeBlanc. I am really appreciative for having her in my defense. She expressed many valuable comments and questions.

My sincere thanks also goes to other lab-mates and technicians: Craig Garen for the days and nights he spent making proteins, without him the research in this thesis would not have been possible. I also want to thank Meijing Wang, a former technician in Woodside's group. She was a valuable member who taught me how to make handles. My special thanks to Dr. Derek Dee, former post-doc, who patiently helped me in my work with PrP, when I started my research in the biochemistry laboratory. Furthermore, my work with click chemistry was powered by his broad knowledge in biochemistry. Most of the mouse PrP measurements using traditional chemistry were done with the help of Dr. Dustin Ritchie. He had brilliant suggestions to improve the method of handle attachment. Analysis of PrP and tetrapyrrole paper was done with the help of an experienced molecular physicist, Dr. Krishna Neupane. He taught me a lot of analytical skills when I started my research in Woodside's group. Making beads for the experiments is a crucial step, one which Dr. Supratik Sen Mojumdar provided me with invaluable guidance in. He also had great suggestions when I had issues in

data analysis. The problems and issues related to optical tweezers were solved by Dushanth Seevaratnam and Daniel Foster, former PhD student in Woodside's group. Special thanks to Noel Hoffer and Uttam Anand for their critical reading of my thesis. Their invaluable comments helped me to express my work in a more appropriate manner. Lastly, thanks to all other current and former members of Woodside's group, they were helpful in all my research steps and made the lab environment friendly and a nice place to work.

Finally, I must express my very profound gratitude to my parents and my sister back home, and to my fiancé. Their endless love and unfailing supports were the major encouragement on doing my thesis. And to Hossna and Fatemeh my close friends, thanks for their help and support when I was new in Edmonton. They always make my life wonderful, so that I think I have a family here.

I dedicate this thesis to my parents. For their love, support and encouragement. Thank you for teaching me to believe in myself and to follow my dreams.

Contents

1	Introduction	1
1.1	Basic idea of prion misfolding and prion diseases	1
1.2	Protein folding, misfolding and aggregation	3
1.3	Challenge of understanding prion disease and introducing single molecule as a way to overcome the challenge	7
1.4	Brief overview of therapy approaches for prion diseases	11
1.5	Anti-prion compounds	12
1.6	Introduction to Force Spectroscopy	14
1.7	Overview of thesis	17
2	Single Molecule Force Spectroscopy with optical traps	18
2.1	Basics of optical tweezers	18
2.2	Mechanism of measurement	19
2.3	Types of SMFS measurements	21
2.4	Data analysis	23
2.4.1	Identifying distinct structural states	24
2.4.2	Size of the structure	27
2.4.3	Energy landscape profile	28
3	SMFS measurements of MoPrP folding	32
3.1	Motivation	32
3.2	Sample preparation	33
3.2.1	Protein preparation	33
3.2.2	Handle attachment using disulfide bonds (S-S bond)	37
3.2.3	Introduction to click chemistry	38
3.2.4	Handle attachment using click chemistry	42
3.3	Results	43
3.3.1	FEC measurement	43

	3.3.2	Fluorescent experiment to check internal Cys labeling for PrP	45
4		Pharmacological chaperone reshapes the energy landscape for folding and aggregation of the prion protein	48
	4.1	Introduction	48
	4.2	Results	49
	4.2.1	Force-extension curves of monomers PrP	49
	4.2.2	Energy landscape for PrP unfolding	52
	4.2.3	Fe-TMPyP can hinder native folding	54
	4.2.4	Effects on PrP dimers	56
	4.2.5	In vitro aggregation	58
	4.3	Discussion	60
5		Pentosan polysulphate (PPS) as an anti-prion compound	65
	5.1	Motivation	65
	5.2	Bulk measurements	65
	5.2.1	SPR analysis	65
	5.2.2	ITC measurement	69
6		Future work	74

List of Figures

1	Protein translation	4
2	Notional cartoon of an energy landscape in one dimension	6
3	Energy landscape cartoons depicting native folding and aggregation	8
4	Illustrations of single-molecule techniques	10
5	Single-molecule force spectroscopy of a single PrP molecule	16
6	Comparison of different assays in optical tweezers	20
7	Experiment setup and outcomes	26
8	NMR structure of mouse prion protein (121-231)	33
9	2Cys-MoPrP sequence with His-tag	34
10	15% SDS-PAGE gel of 2-cys-moPrP	36
11	circular dichroism analysis of 2-cys-moPrP	36
12	Reaction of Amine compound with NHS Ester derivative	39
13	Reaction of sulfhydryl compound with maleimides derivative	39
14	Handle labeling with TCO	41
15	Protein labeling with Tz	41
16	Protein handle attachment with click chemistry	42
17	Commparation between thiol handle attachment and click handle attachment	43
18	Force spectroscopy measurements of MoPrP	44
19	Overlaying 60 unfolding FECs of MoPrP	45
20	SDS-PAGE gel of 2-CysMoPrP and WT-MoPrP labeled with Tz (protein was reduced with TCEP)	46
21	SDS-PAGE gel of 2-CysMoPrP and WT-MoPrP labeled with Tz (protein was reduced with MEA)	47
22	Force spectroscopy of PrP with Fe-TMPyP	52
23	Effect of Fe-TMPyP binding on unfolding energy landscape	54
24	FECs without discrete transitions	56
25	FECs of PrP dimer	58

26	Effect of Fe-TMPyP on ensemble aggregation kinetics	60
27	Cartoon of Fe-TMPyP effects on PrP folding	62
28	SPR sensorgrams of purified recPrP binding to immobilized PPS	67
29	Recovered SPR sensorgrams of purified recPrP binding to immobilized PPS	68
30	linear fit to the ligand concentration dependence of γ	68
31	One site model fit to the PPS titration into ShPrP with background titration .	71
32	One site model fit to the PPS titration into ShPrP	72

List of abbreviations

Prion protein	PrP
Cellular form of prion protein	<i>PrP^C</i>
Scrapie form of prion protein	<i>PrP^{Sc}</i>
cysteine	Cys
Syrian hamster prion protein	ShPrP
Mouse prion protein	MoPrP
Circular dichroism	CD
Kilodalton	KDa
Transmissible spongiform encephalopathies	TSEs
Nuclear magnetic resonance spectroscopy	NMR
Amyotrophic lateral sclerosis	ALS
Bovine spongiform encephalopathy	BSE
Creutzfeldt–jakob disease	CJD
New variant creutzfeldt–Jakob disease	nvCJD
Single molecule	SM
Fluorescent resonance energy transfer	FRET
Atomic force microscope	AFM
Surface plasmon resonance	SPR
Pentosan polysulphate	PPS
Fluorescence correlation spectroscopy	FCS
Double strand DNA	dsDNA
Force extension curve	FEC
Single-molecule force spectroscopy	SMFS
Worm like chain model	WLC
Isopropyl- β , D-thiogalactopyranoside	IPTG
Dithiothreitol	DTT
Immobilized metal affinity chromatography	IMAC
2,2 -dithiodipyridine	DTDP
Amino acid	aa
Hidden Markov model	HMM
Point spread function	PSF
Single molecule	SM
Iron(III) meso-tetra (N-methyl-4-pyridyl-prophine)	Fe(III)-TMPyP
Tetrapyrrole	TMPyP
Syrian hamster prion protein	ShPrP
Isothermal titration calorimetry	ITC
Thioflavin T	ThT
Protein misfolded cyclic amplification	PMCA
Maltose binding protein	MBP

Poly-histidine tag	His-tag
Molecular weight	MWT
Sodium dodecyl sulfate polyacrylamide gel electrophoresis	SDS-PAGE
N-Hydroxysuccinimide	NHS
Trans-cyclooctene	TCO
Tetrazine	Tz
Maleimides	Mal
Wild type MoPrP	WT-MoPrP
Thioflavin T	ThT
Misfolded cyclic amplification	PMCA
Maltose binding protein	MBP
Recombinant PrP	recPrP
Surface plasmon resonance	SPR
Resonance units	RUs

1 Introduction

1.1 Basic idea of prion misfolding and prion diseases

It is widely accepted that prion diseases—the misfolded prion aggregation—are associated with the misfolded form of the prion protein (PrP^{Sc}) [1]. Prion disease can introduce a new way of transmission of infectious diseases which is caused by the replication of a misfolded structure by templated conversion rather than replication of an infectious organism (as for viruses and bacteria) [2], [3]. Prion diseases manifest as structural conversion of cellular prion protein (PrP^C) into a transmissible, misfolded form of prion protein (PrP^{Sc}). Prion protein diseases are special because of the direct interaction between PrP^{Sc} as a template and PrP^C to drive the formation of the infectious prions [4], [5]. This means that, the stable misfolded protein can convert the native form of prion protein and help itself to reproduce [6], [7]. In a nutshell, protein aggregations in different neurodegenerative disorders—such as Alzheimer’s disease, amyotrophic lateral sclerosis (ALS), Parkinson disease, and prion diseases—work as toxic agents inside and outside of a cell [8].

PrP is a membrane-bound protein with molecular mass of 33-35 kilodalton (kDa) and in its native form it is a non-infectious protein. PrP^C is mostly localized on the cell surface where it is attached to the lipid bilayer (a thin polar membrane made of two layers of lipid molecules that works as a barrier to keep proteins where they are needed and prevent diffusion of them into the other locations where they are not supposed to be) [9]. Notably, the converted form of prion protein or scrapie form of the prion protein (PrP^{Sc}) is the most important factor in most transmissible spongiform encephalopathies (TSEs) infections or prion diseases [3].

(PrP^C), a normal form of the prion protein which is mostly expressed in the brain but occurs in many other tissues throughout the body, is different conformationally from the misfolded form of the protein [10], [11], [12]. The protein can be found in different isoforms; for example, the normal isoform which is called the cellular form of the prion protein and the abnormal/ disease-causing isoform which is called the misfolded form of the prion protein [13]. Scientifically, Nuclear magnetic resonance (NMR) structure of cellular prion protein shows that the protein is rich in alpha helical structure [14], [15]. Moreover,

the results expressed from circular dichroism (CD), a method often used in chemistry to analyze the structural form of a protein, show that prion protein can be converted to an insoluble amyloid form of the PrP with a beta sheet rich structure [1]. Conversely, the normal form of the prion protein is alpha-helix-rich, soluble in mild detergents and protease¹ sensitive [16], [17], [3].

Prion infections of different species can occur in different ways. For instance, the oral route is the initial step of infection in sheep scrapie, bovine spongiform encephalopathy (BSE) of cattle and new variant creutzfeldt–Jakob disease (nvCJD) [18]. Thereafter, the initial steps of replication begin in a peripheral compartment before brain conversion begins [18].

Two concerns associated with prion protein aggregation are finding the structure of PrP^{Sc} and the associated conversion mechanism. Resolving these two concerns makes it possible to overcome problems of diseases [19]. What has made the second concern more controversial is that we are not certain of the structure of the scrapie form of PrP. This uncertainty impedes us in clearly predicting the conversion mechanism [20], [21].

Prion protein can aggregate into different shapes and forms; for example, oligomers, amorphous aggregates and amyloids [7]. These scrapie-associated fibrils may be observed using electron microscopy or light microscopy when the amyloid plaques are large enough [22], [23]. Although the conversion mechanism is not completely known, there is some evidence that empowers the idea that the scrapie form of the PrP works as a template for cellular form of PrP, infects PrP^c , and promotes the conversion mechanism [3]. Conversely, we must consider the possibility that all of these forms or structures are not infectious [7].

We can simplify the task of addressing the early events in PrP aggregation by *i*) understanding the different folding pathways available to the protein, *ii*) identifying those that lead to misfolding and aggregation through the use of single-molecule methods, and *iii*) investigating how these pathways respond to protein-protein or ligand-protein interactions [19]. The ensemble approach is an average study on prion protein aggregation. However, the single molecule approach is a way of looking at one single molecule over a period

¹Protease is any enzyme that can cleave a protein. Specifically, protease can hydrolyze proteins by breaking the peptide bonds that link amino acids together in a polypeptide chain.

of time [24], [25]. There are some drawbacks in using ensemble method. First of all, initial conversion starts with misfolding of only a few molecules, making this process and its features very challenging to observe using this method. Secondly, the conversion may involve different pathways and intermediates which may not be possible to be detected in ensemble approach [16]. And finally, in many cases, in order to stabilize and observe non-native states, we need chemical denaturants. Chemical denaturants have complex, global effects on the solution and have a behavior that may bias what is seen in misfolding. Consequently, an alternative approach that can overcome all these problems is needed. The single molecule approach gives us a chance to observe these events at the single molecule level using different types of instruments [26].

As a way to overcome the diseases, there is a chance of using some molecules as potential drugs which have anti-TSE effects. In that case, anti-prion drugs reduce the misfolding rate of the proteins and leads to a reduction or halting of the disease [8]. Although some small molecules are the most effective known anti-TSE compounds—for example PPS, tetrapyrrole, anti-*PrP^{Sc}* antibody—the mechanism of action of these compounds remains unclear [27].

1.2 Protein folding, misfolding and aggregation

Recall that hereditary information is stored and passed on in a one dimensional sequence of DNA base pairs. To go from heredity to biological function, messenger RNA which is produced from DNA is needed. A ribosome decodes messenger RNA to produce a specific amino acid chain. The produced amino acids contain sufficient information to determine a protein's geometrical 3D structure [28], [29]. The folding of proteins into compact 3D structure is the important subsection of self-assembly in biological studies [30] (Figure 1).

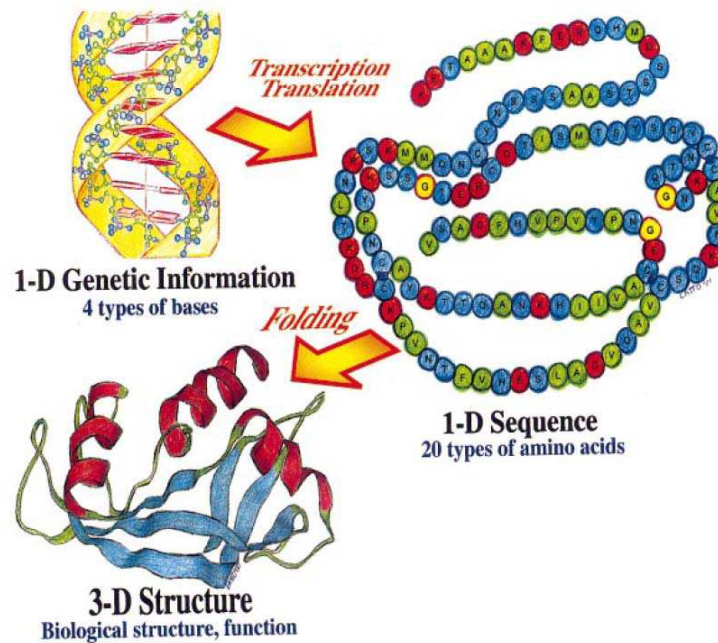


Figure 1: All information necessary for the structure and function of a living organism is usually contained in the 1D sequence of base pairs in the DNA molecule. This information is eventually translated to the specific sequences of amino acids in protein chains. This 1D information encodes, through the complicated process of folding, for the 3D information contained in the native structure in which the protein is functional. Folding is non-local process in that it involves bringing parts of the chain remote in sequence close together in space. Figure adapted from [29].

To understand the folding process which is complex, we need to know about the concept of energy landscape. Energy landscapes provide us an opportunity to understand the structure formation in biological macromolecules, such as proteins [31], [32], [33]. An energy landscape is a surface describing the energy of every possible conformation. Theoretically, protein can exist in an infinite number of conformations along its energy landscape, but in reality, the proteins fold from the secondary structure which is the chain of amino acids to the tertiary structure, when typically the lowest free energy is possessed. As mentioned, the number of possible conformations of any polypeptide is so large, that the system needs a huge length of time in order to search through all possibilities. Therefore, the searching is not required to pass over a series of mandatory steps between specific partly folded states, however the system performs a stochastic search of many conformations accessi-

ble to a polypeptide chain, taking only microseconds to do so [34], [35], [31]. Polypeptide chains are able to find the lowest energy structure through a diffusive search that is not purely random process, but biased by the stability of native-like interactions between residues [34], [35], [31]. In addition, only correctly folded proteins with low enthalpy and entropy operate properly in the cell environment and can interact selectively with their natural partner [31], [30]. Moreover, native states of proteins generally refer to the condition that proteins are thermodynamically stable under physiological conditions and the global free energy of all kinetically accessible structures is at a minimum [29], [30].

Describing free energy landscapes on a multidimensional surface is a bit hard to understand; so, a single dimensional coordinate is introduced for simplicity (Figure 2). In addition, since our experiments are almost in 1D, describing free energy landscape on a 1D surface is reasonable. As proteins fold rapidly, the general thought suggested the funnel-shape landscape to minimize the time needed to arrive at the native structure. In figure 2 unfolded molecules have high enthalpy and high entropy, however folded molecules have the lowest enthalpy and entropy. Notably, the presence of energy barriers within the energy landscape slows down the folding process, owing to the fact that decreasing enthalpy and entropy during folding are not synchronized. The folding landscape is not unique, because it is implicitly a function of the environmental conditions [31].

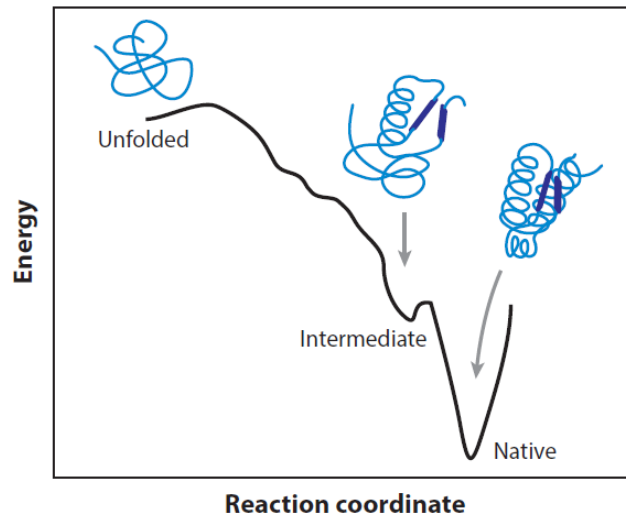


Figure 2: Notional cartoon of an energy landscape in one dimension. An unfolded molecule has high energy and high entropy, whereas a folded molecule has low energy and low entropy. The funnel-like shape of the landscape leading to the native state may be punctuated with barriers and metastable intermediates. Figure adapted from [36].

If a protein does not fold properly or misfolds—right after synthesizing or in later process—it can have inappropriate interactions with other molecules within the cellular environment unless a range of strategies are taken into account by living cells to prevent such behavior [37], [38], [39]. These strategies would be helping protein to unfold and refold into the correct shape by molecular chaperones or removing misfolded proteins once they have formed through the action of the proteasome. Some diseases are associated with the incorrectly folded proteins (such as cystic fibrosis and some types of cancer) while others are associated with the high propensity of proteins to misfold and ignore all protective processes in the cell to form intractable aggregates within cells (Alzheimer’s and Parkinson’s diseases, Spongiform encephalopathies and type II diabetes). Therefore, failure to fold correctly, or the inability of maintaining the correct shape can give rise to the malfunctioning of the living system and increase the chance of diseases [37], [39].

Almost all proteins can form amyloid structures under certain conditions. Amyloids are not typically infectious but they are in some cases. Aggregation of a specific protein results in specific amyloid diseases. These amyloid fibrils are insoluble and usually composed of

a highly-ordered β *sheet* *rich* structure [40]. The small oligomers are thought to be the most toxic species in neurodegenerative diseases. Moreover, they can decrease the quantity of protein that can perform its normal function [1]. For example, prion protein can misfold and aggregate into a form which is rich in β *sheets*, eventually, forming insoluble amyloid fibrils [21], [41].

Understanding the molecular misfolding and aggregation process is still unclear. The nucleated-growth model is the preferred model for amyloid formation. The conversion time includes a lag phase—the time needed to form misfolding nucleus— that is followed by a rapid amyloid polymerization process [42], [43] [44]. Moreover, with the presence of different pathways within the aggregation process we need a molecular method to know more detailed mechanism underlying protein misfolding [19].

1.3 Challenge of understanding prion disease and introducing single molecule as a way to overcome the challenge

Generally, there are many factors which make the study of prion diseases problematic. Figuring out prion diseases has been complicated by conversion of PrP into the different misfolded states. Consequently, we need an approach to distinguish the pathways which result in misfolded states from the other pathways. In addition, the unknown conversion mechanism is a controversial topic in prion diseases which has made this problem all the more difficult to solve.

Finding these pathways are not easy due to the complexity in understanding the energy landscape [19]. A protein is searching through different configurations to pick up a native structure which is usually lowest energy structure. In figure 3, the cartoons of energy landscape related to native folding and aggregation are depicted. The landscape represents different states such as native, partially folded intermediate, unfolded, misfolded, soluble oligomers, or insoluble aggregate with energy barriers that separate all the states. According to funneled energy landscape, high-entropy and high-energy unfolded states located at the top of the funnel, fold along any variety of paths down to the low-energy, low-entropy native conformation. In figure 3, misfolding and aggregation states are also illustrated and separated by substantial kinetic barriers. The nonnative structure is a connector between folding

landscape and the inter-molecular aggregation. This means that a native form of a protein can be misfolded into a non-native structure and then can be aggregated into oligomers or amyloids [45], [46].

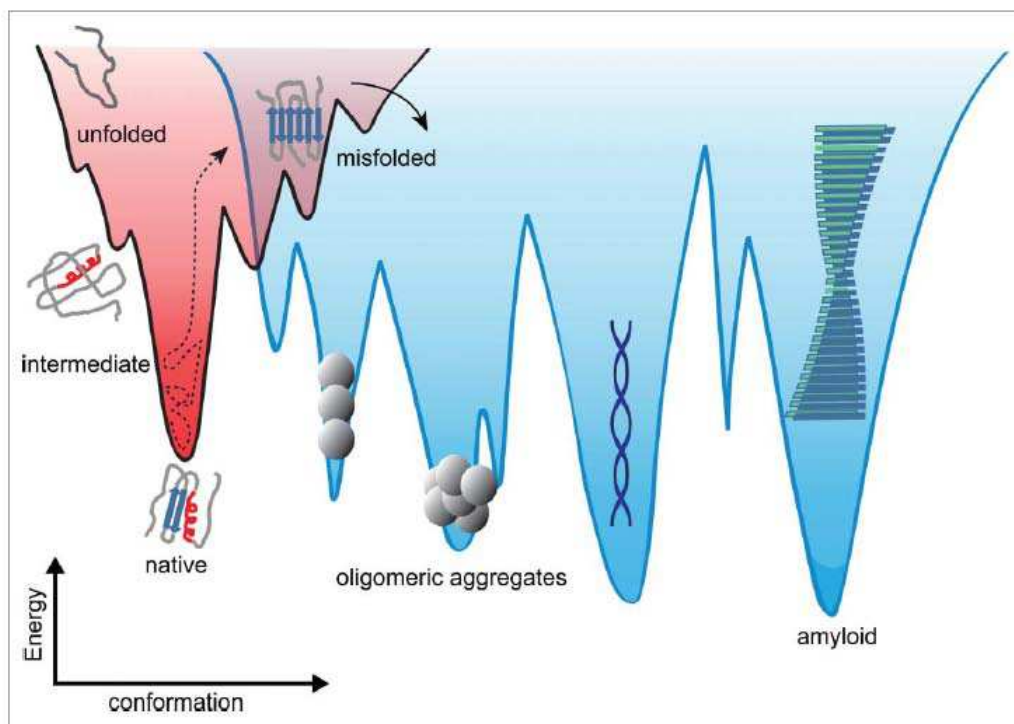


Figure 3: Energy landscape cartoons depicting native folding (left) and aggregation (right). Nonnative species often connect the 2 regimes. The landscape is expected to be more rugged for aggregation, having deeper kinetic traps. Single-molecule force spectroscopy can measure the critical landscape properties like the energetic stabilities of the different states (including intermediates), the heights of the energy barriers between states, the position of the barriers along the reaction coordinate, and the diffusion coefficient that connects the landscape properties to the observed kinetics of structure formation. Figure taken from [47].

It is also possible for a protein to aggregate into a misfolded state. Moreover, the ensemble approach which is an average study is not the preferred way to characterize the properties of rare or short-lived states. It is also challenging to differentiate the properties of subpopulation states via the ensemble approach [48]. This means that looking at the system with a 'blurry' method does not give a good picture of what is going on. Consequently, single molecule spectroscopy is introduced as a good way to overcome this problem by looking

at single molecules one at a time. The approach can help us to investigate protein folding mechanism as well as to observe distinct subpopulation, transient states, and finally, to determine the folding pathways and energy landscape for the molecule of interest [26].

Single molecule (SM) method, which is a powerful tool in the area of biophysics, can aid us in dealing with biological problems in vitro, providing near atomic resolution. This method is very useful in biological studies to give us detailed information of microscopic behavior. Moreover, SM method is a way to identify and characterize different subpopulations and very rare events [49]. Interestingly, we can observe rare and short-lived states directly by monitoring a single molecule over a period of time [49]. In this technique, proteins can be studied at very low concentration (pM) which provides us with an opportunity to study the initial states of aggregation [49]. Using this method, rare transition states, misfolded states and pathways [50], kinetics, thermodynamics of mechanical response and folding transitions [51], [50], [52] [53], mechanisms of molecular motion and even the interactions that stabilizes non-naive structures can be observed. The single molecule method offers a unique means of measuring the properties of the free energy landscape directly [54]. In addition, for the first time, the transition path time was measured using this method [55], [56]. There are different types of complex and sensitive instruments and techniques that are widely used for making high resolution measurements, namely, particle tracking, fluorescent resonance energy transfer(FRET), magnetic tweezers, force-mode atomic force microscope (AFM) and optical traps [54] (Figure 4).

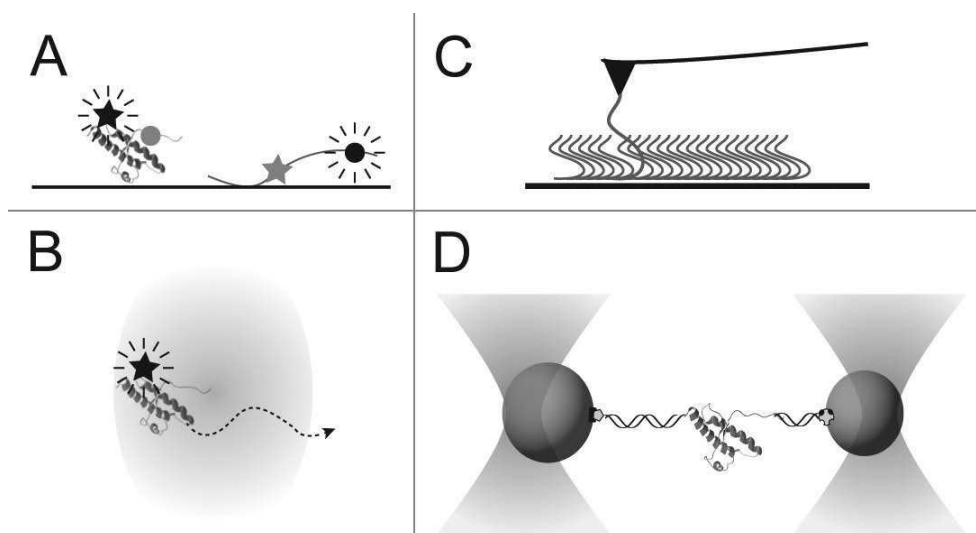


Figure 4: Illustrations of single-molecule techniques. (A) In FRET, the protein is labeled with two dyes, a donor (circle) and acceptor (star), and the donor is excited. Energy transfer to the acceptor is high when the dyes are close (left), low when they are far apart (right). (B) In FCS, fluctuations in the fluorescence of a labeled molecule are measured as it diffuses through a confocal excitation volume and used to determine the diffusion time. (C) In AFM, the tip is used to pull on a molecule tethered to the surface (here, a monomer is pulled out of a fibril). (D) In optical tweezers, beads trapped by laser beams are used to pull on the ends of a protein molecule tethered between them. Figure taken from [19].

. The first method for measuring biological motion took place with the use of some micron sized particles that can be attached to a molecule. With this approach, the position of the molecule can be tracked through a microscope [57], [58]. Fluorescent dyes are a good replacement for particles when the reporter particles interfere with the measurement due to the large size of the particles [59]. The second method of producing high quality measurements of biological molecules is fluorescence resonance energy transfer (FRET). In this case, the method uses two fluorophore, one as an excited fluorophore excited by light (donor), the other one as an acceptor fluorophore. Recently, single molecule methods are being used in figuring out misfolding of different proteins; for example, alpha-synuclein, A-beta, calmodulin, coiled-coils, prion proteins, and etc. [54]. In addition, to find the effects of therapeutic agents on the proteins, single molecule methods are powerful tools [60], [61].

1.4 Brief overview of therapy approaches for prion diseases

Many therapeutic strategies have been tried, but there are still no successful treatments that prevent or inhibit the disease. Some of the most explored methods include immunotherapies and small-molecule drugs inhibit misfolding and aggregation. Knowing the role of the immune system can improve therapeutic approaches [3]. Anti-prion protein antibody may offer a solution to prion diseases. Antibody binds to the protein to inhibit misfolding/aggregation and/or triggering the immune system to help clear the infection. If we assume that the immune system could not respond in a prion affected specie, the use of anti-prion protein antibody would be reasonable. In this case, the species' immune system identifies PrP^c and PrP^{Sc} as antigens using the injected antibody [62], [63]. Several recent studies show the ability of antibodies to clear scrapie-infected cells of PrP^{Sc} [3]. The antibodies are generally directed against PrP^c [3]. 6H4 is a non-selective antibody for prion protein which can block the scrapie form in mice experimentally [64]. The idea is that the presence of antibodies in the cell can interfere with the intermolecular interactions of PrP^c or can change compartmental cycling of this protein. Consequently, the rate of conversion of PrP^c to PrP^{Sc} decreases [3].

On the other hand, there are some disadvantages in using antibody against PrP^c in vivo. Firstly, PrP^c is an over-present protein. Using anti- PrP^c antibody can interfere in a way that is not specific [65], [66]. Secondly, anti-body against prion protein can disarrange the balance of PrP^c which can lead to autoimmune disease. Finally, having anti- PrP^c antibody in the cell can interfere with the cellular function of the protein [67].

In order to resolve these issues, anti- PrP^{Sc} antibody may be used as an alternative to anti- PrP^c antibody [68]. The advantages of using anti PrP^{Sc} anti-body is two-fold: First, kinds of anti-bodies have no toxic effects, and second, they do not take normal cell surface protein as antigens. Hence, they do not interfere with the normal cell [69]. The ability of monoclonal and polyclonal anti PrP^{Sc} anti-body to recognize PrP^{Sc} as antigen, proved the possibility of prion infectious therapy via anti-bodies [70]. Recently, vaccine therapies have also been introduced by injecting vaccines containing amyloid- β ($A\beta$) fragment of amyloid precursor protein of Alzheimer's disease. By introducing $A\beta$ fragment to the immune system, it

appeared that there was an effective therapy for Alzheimer's disease. Unfortunately, after development of encephalopathy in some cases, the use of this vaccine has been stopped. However, with anti PrP^{Sc} anti-body has prevented neuro-invasion in cattle and human and improvement of encephalopathy in the brain [71].

1.5 Anti-prion compounds

Many ligands capable of binding to human PrP have been reported. Some of these ligands that can not interact with PrP, behaved as nonspecific polyionic aggregates. On the other hand, some ligands that can interact with PrP can potentially be considered as a pharmacological chaperones [8]. For example, GJP49 and GJP14 are two compounds that showed the ability of having anti-prion effects in silico experiment [72]. Surface plasmon resonance (SPR) results indicated GJP49 and GJP14 bind with 1:1 stoichiometry with PrP^c at the same site in equilibrium experiments [72]. They bind to PrP^c and inhibit the pathogenic conversion of PrP^c to PrP^{Sc} . In addition, the dissociation constant (K_D) was characterized to be $50.8 \mu M$ [73]. GN8, another anti-prion compound, binds to the same location that GJP49 and GJP14 do [74]. GN8 is an effective anti-prion compound which is unique because of the binding affinity and anti-prion activities in both vivo and vitro experiments [75], [74]. However, there are some anti-prion compounds such as GFP55, that lack high binding affinity and are classified under an ineffective group of compounds [72]. Another compound that can increase SPR signal without any trend toward saturation is quinacrine. An important point for this reaction is that quinacrine binds to PrP^c in a nonspecific manner due to strong hydrophobic interaction. Unfortunately, using quinacrine has side effects; for example, it may bind to other proteins instead of our intended PrP^c ; also, it may accumulate in the brain after long term therapy [73]. Quinacrine can bind non-specifically around parts of helices 1, 2 and 3 which include residues Y225, Y226 and D227. The differences in the compounds binding affinity come from the differences in the binding site of protein for ligands [73]. SPR results of pentosan polysulphate (PPS) shows increasing signal and incomplete dissociation for PPS-PrP reaction. PPS binds non-specifically to C-terminus of PrP^c . This non-specific interaction in vivo actually decreases the concentration of PrP^c and induces its aggregation [73]. In chapter 5, more details about this compound are presented.

In conclusion, we still do not know the mechanisms of anti-prion compounds. But, there are some indications showing that some compounds bind to PrP^C , and some other bind to the other forms of the protein [73].

There are plenty of cellular processes that help to reduce the effects of misfolding. The role of molecular chaperones in the cell is to aid proteins in finding their native structure and prevent misfolding in the first stage of the process which can be an effective means of alleviating the disease in disease related proteins [76], [77]. Hence, drug chaperones are then being added as a way to try to help prevent misfolding and decrease the speed of infection within cells [73]. In addition, single molecule approaches are also useful methods of investigating the mechanism of the molecular chaperones. The main result revealed from this method is that the molecular chaperones can help proteins refold to their native structures, by unfolding the misfolded proteins and giving them another chance to fold into the correct shape, altering the folding rate of domain and blocking tertiary contacts in the transition state [78], [79].

Prion protein should pass over a high-energy barrier existing between native state and scrapie state to be misfolded. Hence, naturally, the protein can pass rarely over this barrier unless some unknown causes occur. Unfortunately, some compounds; for instance, GN8, GPJ49, GPJ14 and quinacrine can cause residual fluctuations on a time scale of micro- to milliseconds after binding to the prion protein [80]. These fluctuations can increase the risk of conversion. However, pharmacological chaperones help the protein by decreasing these fluctuations. Therefore, they stabilize the native form of the protein. This protection can be done by reducing the energy level of the native state of the protein. Hence, passing the barrier between PrP^C and PrP^{SC} would be difficult for the protein and the chance of pathogenic conversion decreases [73].

The literature on protein structures shows that the native structure of the prion protein is very similar for different species. But, it is unclear if there are differences in their functions due to the lack of information. The conversion structure and the number of conversions for each molecule as well as the mechanism of conversions is still unknown [81], [82], [21], [20]. In addition, effects of many compounds on PrP^{SC} and their efficiency directly depend on the conversion structure they are dealing with. Thus, they may cause more con-

version to PrP^{SC} rather than the PrP^C conformation. On the other hand, pharmacological chaperones—which are independent from PrP^{SC} —affect the known native structures and mainly the partly folded structures. As a result, they can act to favor native folding [73].

As mentioned before, an effective treatment has not been introduced for prion diseases [83]. However, developing the pharmacological molecular chaperones which mimic the cellular chaperones activities has been a key point in therapy approaches. Because of the unclear mechanism of action between protein and molecular chaperones, the therapeutic strategy is still controversial [27]

The focus of this thesis is on the pharmacological chaperons, specifically molecules that are thought to prevent misfolding by binding PrP^C . Iron tetrapyrrole is a candidate to act like a cellular chaperones and stabilize native structure of the prion protein.

1.6 Introduction to Force Spectroscopy

As a solution to the difficulties associated with ensemble measurements, biophysical techniques with the ability to observe the motion of single molecules down to the nanometer scale or below are introduced. There are many measurement tools that provide new insight into the mechanism of a single molecule. For instance, centroid tracking, fluorescence resonance energy transfer, magnetic tweezers, atomic force microscopy, and optical traps. All of these methods provide an opportunity for detecting molecular motion, at near atomic resolution in vitro experimental conditions. The greatest advantage of using single molecule studies, is in the investigation of the kinetics and thermodynamics of mechanical responses and folding transitions. It is also possible to reveal other complex features such as the mechanism of translocation, folding pathway, properties of transition states and enzymes activities and population heterogeneity [54], [49].

We can classify the single molecule measurements tools into two classes: the one by which we can track the motion of labeled molecules without applying significant external forces; such as, centroid tracking, fluorescence correlation spectroscopy (FCS) and FRET. The other class introduces an approach with measuring motion while the molecule is under external loads. The methods that constitute this class are; magnetic tweezers, AFM and optical traps. [54].

The greatest advantage of force based measurements is that by increasing the stiffness of the molecule of interest, we can increase the resolution of the measurement. And also, there is a chance to map the energy landscape easily. All the data are collected while applying an external force to single molecule in order to destabilize the structure. Then, the length of the protein of interest is measured. In order to apply force, two sets of double stranded DNA (dsDNA) handles are attached to the protein. Each end of any set has a distinct tag used for attachment to different sized beads. The construct, consisting of the handles and the molecule of interest, acts as a spring [54].

In our lab, we focus on optical tweezers (optical trap). In optical tweezers, radiation pressure is applied using a focused laser beam on small dielectric beads which are attached to both ends of the dsDNA handles [54]. The trapped beads are polarized by the strong electromagnetic field of the laser. As a result, a force proportional to the gradient of light intensity according to $F \propto \alpha \nabla I_0$ occurs, where I_0 is the laser light intensity at the specimen and α is the bead polarizability [84].

The applied force can be adjusted using the intensity of the laser light or by adjusting the position of the beads with respect to the trap center [54]. If the measurement is performed in living cells, in order to reduce the molecular damage from intensity of light, the wavelength, which is used for generating the applied force, is near infrared. This region of wavelength is near-transparency for most biological materials [85]. Then, the position of the beads can be determined by collecting the laser light scattered by the beads. The light scattered by the beads, from either the trapping laser or a separate detection laser is collected by a photo-sensitive detector [86]. By moving the beads apart, the tension applied to the molecule increases. As a result, the extension of the molecule increases. Force extension curves (FECs) were created by measuring the extension of the PrP constructs while moving the traps apart at a constant rate to ramp up the force [69]. We call this type of curves force extension curves (FEC) (Figure 5). The strategy of the method will be fully explained in chapter 2.

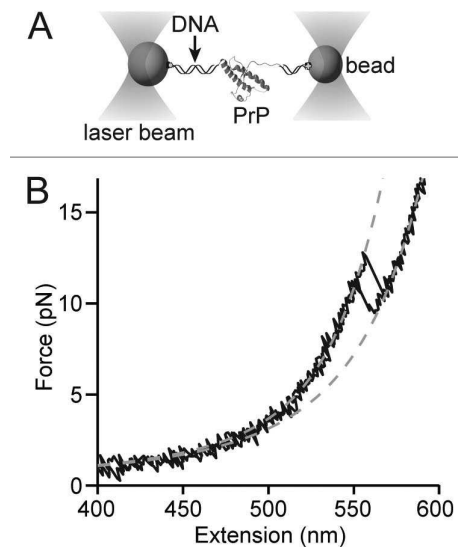


Figure 5: Single-molecule force spectroscopy of a single PrP molecule. (A) Experimental scheme using optical traps. Cysteine labeled PrP is attached to DNA handles linked in turn to beads held by optical traps. (B) Force-extension curves show that as the force increases, the handles stretch until the PrP structure unfolds suddenly as a two-state system. WLC fits (dashed lines) to the folded and unfolded parts of the curves reveal a contour length change matching the result expected for PrP^C . Figure taken from [19].

To conclude, single molecule experiments provide an opportunity to probe the properties of individual molecules instead of an ensemble of molecules. Ensemble measurements can reveal the average properties of molecules without any details of the stochastic fluctuations. In contrast, with single molecule studies, we can observe even rare distinguished events because of the ability to probe very fast dynamics (typically, millisecond or even less) [25], [24], [16], [26].

The basics of single-molecule force spectroscopy (SMFS) are defined by applying an external force to the single molecule in order to denature the molecule. Moreover, the most important benefit of this approach is that one can apply force in any specific part of the protein as well as perturbing the structure of the protein in physiological pH without using any denaturing buffer. The mechanism of conformational changes of molecule in response to the applied force is unfolding and folding when the force increases and decreases respectively. In addition, extension changes related to the tension applied to the molecule can be monitored by the motion of the force probe. The SMFS method is an effective way to reveal

the structures of molecules. Interestingly, using this method makes it possible to apply a wide range of force to a single molecule. As a result, we can have structures with a wide range of stabilities [87].

In order to study protein folding at the single molecule level, many force probes are available including AFM, optical tweezers and magnetic tweezers. The key point that affects choosing the appropriate force probe is the level of force needed to unfold a protein. For example, for some proteins high force is required; hence, we need AFM to apply force to the intended molecule. In contrast, optical tweezers and magnetic tweezers are ways of manipulating a protein in low force regime [54], [88].

1.7 Overview of thesis

The rest of the thesis is organized as follows. Chapter 2 describes single molecule force spectroscopy method, optical tweezers, and the most important outcomes of optical tweezers. Chapter 3 introduces a real measurement on mouse prion protein (MoPrP). The force-extension results explained in this chapter have been collected from samples which are prepared via either traditional chemistry in our lab (thiol chemistry) or newly developed chemistries (click chemistry). Chapter 4 covers the effects of tetrapyrrole compound as a pharmacological chaperone on ShPrP. The result of this chapter is accepted to be published in the Nature Communications journal in 2016. The thesis ends with the use of pentosan polysulphate (PPS) as well as many compounds that have been reported for anti-prion protein compounds in the study of ShPrP.

2 Single Molecule Force Spectroscopy with optical traps

2.1 Basics of optical tweezers

Optical tweezers is a high resolution and sensitive instrument for probing conformational dynamics at the single molecule level [89]. The instrument gives us a chance to study phenomena ranging from folding and ligand binding to enzyme function, molecular machines, and protein aggregation [89]. To perform SMFS measurements, I used optical tweezers. In optical tweezers experiments, a molecule is attached via DNA handles to two micron sized beads which are trapped by tightly-focused laser beams. By moving the laser beams apart, force is applied to the molecule, causing mechanical denaturation of the molecule [90], [48], [91]. The extension of the molecule can be measured from the distance between the beads and plotted against the applied force, which is measured from the displacement of the beads from the center of the trap [90], [48]. This force versus extension plot is the typical result taken from optical tweezers measurements [19].

In my experiment, the protein is attached covalently through disulfide chemistry to DNA handles and the handles are attached specifically to micron-sized beads through avidin-biotin or dig-antidig linker [91]. The intense light associated with optical traps is in the infrared spectrum with a wavelength of 1064nm. This wavelength was chosen to minimize the damage to biological molecules [54]. The light is emitted via laser diodes and directed onto the beads by a series of optical instruments. Light scattered by the beads is collected by two cross-axial photo-detectors and used to track the position of the beads [54].

Optical tweezers have a wide range of application, from investigating the folding properties of nucleic acids to characterizing folding and misfolding properties of different proteins. We can extract the shape of the folding energy landscape, the structure of the construct as well as the number of sequences under high resolution measurements. Several measurement methods are possible using optical tweezers: equilibrium measurement and non-equilibrium measurement [54]. Both methods are expanded in detail in this chapter.

2.2 Mechanism of measurement

There are three common configurations which force may be applied to a single molecule by optical traps. In the first method, a bead on one end is held by a micro-pipette and the other bead is held by an optical trap. In the second method, the molecule is tethered on one end to the surface by a DNA handle and the other end of the molecule is tethered to a bead which is held by the optical trap. Finally, in the third method, two beads, each tethered to opposite ends of the molecule are trapped by the optical tweezers (Figure 6). This third method is preferential in our lab based on the properties of the system under study and the required resolution in our measurements with optical tweezers. due to the thermal heating of the objective, stage settling and laser pointing fluctuations, the surface-based assay is susceptible to relative drift between the surface and the trap, however, the third geometry that we use in our measurements has minimized these kind of problems. Moreover, using optical traps on both ends of the molecule which is a differential measurement can decrease the noise of measurement [92], [93]

The force is transferred to the molecule via the beads held in a trapping potential arising from the gradient force of a focused laser beam. The potential is Hookean within the regime of the focal point of the laser beam. This means that the produced restoring force is linear with the displacement of the bead from the center of the trap [94], [95]. Achieving the high resolution of the bead displacement is possible in this kind of measurement [95].

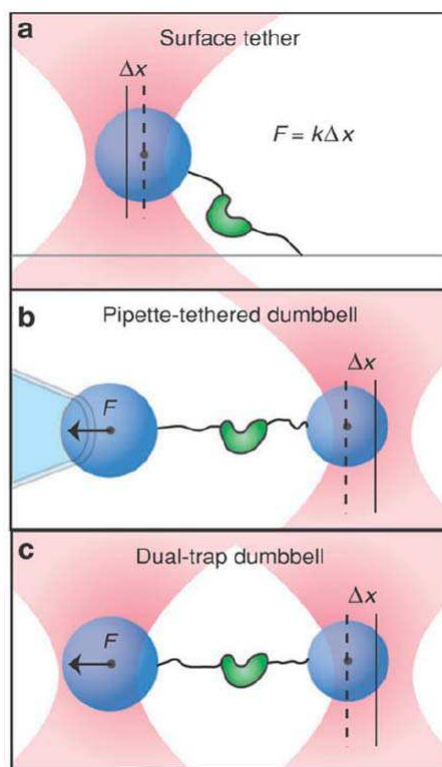


Figure 6: Comparison of the (a) surface-based assay, (b) dumbbell-based assay using one optical trap and a micropipette, and (c) dumbbell-based assay using two optical traps. Force is recorded by measuring the displacement of the bead from the center of the optical trap using light scattered by the bead. Figure taken from [54].

Notably, to reduce the probable interaction between the beads and protein, the beads are not attached to the protein directly. In other words, we use handle—such as double stranded DNA (dsDNA)—between beads and protein [54]. DsDNA handles can separate the beads spatially and minimize potential interaction between the beads and protein. Protein-ligand combinations such as biotin-avidin or digoxigenin-anti-digoxigenin are usually used to attach DNA handles to beads [96]. Handles can be attached to both ends of the molecules via two different chemistries. The first chemistry used in our lab in order to attach dsDNA to both ends of the protein was thiol [97]. The second chemistry, which is the most recent method in our group, is click chemistry introduced by one of our former postdoctoral fellows, Derek Dee. This chemistry is explained in detail in the next chapter. What is important in both chemistry is that Cys residues are reduced by reducing agent in the protein of interest

at the desired attachment points [96], [98].

Attaching handles to the reduced Cys of the protein is a means of controlling the location at which the force is applied by the laser beam. This means that if one changes the location of handles attached to the protein, they can use another geometry to apply the force [99]. The protein-handles reaction using disulfide bond has certain disadvantages. For example, it can lead to non-specific binding of handle-handle instead of protein-handle. Moreover, with the presence of this kind of non-specific interaction finding a single molecule on the microscope is a bit hard. Protein and DNA handles can have a non-specific interaction. So, the interaction is negligible at the forces required to unfold the protein [87].

The measurement with optical tweezers can be done in several ways using different regimes of statistical mechanics. The first condition is measurement in the non-equilibrium regime including constant pulling speed as well as increasing applied force [100]. The second condition is equilibrium measurement to record data from a single molecule which means that the control variable for the measurement is kept constant [88]. Both approaches are very useful and essential in measurement with optical tweezers. Under these circumstances, we can obtain congruent results which confirm the validity of each, individual measurement. The observables in constant speed measurement (non-equilibrium) are the extension (reaction coordinate) of the molecule of interest and the applied force to the molecule; while, extension and time at which events occur are the parameters for constant force measurement [26], [87].

2.3 Types of SMFS measurements

There are several different types of measurements—non-equilibrium measurements and equilibrium measurements—which are analyzed in different ways but yield similar information. In non-equilibrium measurements, changes are fast on the time-scale and the molecule can respond by changing the structure. In this type of measurement, force is either rapidly ramped or suddenly jumped. Moreover, the extension of the molecule and the applied force are measured while the protein is not in thermal equilibrium. However, in equilibrium measurements the fluctuation in molecular structure is measured while either the force or separation between the traps is kept constant [91]. Each types of measurements has its

own advantages, so it is always useful and reasonable to apply both methods to a desired molecule. In addition, similar information about folding can be extracted from equilibrium and non-equilibrium measurements; so, we can further validate the results.

Non-equilibrium measurements of folding

The most popular type of measurement is non-equilibrium which is typically done at a constant pulling speed. Clearly, the extension of the molecule increases as the tension force rises by moving the laser beams apart. The measurements are analyzed by plotting the force applied to the molecule as a function of the molecular extension. The resulting curve is called a force-extension curve (FEC). Specifically, the force increases non-linearly when the construct is stretched by moving the traps apart. As a matter of fact, the speed at which the separation occurs is the key control parameter in the force-ramp measurements. The shape of FECs is characterized as starting at a very low force, then increasing non-linearly along the reaction coordinate (extension) [91], [69]. The force goes up gradually until a sudden decrease in force as well as an unexpected increase in extension happen, which generates a characteristic sawtooth-shaped “rip” in the FEC (7-B). By measurements of folding with the high number of pulls, the variations in the unfolding forces can be observed (7-D). Important data can be extracted from this distribution of unfolding forces. This rip is associated with a cooperative change in the structure. To put it more simply, this is the point that a molecule unfolds. It is possible to have more than one rip in an FEC meaning that the protein contains the presence of multiple, independently-stable domains (7-C). Generally, a FEC with one rip involves two states: folded state and unfolded states [49], [89].

Another key point is that we can record data in both ramping up and down the force to measure unfolding and refolding of the molecule (7-A) [69]. The first case and the second case are called unfolding and refolding respectively. It is possible that the refolding and unfolding curves do not match. This asymmetry indicates the dissipation of energy. Repeating the unfolding measurement can increase our statistics to analyze data. The main problem in pulling the molecule is the stiffness of the handles and protein which is not very strong, creating a high probability for breaking the tether.

Multiple unfolding and refolding transitions can be observed in a single FEC in the force-

ramp measurements (Figure 7-E Black). In extreme case, the higher the unfolding/refolding rate is, the smoother and more gradual the extension changes (Figure 7-E Gray). Whereas, slower unfolding/refolding rate compared to the speed of separating the traps results in out of equilibrium measurement of the folding [87].

Equilibrium measurements of folding

Basically, equilibrium measurement refers to a type of measurement in which the force or the separation between the traps remains constant. In the first possibility, the applied force is fixed to a specific value and the behavior of the molecule is recorded. Although, the second possibility allows us to set the trap separation to a predetermined distance, thereby, some initial level of tension is applied to the protein. To be more specific, in a constant position measurement, while the structure of the protein fluctuates in response to the tension, the applied force reduces and increases when the protein unfolds and refolds respectively [49]. In contrast, in a constant force measurement, the force remains constant using a force clamp. The extension of the molecule is measured as a function of time in a constant force measurement [89].

The equilibrium measurement has some significant advantages. First of all, it is easier to make high-resolution measurements using equilibrium measurements rather than non-equilibrium measurements, mainly because some variables are fixed. Secondly, some rare states that were difficult to be observed in the non-equilibrium measurements can be recorded [49], [101]. On the other hand, non-equilibrium methods can give us access to the behaviors not seen in equilibrium. Therefore, both equilibrium and non-equilibrium methods are essential measurement methods [49]. All measurements described in this thesis were done so under non-equilibrium conditions.

2.4 Data analysis

After collecting data, we need to know a way to analyze this raw data from high resolution optical tweezers. Initial results that can be obtained from optical tweezers are the extension of the molecule, the force applied to the molecule and the time at which events occur. Extension of the molecule is reaction coordinate for the folding transition describes the progress of

folding [89]. We can extract a lot of information from optical tweezer experiments, such as the number of intermediate states [102], contour length changes of protein between folded and unfolded states, size of the structure, the number of amino acids, the rates of transition between different structural states [103], [104], energy landscape parameters as well as the shape of the energy landscape [105], [106]. Some of these outcomes are introduced in the following section.

2.4.1 Identifying distinct structural states

Both constant speed and constant force measurements are required high resolution data in order to observe intermediate states. In the first case, the intermediates appear like multiple successive rips (Figure 7-C). However, in constant force measurements, multiple steps in extension are signs of having the intermediates structural states. After finding the length of each intermediate state, it is time for mapping the state trajectory of the molecule. To do this kind of analysis, we need to generate the distribution of extension values first. Then, if peaks are well separated in the histogram, different analyses may be used to find the state trajectory. For example, the threshold analysis is often used [107]; and in some cases that peaks are not well distinguished, hidden Markov model (HMM) is a method to deal with this problem [108]. Optical tweezers are capable of extracting useful information about intermediate states; however, we need to take into account that, since we only measure length changes, it is possible to have more than one state with the same length. In this case, we need other parameters to distinguish the states; such as, the force which is needed to unfold the structure, or the lifetime of the intermediate state at a given force [49], [91]. It is important to keep in mind, even if enough evidence does not exist to prove intermediates, we cannot conclude that intermediate states are absent. In order to observe those hidden intermediate states, we may need to change the type of measurement or the location where the pulling handles are attached to the protein [49]. In addition, there is also a chance of hiding an unstable intermediate between two stable states. In this case, the stable state has a high unfolding force, much higher than that unstable intermediate. As a result, we cannot see the intermediate state because all portions of the molecule unfold at the same time [87].

Simple polymer models, such as worm like chain (WLC) model [109], is used in all

measurements to connect the extension changes (which are force-dependent) to the contour length changes (which are absolute) [110]. In our measurements, one of the WLC models can be used to fit the data of optical tweezers over a wide range of force (1-100 pN) encountered in optical tweezers (Figure 7-D). This model is called Marko-Siggia model whose equation [109] is

$$f(x) = \frac{k_B T}{l_p} \left[\frac{1}{4} \left(1 + \frac{x}{L_c} + \frac{F}{K} \right)^2 - \frac{1}{4} + \frac{x}{L_c} - \frac{F}{K} \right]. \quad (1)$$

x is the measured extension of the chain;

F is the applied force to the protein of interest;

l_p is the persistence length of the chain;

L_c is the contour length of the unfolded protein;

k_B is the Boltzmann constant; and

K is the enthalpic elasticity of the chain.

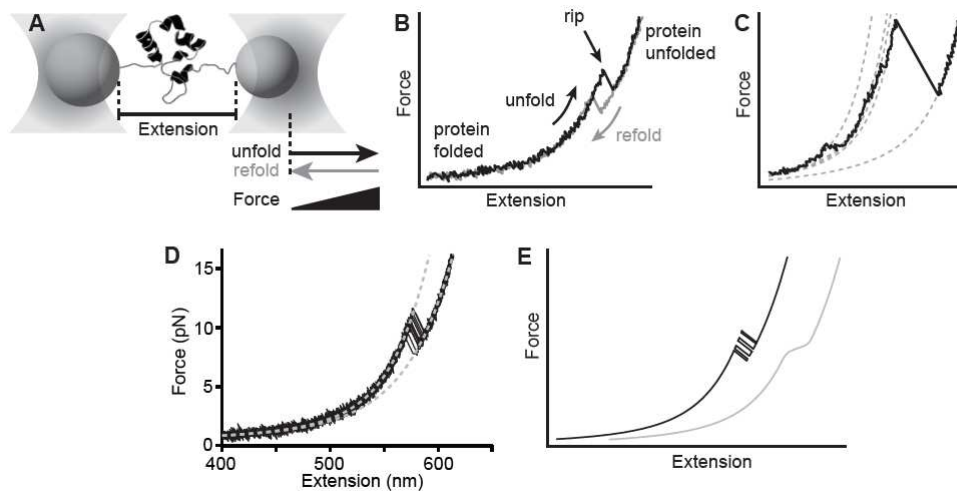


Figure 7: (A) The two beads are moved apart to increase the tension on the protein molecule tethered between them, and brought back together to decrease the tension. (B) Force-extension curves of the protein PrP resulting from ramping the force up (black) and down (grey) show a non-linear increase in the force as the handles are stretched out, followed by a rip when the protein unfolds. Hysteresis between the unfolding and refolding curves indicates that the protein is out of equilibrium, owing to a high ramp rate. Taken from Ref. (19). (C) Multiple rips are seen in the unfolding of an oligomer of α -synuclein, indicating the presence of multiple, independently-stable domains that unfold sequentially. Dotted lines show worm-like chain fits to the different states; three intermediates are seen here. Taken from Ref. (75). (D) Repeated unfolding measurements of PrP show variations in the unfolding force, reflecting the stochastic nature of the transition. All FECs are well fit by the WLC model. Taken from Ref. (18). (E) Multiple unfolding and refolding events can be observed when the protein kinetics are fast compared to the ramp rate but slow compared to the sampling rate (black). When the kinetics are fast compared to the sampling rate, individual rips become averaged (grey). [87].

As mentioned before, the change in contour length can be found using non-equilibrium measurement. The procedure to obtain contour length change (ΔL_c) begins by fitting FEC with the WLC model as described above. As discussed, protein is attached to two dsDNA handles with one on each of the ends. When the protein is folded, the handles act as a flexible chain. In order to fit the FECs, the construct should be seen as two independent chains in series: one for the DNA and one for the unfolded protein. Consequently, the first part of FEC needs to be fit using parameters for DNA. However, the second part of FEC, while the protein is unfolded, needs to be fit using parameters related to the protein. For example,

typically, persistence length for a dsDNA molecule should be in the range of 30 to 50 nm. In contrast, this value is between 0.6 to 0.8 nm for protein. Also, crystallographic value for contour length is 0.34 nm per nucleotide for a molecule of dsDNA. Conversely, this value is 0.36 nm per amino acid for a protein molecule. Moreover, the enthalpic elasticity of dsDNA is 1000-1500 pN. The same is about 2000 pN or even higher for protein [87].

The analysis to find ΔL_c in constant force measurement is very similar to non-equilibrium measurement. The difference is that in this type of measurement, we use the same equation as in (1) with known parameters. For constant force measurement, we are interested to use the found parameters from force-ramp data instead of using literature parameters. Similarly, for constant trap position, where the force changes and the molecule folds and unfolds, the procedure of finding ΔL_c is the same as constant force. The difference between forces in the folded and unfolded positions must be considered [87].

2.4.2 Size of the structure

Interestingly, the number of amino acids can be calculated after finding ΔL_c [69]. This value is very precise because of the high resolution measurement of optical tweezers. Note that finding the number of amino acid is possible with the flowing equation [1].

$$N_{aa} = (\Delta L_c + d_T) / L_c^{aa} \quad (2)$$

In this equation, d_T is the end-to-end length of the folded protein structure and L_c is the length of each amino acid [69]. It is important to know the value of d_T in order to find the accurate result for the number of amino acids (aa). When we are looking at a molecule with transitions between two structured states, we need to know changes of d_T between two structures [111]. This can be obtained via a high resolution structure. If this high resolution structure is not available, d_T is not accurate and the number of aa can be found using an approximate calculation. As the last point, if the value obtained by a single molecule measurement does not match with the crystal structure of the protein, it is likely that the protein is not folded properly [87].

2.4.3 Energy landscape profile

Energy landscape theory gives us information about the folding of the protein from high energy unfolded to the low energy folded state through all possible conformations [36]. Naturally, a molecule searches among different possibilities over the energy landscape to find a minimum energy structural state [112]. If we can find a way to measure the energy landscape, the result opens a window to the properties of folding transitions. Actually, measuring the energy landscape is a very difficult task within biophysics and is accomplished through the use of different approaches such as single molecule measurements. Non-equilibrium measurements as well as constant force/constant trap separation measurements provide an opportunity to obtain energy landscape profiles along the reaction coordinate x , which is molecular extension [113]. In the following section, a brief description of these analytical methods is provided.

- Reconstructions from equilibrium measurements

In order to extract the energy landscape, data sets of extension versus time is collected using constant force measurements. After that, we need to calculate the probability of extension, $p(x)$. The inverted Boltzmann relation is applied in order to discern the landscape profile associated with the desired molecule [87]:

$$G(x) = -k_B T \ln[P(x)], \quad (3)$$

where k_B is the Boltzmann constant. When we intend to use constant force measurements, it is essential that the applied force be kept constant throughout the folding process. In order to maintain a constant force, we can use an active force-clamp. One drawback of using an active force clamp is that the time needed to receive feedback about the beads position and to adjust the trap position such that the force on the molecule remains constant, is slower than the timescale of the structural transition [36]. Passive force clamping is a means of avoiding this issue. In a passive force clamp the stiffness of one of the traps is kept constant at zero [101].

It is also possible to reconstruct the landscape using constant-trap measurements in a similar way to that of the constant-force measurement. Under such conditions the force on the molecule varies in order to compensate for changes in the molecular extension which in turn maintains a constant trap separation [36]. The landscape was reconstructed empirically by Rief and colleagues by performing the deconvolution point-wise, using a position-dependent PSF [114] then, the mechanical dynamics model of Thirumalai et al. was also applied [115].

The major limitation of any landscape extraction method arises from instrumental distortions. As mentioned before the construct is made of protein, beads and two dsDNA handles. The dynamics of the intended protein are convolved with the dynamics of the beads due to their rotations and interactions through the linking handles. If $p(x)$ is the intrinsic distribution of the molecular extension, and the instrumental point spread function (PSF), denoted as $S(x)$ is known, the measured distribution of the extension would be given by $P(x) = S(x) * p(x)$ [36]. So, in order to remove the effects of the beads and handles, thereby obtaining the intrinsic distribution of the protein extension, the PSF must be taken into account. We can easily make a construct without any protein and implement the non-linear deconvolution algorithm [116]. Another approach to find PSF is the use of theoretical model powered by Thirumalai. In this model, deconvolutions are shown for protein, DNA, and beads even when there is no chance of measuring instrumental PSF directly from the instrument [115].

- Reconstructions from force-ramp measurements

Sometimes, because of a high energy barrier, and as a result slow folding rate, reconstruction of the energy landscape needs to be done from non-equilibrium measurements. Optical tweezers provide an opportunity to use force-ramp or force jump measurements in order to extract the energy landscape. In this method, free energies from measurements of the non-equilibrium work performed during force-ramp measurements can be recovered using fluctuation theorems, like Jarzynski's equality [105]. The Jarzynski equality, which uses the raw data from constant speed experiments,

has recently been improved by the work of Hummer and Szabo [117]. The equation demonstrates free energy versus reaction coordinate (x) which is extension of the molecule [87]. This method has been used to computational and laboratory experiments but never validated experimentally [118], [119], [120], [121]. DNA hairpins were used to compare the folding landscapes for DNA hairpins reconstructed from this approach experimentally with those reconstructed from equilibrium measurements [122]. After comparing landscape profiles obtained from the non-equilibrium reconstruction and those from equilibrium probability distributions, a good agreement was found [113], [122].

- Model-dependent approximations of the landscape

As mentioned, full landscape can be reconstructed through model-free approaches such as force-ramp measurement and constant force measurement (Dudko and colleagues have shown the equivalence of the results of both experimental conditions [123]). However, the key features of landscapes can be characterized using model-dependent approximations. The Dudko technique is a model-dependent approach that can be used to reconstruct the energy landscape [124]. It has previously been demonstrated that when a load is applied to protein, the free energy barrier, will usually move closer to the folded state of the protein. One advantage of the Dudko technique, is that it accounts for this barrier movement (Bell-Zhurkov model and Evans and Ritchie model [125]). Dudko model derives the unfolding force distribution shape as a function of landscape parameters under the assumption of specific landscape profiles [36].

$$p(F) \propto \frac{k(F)}{r} \exp \left\{ \frac{k_0}{\beta \Delta x^\ddagger r} - \frac{k(F)}{\beta \Delta x^\ddagger r} \left(1 - \frac{\Delta x^\ddagger F}{\Delta G^\ddagger} \nu \right)^{1 + \frac{1}{\nu}} \right\}, \quad (4)$$

where

$$k(F) = k_0 \left(1 - \frac{\Delta x^\ddagger F}{\Delta G^\ddagger} \nu \right)^{\frac{1}{\nu} - 1} \exp \left\{ \beta \Delta G^\ddagger \left[1 - \left(1 - \frac{\Delta x^\ddagger F}{\Delta G^\ddagger} \nu \right)^{\frac{1}{\nu}} \right] \right\}$$

in which Δx^\ddagger is the distance to the transition state and ΔG^\ddagger refers to barrier height. In equations ν is a parameter showing the shape of the landscape. For example for a

linear-cubic potential barrier shape ν is $2/3$ and for cusp shape ν would be $1/2$. Similar expression for refolding forces is also given by landscape theory. The expression for the rates in (4) can be used to fit the force-dependent kinetics to obtain landscape parameters [124].

3 SMFS measurements of MoPrP folding

3.1 Motivation

Bovine (cow) prion disease BSE can be transmitted from cows to humans in the form of vCJD disease [126]. The prion protein is a high disease susceptible protein. For this reason, prion protein is an interesting subject for scientists [127]. As mentioned in the previous chapters, prion's infectious form, PrP^{Sc} , can act as a template for normal prion protein cells. Consequently, studies of prion protein, its structure and function, may be a key points in decreasing the likelihood of development and transmission of prion diseases. The method used in our lab for studying prion protein at the single molecule level, is optical tweezers. By using this instrument, we have a chance of revealing the different folding pathways of prion protein as well as determining certain pathways which lead to misfolding and aggregation [26], [19]. The use of single molecule methods has certain advantages, as explained in chapter 1. But, the most important reason is that, by using of the single molecule approach, we can look at single molecules one by one at a time, as apposed to the average effects viewed through ensemble measurements. Also, many pathways, that are rare and non-detectable via other methods, can be observed using the single molecule method [49].

Many papers regarding the folding pathways of the ShPrP molecule have previously been published. The reason of studying MoPrP in our lab is to look at subtle differences in the folding dynamics of mouse and hamster PrP to understand the origins of the different disease behaviors in different species. Knowing about folding and misfolding pathways of both species can also help us to understand more about cross-species transmission diseases due to the transmission barrier as well as the fact that different species have different susceptibility to disease [128].

Mouse prion protein, exactly like ShPrP structurally, contains three α helices and two β strands sheets in the native structure [129]. In other words, it is rich in alpha helices when the protein is in the native form. **ShPrP(89-231)** and **mouse PrP(89-231)** are different in eight amino acids [129]. Basically, MoPrP starts from some non-structured residues. Then, β strand 1 starts and turn 1 comes after that. Helix 1 after turn 1 is followed by turn 2, strand 2 and turn 3. Then, turn 4 connects helix 2 and 3 [129].

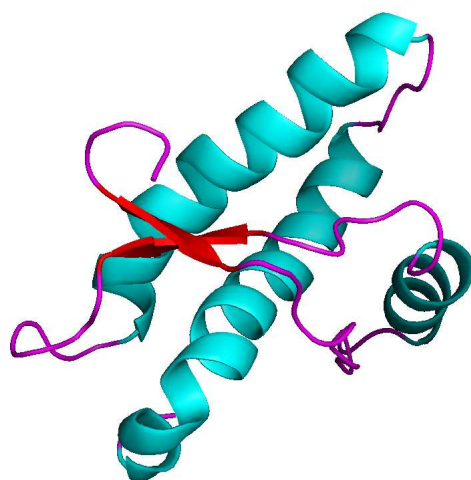


Figure 8: NMR structure of mouse prion protein (121-231). Figure adapted from [130]

3.2 Sample preparation

3.2.1 Protein preparation

The mouse sample that we were looking at was the truncated form of mouse prion protein (amino acids 89 to 231). We looked at the truncated PrP which is a shorter version of PrP. Because the N-terminal domain of the full version is flexible and unstructured, we cannot see any trajectory describing folding and unfolding of this region by optical tweezers [131]. First of all, the protein expression starts by protein engineering with cysteine residues at each terminus and cloning into pJ406-2cys-MoPrP expression plasmid with N-terminal poly-histidine tag. The first 20 residues (specifically MGSSHHHHHHSSGENLYFQG = 20 residues) contain poly-histidine tag (His-tag) of protein. The purpose of adding the His-tag is to facilitate the purification process and amplify the yield of the highly purified protein.

In the next stage of the process, the isolated colony from the plate is grown within a liquid LB medium (containing $100 \mu\text{g}/\text{mL}$ ampicillin), incubated at 37 degrees and shook at 225 rpm overnight. Growing colonies is accompanied with monitoring the optical density at 600 nm overtime. When the $OD_{600\text{nm}}$ reaches 0.6-0.7, PrP induction is induced by adding isopropyl- β , D-thiogalactopyranoside (IPTG) to achieve the final concentration.

After induction, the culture is allowed to incubate for 4 hours. The E. coli cells are then

harvested by centrifugation in 500 ml bottles at 5500 x g, 20 min at 4 degrees in a Beckman Allegra 25R refrigerated bench-top centrifuge. The last step of expression is to wash the resulting bacterial pellet with 1X PBS in order to aliquot into appropriately labeled 50 ml tubes. So, each tube contains equivalent of 500 ml of culture. The same centrifugation as above is repeated. Then, the 1 PBS from the pellet is decanted and the bacteria is frozen at -80 to await purification.

MGSSHHHHHSSGENLYFQG C (89) GQGGGTHNQW NKPSKPKTNL KHVAGAAAAG AV
 VGGLGGYM LGSAMSRPMI HFGNDWEDRY YRENMYRYPN QVYYRPVDQ YSNQNNFVHD
 CVNITIKQHT VTTTTKGENF TETDVKMMER VVEQMCVTQY QKESQAYYDG RRS C (231)

Figure 9: 2Cys-MoPrP sequence with His-tag, the external and internal cysteines are specified with red color. Blue residues are different in ShPrP [131].

Protein purification is the next process required in preparing an appropriate MoPrP sample. As the first step, one or more bacterial pellets are thawed from -80 storage, after which each pellet is re-suspended in lysis buffer (50 mM sodium phosphate buffer, pH 7.4, 500 mM NaCl, 6M guanidinium HCl, 20 mM imidazole, 0.5 mM phenylmethylsulfonyl fluoride). Then, the sample is sonicated on ice using a Branson sonicator set to 6 20 seconds, 50% power output, allowing the sample to sit on ice 30 sec to 1 min between each 20 second interval. After making sure the lysate is no longer viscous, dithiothreitol (DTT) and Tween-20 are added to reach a final concentration of 0.5% v/v.

Next, to clarify the sonicated preparation, the sample is centrifuged in the Beckman Allegra 25 R in the JA-14 rotor at 30000 x g, 90 min, at 4 degrees . The supernatant is retained and filtered with 0.45 um syringe filter in preparation for column chromatography. Then, a 5 ml Ni-immobilized metal affinity chromatography (IMAC) column is equilibrated by attaching it to the AKTA Purifier and flowing 5 column volumes (5 cv; 25 ml) of equilibration buffer (50 mM sodium phosphate buffer, pH 7.4, 500 mM NaCl, 6 M GuHCl, 20 mM imidazole) through the resin. After that, the protein sample is applied using the sample pump at a flow rate of 1 ml/min while the unbound protein is washed thoroughly from the col-

umn using the equilibration buffer until the absorbance (at 280 nm) reaches baseline again. Eluting the bound protein (the His6-tagged PrP) from the resin by using sufficient volume of elution buffer (50 mM sodium phosphate buffer, pH 7.4, 500 mM NaCl, 6 M GuHCl, 500 mM imidazole) is the next step in the process.

To determine the purity, Molecular Weight (MWT) and amount of purified protein 15% sodium dodecyl sulfate polyacrylamide gel electrophoresis (SDS-PAGE) gel is needed (Figure 10). The expected MWT is 19 kDa. SDS-PAGE gel results are used to pool good fractions in order to do the refolding step.

Sufficient fresh Refolding buffer (1.1 M GuHCl, 55mM Tris-HCl, pH 8.2, 21 mM NaCl, 0.8 mM KCl, 1 mM reduced glutathione, 1 mM oxidized glutathione, 1 mM EDTA) is prepared to dilute the pooled sample volume 1:10. The pooled protein is added to the refolding buffer drop-wise while being stirred. The sample container is then covered with aluminum foil and left to incubate at 4 degrees, overnight, while being constantly stirred. The next day, the sample is centrifuged at 30000 x g, for 1 h, at 4 degrees in order to remove any precipitate. Then, the supernatant is removed and used to load into 6-8000 kDa cutoff dialysis tubing. Dialyzing should be done in 4 L of dialysis buffer (ammonium acetate pH 4.5) for 3 h at 4 while stirring. The dialysis buffer is then changed to a fresh 4 L buffer and dialyzing is continued overnight. Next, the dialyzed sample is centrifuged from the bag and the supernatant is retained.

It is recommended to analyze the sample (CD at this point, and 15% SDS-PAGE) before freeze drying. Once the CD (Figure 11) and SDS-PAGE analysis confirm we have what we want, the concentration is measured and the protein is aliquoted into individual 50 ml tubes so that each contains 2-3 mg of protein. Liquid N_2 is used to freeze the samples in the tubes. The samples should be stored at -80 until required. All the steps of expression and purification of the proteins have been done by Craig Garen in our lab.

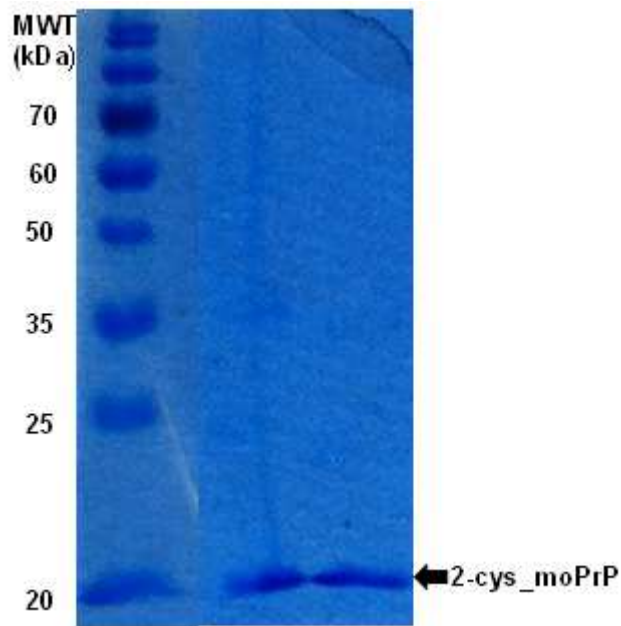


Figure 10: 15% SDS-PAGE gel analysis of 2-cys-MoPrP. Picture credit: Craig Garen

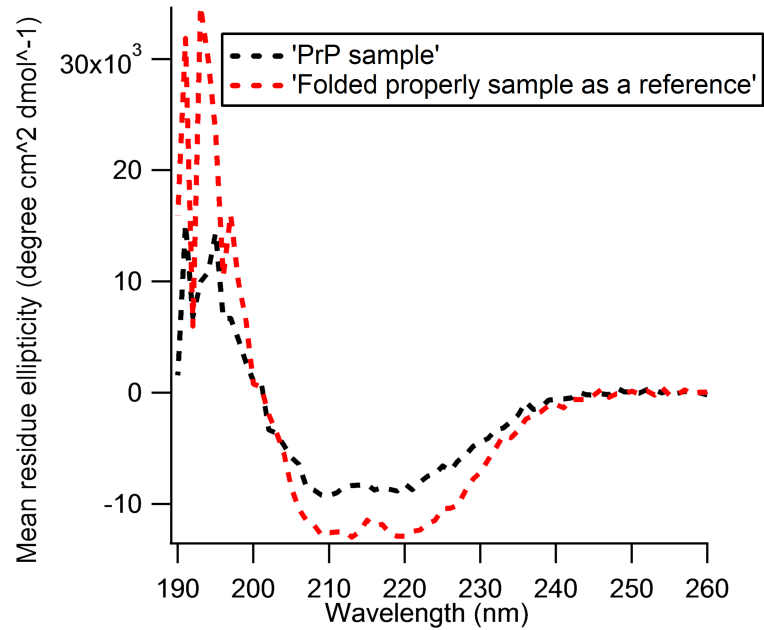


Figure 11: circular dichroism analysis of 2-cys-moPrP. presence of two minimums in the signal can confirm the α helices rich structure for native form of PrP

3.2.2 Handle attachment using disulfide bonds (S-S bond)

A common approach for attaching DNA handles to proteins is through a disulfide bridge to any cysteine residues exposed on the surface of the protein. In order to study misfolding pathways of single molecules of mouse PrP (monomers), the third geometry explained in chapter 2.2 was used. To achieve this geometry, we need to attach two double stranded DNA handles, one on each end of the mouse prion protein (residues 90 to 231). Then, polystyrene beads are required to be attached to both ends of the construct in order to hold the sample in the optical tweezers, by which force is applied.

To attach the handles to the ends of the proteins, we must first reduce the cysteines in both the handles and proteins. The reduction of correctly folded proteins (typically 15-20 μM) was done with TCEP in a 1:10 molar ratio for 30 min at room temperature in sodium acetate pH 4.5 buffer. After the reduction, the extra TCEP was removed using 10K spin filtration. Then, the proteins were immediately activated using 2,2'-dithiodipyridine (DTDP) in a 1:70 molar ratio overnight, in a 4 degree fridge. In the same manner, handles prepared by PCR were reduced with TCEP in a 1:500 molar ratio for 30 min at room temperature in pH 4.5 buffer. One handle was 798-bp in length containing a thiol group on one end and a biotin on the other. The other handle was longer with a length of 1261-bp, containing a thiol group and digoxigenin instead. For an easy gel identification, two different lengths of the handles are needed. The concentration of handles are typically around 20 μM . After protein incubations, both activated proteins and reduced handles were immediately reacted with each other. Next, the extra DTDP and TCEP were removed from the construct using zeba spin desalting columns for at least 3 times spins.

In order to form dumbbells, protein-DNA constructs were incubated at approximately 100 pM with 30 pM polystyrene beads (600 nm diameter labeled with avidin, 800 nm diameter labeled with anti-digoxigenin). Then, 50 mM MOPS buffer, pH 7.0, with 200 mM KCL and an oxygen scavenging system (8 mU μL glucose oxidase, 20 mU μL catalase, 0.01 percent $\frac{wt}{vol}$ D-glucose) were used to dilute dumbbells to approximately 500 femto M [132]. In the end, the sample was inserted into a flow cell for the optical traps. The optical tweezers were then used to apply tension in order to denature a single molecule MoPrP. As a result,

the structural changes of a single molecule were monitored via the end-to-end extension of the molecule.

The internal Cys were assumed to be labeled using a disulfide bridge, so we needed to change protocols of the handle attachment to the protein. Also, the S-S bond yields lots of tethers that have bonds between handles without protein included. In addition, this chemistry does not allow us to change the oxidation state of the buffer. The new method of handle attachment in our lab is known as click chemistry and is introduced by Derek Dee, our former post doctoral fellow. I also did some experiments to compare the traditional protocol and the new protocol as well as optimizing the new method.

3.2.3 Introduction to click chemistry

One of the most popular categories of probe-molecule reaction is cycloadditions. Cycloadditions is divided into two categories: dipolar cycloadditions and diels-Alder cycloadditions [133]. The most popular bioorthogonal cycloaddition is azides [134]. Azides are 1,3 dipoles which are able to react with alkynes [135], [136], [137]. Specifically, azide-alkyne cycloaddition is called click-chemistry. Click-chemistry can be done in aqueous environment and makes a robust attachment [138], [139]. One of the most important advantages of this reaction is the speed of the reaction which is appropriate for biological system [140], [141], [142]. With the fast ligation chemistry, the assembly of complex biomolecules with low concentration is possible [133], [143]. As a result, an intracellular assembly of molecular structure which can not cross cell membranes due to the large molecular structure can be done very fast with this method [143]. The other category of cycloadditions (similar to click chemistry) is diels-alder cycloadditions [143]. There are three different chemistries used in order to complete the handle attachment via click chemistry. The first chemistry is N-Hydroxysuccinimide+amine (NHS+amine) in order to make DNA handles with Trans-cyclooctene (TCO) primers. The second chemistry is maleimides+HS in order to make protein labeling with tetrazine (Tz). And the last chemistry is TCO+TZ in order to complete the handle attachment. The mechanism of each chemistry is now explained and its application to the handle attachment process is clarified.

1. NHS and Amine reaction:

A wide range of amine-reactive cross-linking reagents use NHS ester to make amide bonds. After the reaction between the NHS and amine compound, an acylated product and NHS leaving group are produced (Figure 12). The reaction with primary and secondary amines creates a stable bond. In protein molecules, NHS can react with α – amines which is located at N-terminals and ϵ – amines of lysine side chains [97]. In the click protocol, in our lab, we need to label DNA handles. But, DNA does not have any primary amines in it, so an amine added chemically at the end of the DNA when the primer for the handle is synthesized.

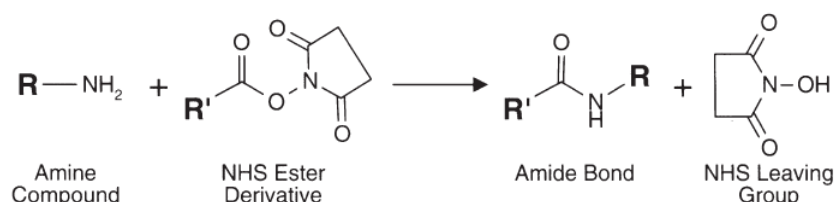


Figure 12: Reaction of Amine compound with NHS Ester derivative. Figure adapted from [97]

2. Maleimides and HS reaction:

Maleimides (Mal) with double bonds can react with sulfhydryl groups (SH group) to form stable thioether bonds. Maleimides reactions can be done in pH range of 6.5 to 7.5 [144], [145]. In this reaction, one of the carbons adjacent to the maleimides' double bond is responsible for the reaction and generates the additional product (Figure 13). The SH group in Cys residues of the protein is used in this chemistry.

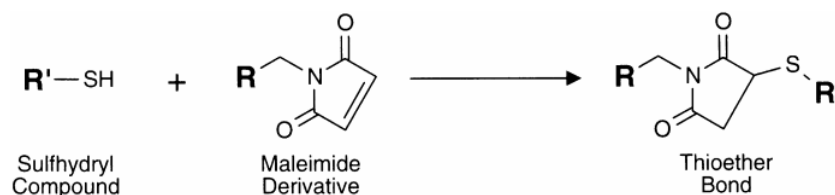


Figure 13: Reaction of sulfhydryl compound with maleimides derivative. Figure adapted from [97]

3. Introduction to TCO-Tz reaction: Diels–Alder reactions can be reversible under

certain conditions ². Trans-cyclooctene (TCO) is an example of a strained molecule that uses an inverse diels-alder chemistry to react with high affinity binding with tetrazines [143]. The reaction can be done in the aqueous environment in the presence of proteins [143]. TCO-tetrazine reaction is the fastest bioorthogonal transformations without need for catalysis, with the reaction rate between 10^3 and $10^6 M^{-1} S^{-1}$ [146], [147]. Their rapid reactivity with only small amounts of reagent is a notable feature of TCO-tetrazine which can even be used in vivo environment [148], [149], [150]. The key point in tagging biomolecules is that one of the chemicals we want to use in the reaction should be attached to the target molecule [133].

After understanding each chemistry in details, their applications in the handle attachment process are introduced. The main reaction used to attach handles to proteins is Tz and TCO. Therefore, one reagent (handle or protein) needs to be labeled with Tz and the other one needs to be labeled with TCO. In order to do DNA labeling with TCO, we need to label the DNA primers with TCO. Primer labeling uses NHS-Amine reaction. Specifically, the primers have the amine group; also TCO are linked to NHS group via *PEG*₃ (ester-activated PEG compound used for cross-linking, also known as spacer, between primary amines (—NH₂) in proteins and other molecules). Hence, by reacting primers with the amine group and TCO with the NHS group, the labeled primers with TCO will be produced (Figure 14- a). Then, the primers are used to make dsDNA handles which have the TCO tags on one end (Fig 14- b).

²The reverse reaction is known as the retro-Diels–Alder reaction

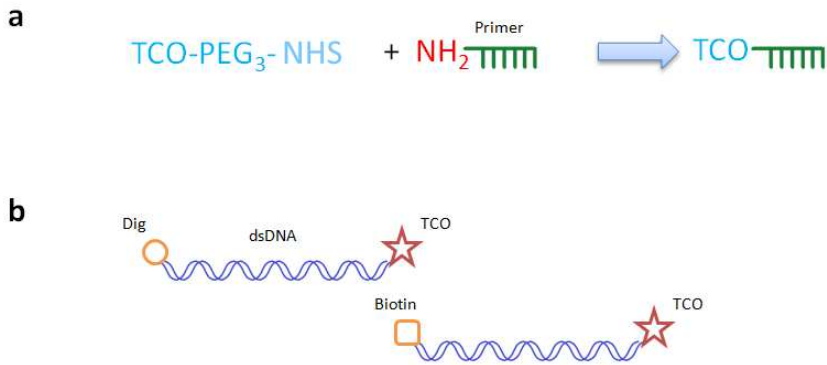


Figure 14: Handle labeling with TCO. (a) Reaction of DNA primer with maleimides linked with NHS. (b) DNA labeled with TCO.

We now must label the protein before we can complete the handle attachment. Firstly, the protein needs to be reduced using a reduction agent such as TCEP. After reducing cysteines, SH bonds in both terminus of the protein are available to be tagged by Tz. Hence, the maleimides compound linked to Tz with a spacer (PEG_5) is used to label protein with Tz (Figure 15).

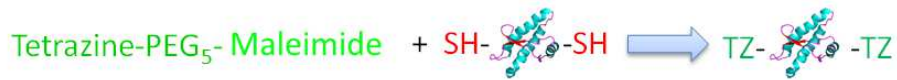


Figure 15: Protein labeling with Tz

After doing both DNA handles and protein labeling, we need to mix both reagents to produce the protein handle attachment (Fig 16). The procedure to do the reaction with required experimental conditions is explained in the next section.

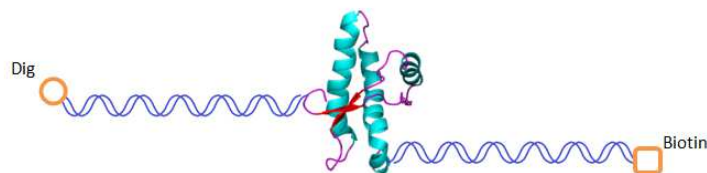


Figure 16: Protein handle attachment with click chemistry

3.2.4 Handle attachment using click chemistry

Tagging a wide variety of biomolecules in cells and other complex environments can be facilitated using bioorthogonal chemistries [133]. To understand the cellular process of small biological molecule, we need a method to probe these small molecules in real time. By probing small biological molecules, we are able to visualize them. The chemistry we want to choose, should be selective and non-perturbing to biological systems [133]. Thus, these kinds of chemistries are called bioorthogonal [151]. The bioorthogonal probes must be stable in aqueous environments [151]. In addition, the reaction between probes and biological molecules should be non-toxic [151]. To start the reaction, it is ideal to begin with a high concentration of PrP (around $100\ \mu\text{M}$) in pH 4.5 buffer (e.g. sodium acetate buffer). Next, the protein is diluted to $10 - 15\ \mu\text{M}$ in pH 7 buffer (e.g. 50 mM Na Phosphate buffer +10 mM EDTA, pH 6.85) with approximately 500 ml to 600 ml volume of the solution. The reason of having protein in high pH buffer is that the protein labeling with Tz should be done in pH 7 buffer.

Similar to thiol chemistry, to do handle attachment using click chemistry, we first tried to reduce Cys residues in both ends of proteins using TCEP. In order to do that, 10-15 μM 2Cys-protein is reduced with 200-300 μM TCEP. Then, the mixture is incubated for 30 min at room temperature.

After that, 40 μM stock solution of lyophilized Mal-peg4-Tz was prepared. The next step would be mixing protein/TCEP solution and Mal-peg4-Tz with a final concentration of $600\ \mu\text{M}$. After an hour incubation, the mixture was diluted to 1 ml with a strong pH 4.5 buffer (e.g. 500 mM NaOAc pH4.5) to avoid protein precipitation.

Then, the excess Mal-peg4-Tz in the mixture was removed using 10 KDa spin filter. In addition, the protein was concentrated using the spin filter. The catalog of spin filters specifies the needed time and speed to achieve appropriate result of removing extra chemical. After that, the concentration of the sample should be checked using a Nano-Drop (for MoPrP absorbance wavelength is 280 nm and $E_{280}^{0.1\%}$ is 1.55).

As the last step, Tz-Protein with TCO-Handles were mixed at approximately 1:1:1 ratio of Handle A:Handle B:Protein. Then, the mixture was incubated at 4 degrees overnight. Click chemistry is a very fast reaction that helps us to gain a huge amount of Handle-PrP-handle product with a low concentration of initial materials. I performed experiments comparing both chemistries, the results, presented in Figure 17 highlight the difference between the final products associated with each method (thiol and click chemistry) after starting with the same initial concentrations of materials.

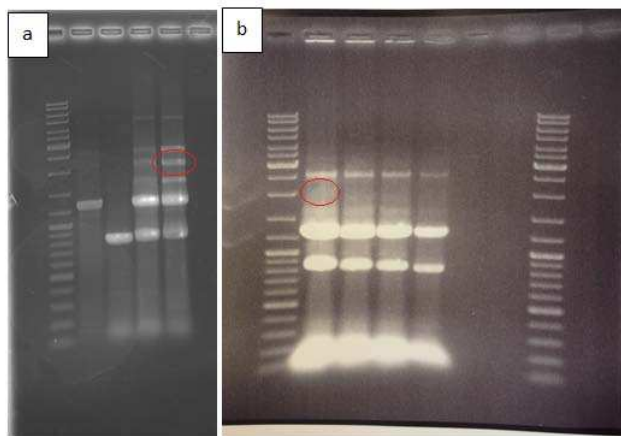


Figure 17: Comparison between thiol handle attachment and click handle attachment. (a) Gel electrophoresis of handle attachment using click chemistry. (b) Gel electrophoresis of handle attachment using thiol chemistry. The desired product is indicated with red circle in both gels. The band is much brighter in the click chemistry lane indicates much higher yield

3.3 Results

3.3.1 FEC measurement

FEC measurements start with moving the traps apart at a constant speed. In unfolding curves by increasing the force, the extension of the molecule increases non-linearly. The FECs show nice unfolding curves on the surface for single PrP molecules. All FECs fit very

well to WLC, and the persistence length (approximately 30 nm) was consistent showing a single molecule between the traps. But, by analyzing the FECs very closely, it was found that the length changes were too short. The contour length changes observed in the FECs are shorter than that expected from the NMR structure for a single PrP molecule [130](Figure 18). In Figure 18, four individual FECs are shown. The contour length changes for these four curves are in the range of 20 to 24 nm which are shorter than those of native form from NMR structure. The structure of MoPrP from literature can be used to calculate the contour length changes and the number of amino acids which are 34.12 nm and 104 respectively related to the native structure [130].

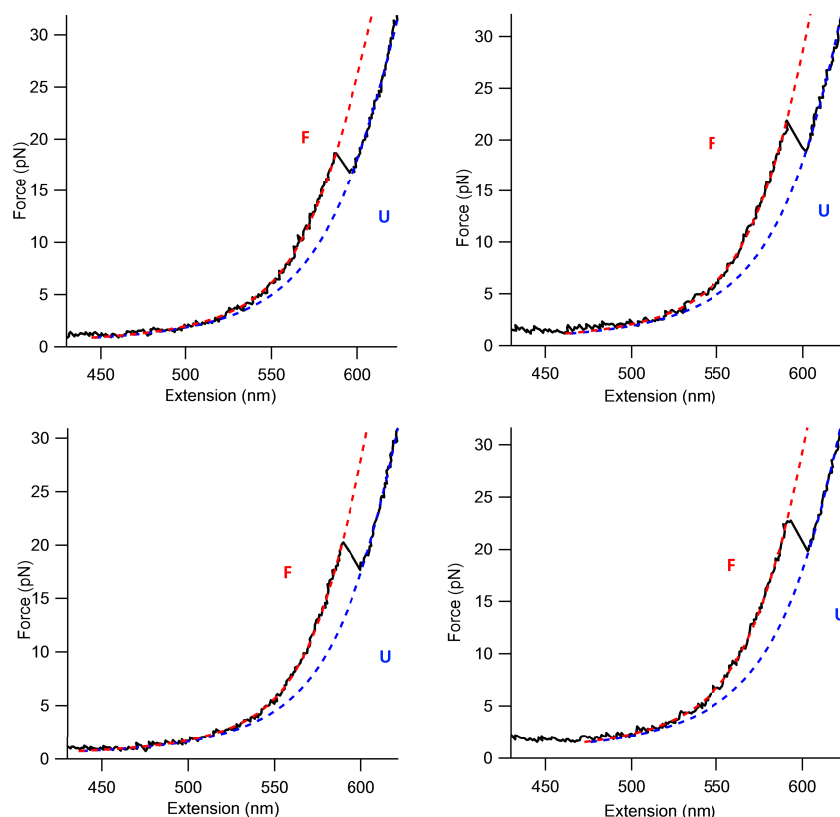


Figure 18: Force spectroscopy measurements of MoPrP. The handles stretch as the force rises monotonically until PrP unfolds, causing a discrete jump in the extension and force (black). The contour length change is found from worm-like chain fits to the folded (red) and unfolded (blue) states to be the value shorter than expected for unfolding of the native state (This figure shows four individual FEC).

To gain a better statistic, successive measurements have been done on each molecule

(Figure 19). Moreover, the value of the contour length change matches the distance between one end of the molecule and the middle Cys. It means that in both cases—the sample prepared with thiol chemistry or click chemistry—the results showed that the handles were connected to an internal cysteine from one end instead of the terminus. The handles should be attached to the external cysteines to obtain the contour length change equal to that of the native form from NMR. We suspected that the handles were attaching to the internal Cys residues because we got the wrong lengths when unfolding the protein. The short contour length changes was a little surprising since it did not happen with the hamster PrP (we got the right length in the previous experiment [69]). To confirm this result, an experiment was performed with fluorescent dye.

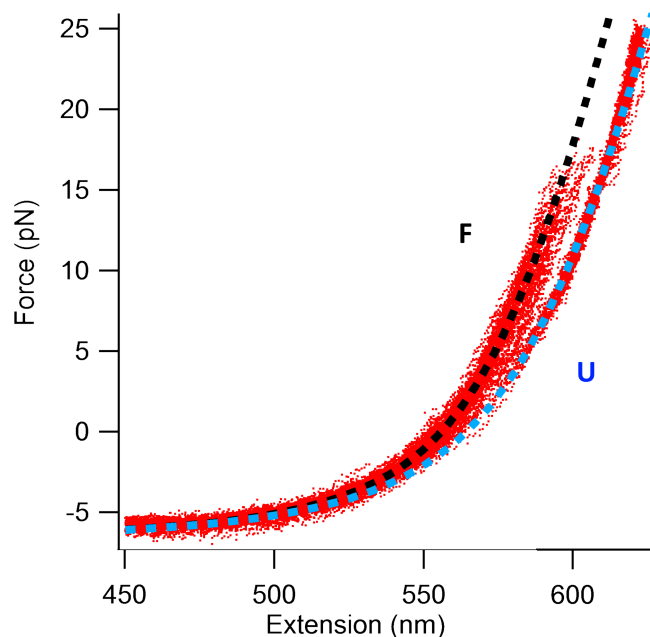


Figure 19: Overlaying 60 unfolding FECs of MoPrP (red). The contour length change is found from worm-like chain fits to the folded (black) and unfolded (cyan) states to be the value shorter than expected for unfolding of the native state.

3.3.2 Fluorescent experiment to check internal Cys labeling for PrP

In order to do this experiment, 2Cys-MoPrP and wild type MoPrP (WT-MoPrP) are required. If we are labeling internal Cys as we expect we may be doing, then after subjecting both protein versions to the labeling protocol we will see fluorescence from both versions. But,

if we are not labeling the internal Cys, then there will be no fluorescence from the WT-PrP.

The process was done exactly the same as the handle attachment process. Firstly, the proteins were reduced with 200 μM TCEP in pH 6.8 buffer and incubated at room temperature for 30 min. Then, reduced proteins were reacted with 400 μM mal-PEG4-Tz for 2 hr at RT. After that, excess Tz removing as well as buffer exchanging to pH 4.5 were done using 10 K spin filter. Then, the proteins labeled with Tz were reacted with Cy5-TCO (florescent dye) instead of handles. The mixture was incubated for 1 hr at RT before running the SDS-PAGE gel. Then, SDS-PAGE gel was run in order to see the proteins with the florescent reader. When the gel running was done, the gel was rinsed in H_2O to remove all free dyes from the gel.

Theoretically, the WT-MoPrP, which does not have any external Cys, should be invisible under florescent reader if the internal Cys remain unlabeled. The result showed labeling for both wild-PrP type and 2cys-MoPrP which means that we are labeling internal Cys rather than only external Cys (Figure 20- a). After fluorescent imaging, the gel was stained with coomassie Blue for 2 hrs, then rinsed in H_2O overnight (Figure 20- a). This experiment was done by Derek Dee.

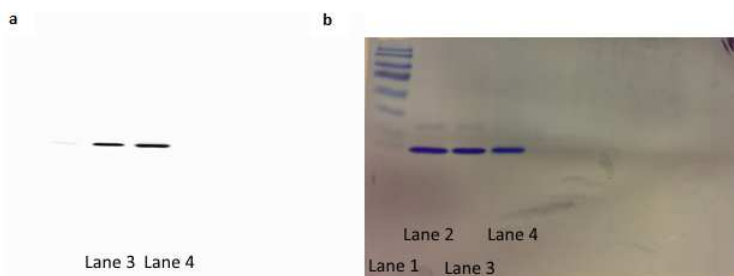


Figure 20: SDS-PAGE gel of 2-CysMoPrP and WT-MoPrP labeled with Tz (protein was reduced with TCEP). (a) Florescent imaging of 2-CysMoPrP and WT-MoPrP labeled with Tz. Lane 1: Protein ladder, Lane 2: WT-MoPrP + Cy5-TCO [not reduced with TCEP], Lane 3: wt-moPrP + TCEP + mal-Tz + Cy5-TCO, Lane 4: 2cys-moPrP + TCEP + mal-Tz + Cy5-TCO. (b) Stained protein gels with coomassie blue.

There are different solutions to solve this problem. The first solution is using a lesser amount of TCEP in order to break the external disulfide bonds of PrP. The second solution

is to use a weaker reducing agent such as MEA. Different concentrations of MEA were tried in an effort to reduce WT-PrP and 2Cys-PrP (Figure 21). The result shows that with 50 μ M MEA, internal cysteines are not reduced. It means that—with the same concentration of MEA— WT-PrP was not labeled with Tz; however, 2cys-PrP was labeled on both terminals. It was revealed, that the apparent short contour length change, was consistent with the internal cysteine labeling, a problem which could be solved by using the MEA reducing agent.

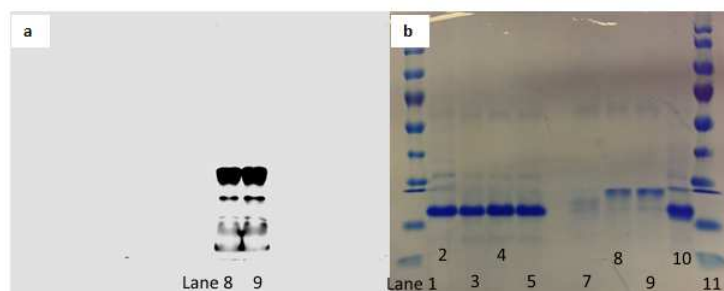


Figure 21: SDS-PAGE gel of 2-CysMoPrP and WT-MoPrP labeled with Tz (protein was reduced with MEA). (a) Florescent imaging of 2-CysMoPrP and WT-MoPrP labeled with Tz. Lane 8: 2cys-moPrP + mal-Tz + Cy5-TCO (10 mM MEA), Lane 9: 2cys-moPrP + mal-Tz + Cy5-TCO (50 mM MEA). (b) Stained protein gels with coomassie blue. Lane 1: DNA ladder, Lane 2: wt-moPrP + Cy5-TCO, Lane 3: wt-moPrP + mal-Tz + Cy5-TCO (5 mM MEA), Lane 4: wt-moPrP + mal-Tz + Cy5-TCO (10 mM MEA), Lane 5: wt-moPrP + mal-Tz + Cy5-TCO (50 mM MEA), Lane 6: empty, lane 7: 2cys-moPrP + mal-Tz + Cy5-TCO (5 mM MEA), Lane 8: 2cys-moPrP + mal-Tz + Cy5-TCO (10 mM MEA), Lane 9: 2cys-moPrP + mal-Tz + Cy5-TCO (50 mM MEA), Lane 10: wt-moPrP + Cy5-TCO, Lane 11: DNA ladder

After improving the method, MoPrP measurements were redone by another graduate student in our group.

4 Pharmacological chaperone reshapes the energy landscape for folding and aggregation of the prion protein

4.1 Introduction

I now turn to the second part of my thesis which is using SMFS to study how anti-prion agents affect the folding of the protein. The conversion from the normal form a protein into a misfolded form is thought to cause many neurodegenerative diseases [1], [7]. Examples of neurodegenerative diseases include Alzheimer's disease, Parkinson's disease, ALS and prion diseases which all have the ability to accumulate misfolded protein, inside and outside of the cell [1], [7], [8]. The normal form of prion protein (cellular form or PrP^C) is a transmissible protein with the structure of three α - helices and two β -strands combined with a large unstructured region. However the misfolded form of this protein has a structure that is rich in beta strands. For example, Creutzfeldt-Jacob disease, scrapie, and bovine spongiform encephalopathy are some prion protein diseases associated with the misfolded prion protein. Although there is no clear description of the normal cellular function of prions, recent studies have shown that anti-prion compounds, may be an effective therapeutic method [8]. Examples of compounds with anti-prion activity include congo red [152] [153], certain polyanions (PPS for instance) [154] [155], 2-aminothiazoles [156] and various heterocyclic compounds [157], [158], [159], [160], [161]. The congo red and ionic tetrapyrrole can stack in the solution and act as polyanion which has a low dissociation constant to the N terminus. So, congo red and ionic tetrapyrrole have been shown to exhibit a propensity to behave as anti-prion compounds. [162], [163]. There are many compounds showed the ability of having anti-prion effects such as GJP49 and GJP14, GN8, quinacrine, PPS and etc. [73]. In our lab, we studied the effects of Fe(III)-TMPyP—which can also behave as an anti-prion compound—on ShPrP. This means that the compound can inhibit the formation of PrP^{Sc} inside the cell culture in vitro [164], [8]. The positive effects of this compound can also be seen in the increasing survival times in animal models [165], [166]. Moreover, this compound can bind to the structural region of prion protein and likely behave such a pharmacological chaperone [8].

As a result, to improve our knowledge of the mechanism of such compounds, we used

the optical tweezers to investigate the behavior of Syrian hamster Prion protein (ShPrP) in the presence and absence of Fe(III)-TMPyP. Previously, ShPrP has been measured in the absence of tetrapyrrole by optical tweezers [167]. Consequently, the energy landscape profile as well as the landscape parameters and properties, have been characterized. Our lab was the first to observe and present single molecule studies on ShPrP combined with Fe(III)-TMPyP. In addition, Fe(III)-TMPyP can bind to PrP with 1:1 stoichiometry. The dissociation constant for Fe(III)-TMPyP has been measured to be 11 μM . The compound binds to the structural region of prion protein. More specifically, it interacts with strand 1, helices 2 and 3 and the loop between strand 1 and helix 2 (Figure 22-a). The structure of the bound complex was modeled from NMR data.

4.2 Results

4.2.1 Force-extension curves of monomers PrP

PrP^C is a cellular form of the PrP which resists against proteases enzymes. Single molecule force spectroscopy of ShPrP(90-231) helps us to understand more about the effect of Fe(III)-TMPyP on ShPrP and its energy landscape. Purified Syrian hamster prion protein (ShPrP) has 2 terminal Cys residues. The method to prepare the sample is the same as our previous protocol [69]. In order to identify the purity of sanitized PrP, SDS PAGE and Western blotting (Anti-prion(109-112) clone 3F4, Millipore) were performed. Circular dichroism (CD) spectroscopy results confirmed the native folding of ShPrP. After that, prion protein was dialyzed in to 50 mM sodium phosphate buffer, pH 7.0 followed by refolding step (similar to our previous protocol) [96]. In order to attach the handles, prion was reduced with TCEP in a 100:1 molar ratio and 30 min incubation time. After that, excess TCEP should be removed using desalting spin column (Zeba, Thermo Scientific). To attach handles, the protein should be activated. Hence, PrP was incubated with 2,2 -dithiodipyridine (Sigma-Aldrich).

Handles that we used for protein attachment are produced using a PCR machine. One with the 798 base pairs, which is labeled with biotin, and the other with 1261 base pairs length labeled with anti-digoxigenin. Then, to create dumbbells, the 100 pM PrP-DNA reaction was incubated with 250 pM polystyrene beads (600-nm diameter labeled with avidin,

800-nm diameter labeled with anti-digoxigenin). In the last step, in order to insert the construct into a sample cell for the optical tweezers, dumbbells were diluted to 500 fM in 50 mM MOPS, pH 7.0, with 200 mM KCl and oxygen scavenging system (8 mU μ L glucose oxidase, 20 mU μ L catalase, 0.01 % w/v D-glucose).

Our previous force-ramp measurement show that there is only one type of population in the absence of tetrapyrrole. Extension increases as force goes up non-linearly. A sudden decrease of force and an unexpected increase of extension result in a rip in the force-extension curve (FECs) (Figure 22-c). The unfolding force is the minimum force that lets protein unfolds. Moreover, in FECs, we could only see two states (unfolding and refolding) without any intermediate states. We used worm like chain (WLC) model to fit FECs of both states. The contour length change (ΔL_c)—which is the change of the protein length after applying force to completely unfold it—was 34.3 nm which is consistent with the value from the NMR structure of ShPrP [111]. Finally, we generated an unfolding force distribution that shows only one peak. The distribution was well fit by Dudko's formula for a single barrier (equation (4)) This single peak demonstrates having one population of natively folded PrP (Figure 22-c inset).

We also measured ShPrP in the presence of 50 μ M Fe-TMPyP. As a result, different behaviors of FECs were observed (Figure 1D). Some FECs show exactly the same behavior as that of FECs without tetrapyrrole (Figure 1D, black) with a very similar unfolding force value. FECs of both unfolding and refolding states can be fit to the worm like chain model (WLC) using equation (1). To fit FECs, we need to fit the folded state (which is basically DNA) and the unfolded state (which is DNA and protein). So, for the DNA description, WLC parameters $L_p = 40$ nm, $L_c = 700$ nm and $K = 1200$ pN were found from fitting the folded state using WLC model. However, for the protein description, WLC parameters $L_p = 0.65$ nm, $L_c = 0.36$ nm and $K = 2000$ pN found from fitting the unfolded state using WLC model.

After fitting the data to the WLC model, the following parameters were obtained: $\Delta L_c = 34.8 \pm 0.5$ nm and $F_u = 10.2 \pm 0.2$ pN (Figure 22-d, gray dashed lines). Results of contour length change and unfolding force show that the protein is natively folded but the results do not show any sign of ligand binding.

The second population (Figure 22-d, red) has the same contour length change seen without tetrapyrrole, but a higher unfolding force: $\Delta L_c = 34.4 \pm 0.4$ nm and $F_u = 15.6 \pm 0.5$ pN. The extracted value for (ΔL_c) after fitting to the WLC model showed natively folded ShPrP. However, higher unfolding force indicated that the protein had been stabilized upon binding the ligand.

Finally, for 25 % of FECs, we could observe shoulder feature instead of obvious rip (Figure 22-d, blue). This behavior and the lack of an obvious unfolding rip indicated that the ligand bound to the unfolded protein and it prevented the protein refolding to the native structure as force decreased.

So, we need a model to fit some FECs with shoulder rather than discrete transition. The shoulder-feature appears because of the rapid semi-equilibrium fluctuation.

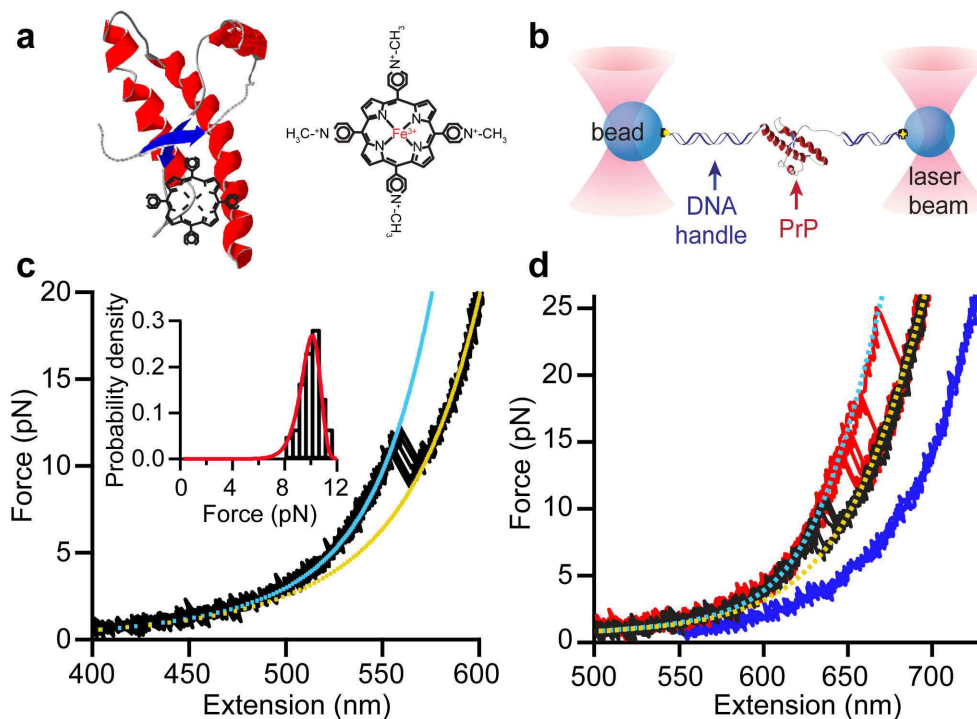


Figure 22: Force spectroscopy of PrP with Fe-TMPyP. (a) Structure of Fe-TMPyP (right). Fe-TMPyP binds PrPC in a pocket as shown on left, interacting with the C terminus of helix 3, N terminus of helix 2, the helix 2-strand 2 loop and strand 1 (model based on ref. 46). (b) Schematic of force spectroscopy assay. PrP was attached covalently to DNA handles linked to polystyrene beads held by laser beams. (c) FECs in the absence of Fe-TMPyP (black), fit by WLC models for the folded (cyan) and unfolded (yellow) states, show a single unfolding event with a narrow unfolding force distribution (inset; $N=4200$) peaked near 10 pN. Red line: fit to equation 3. (d) With 50 mM Fe-TMPyP, three types of FECs were observed, reflecting different states of the protein: natively folded but ligand-free (black), natively folded but ligand-bound (red) and ligand-bound but native structure disrupted (blue). Total number of FECs: 120. The unfolding force distribution for FECs with discrete transitions is much broader than without Fe-TMPyP. Figure taken from [27].

4.2.2 Energy landscape for PrP unfolding

The *Dudko* equation (equation (4)) was used to fit the unfolding force distribution for PrP in the absence of tetrapyrrole [124]. In the experiment with the presence of tetrapyrrole, the same equation was applicable to fit the unfolding force distribution. But, in this case, we needed two equations, one for the unbounded Fe-TMPyP-PrP population and one for the bounded population. Then, the total unfolding force distribution of FECs with discrete

transition is obtained by adding two distributions represented by equation (4). It is interesting that the parameters that we used to fit the unfolding force distribution in the absence of tetrapyrrole, were fixed to fit the unbound distribution in the presence of tetrapyrrole.

By analyzing the distribution of unfolding forces and the associated energy landscape, we gain insight as to the effects of the tetrapyrrole compound on the protein folding action. As we know, a typical unfolding force distribution with a single peak, which is determined by unfolding rate at zero force (k_0), represents an energy landscape with barrier height (ΔG^\ddagger) for the protein unfolding and the distance to the barrier from folded state (Δx^\ddagger) [124]. Previous data from measurements of ShPrP without tetrapyrrole showed an unfolding force distribution with a single peak corresponding to one population of unfolding measurement (Figure22-c, inset). In contrast, the unfolding force distribution of the protein in the presence of tetrapyrrole contained two distinguishable peaks. One of these peaks was relatively narrow and located very close to that of PrP without tetrapyrrole and the second peak was much wider at higher forces. The narrow unfolding force distribution means a compliant protein structure that leads to an extended transition state, which is very sensitive to the force, and hence, exactly represented proteins with no tetrapyrrole bound. The wider unfolding force distribution means the structure has become more brittle with a more compact transition state that is less sensitive to force indicating the presence of protein-ligand complex. We were able to fit the complete unfolding force distribution for two independent state transitions (Figure23-a, red). One fit was for one population of proteins with ligand bound (cyan: ligand-free, blue: ligand-bound) and the other one for the population of protein without tetrapyrrole bound. Landscape parameters indicated some changes after ligand binding: Δx^\ddagger decreased from 9 ± 1 nm to 1.3 ± 0.3 nm; however, ΔG^\ddagger increased from $26 \pm 2 K_B T$ to $36 \pm 7 K_B T$.

85 % of the FECs showed the reaction of the natively folded protein with tetrapyrrole. Assuming binding in equilibrium, the reaction of tetrapyrrole with protein indicated a $9 \pm 3 \mu M$ dissociation constant (K_d). This value has been measured to be $11 \pm 1 \mu M$ using isothermal titration calorimetry (ITC) in equilibrium [8]. From the determined K_d value, we found $\Delta \Delta G = -12 \pm 0.5 K_B T$ which is an estimate of the stabilizing effects of tetrapyrrole binding. A very similar result can be obtained using Jarzynski equality ($\Delta \Delta G = -12$

$5 K_B T$) (equation (5)) [105]. This result is estimated using ΔG from the distribution of work done during unfolding. The distribution of work done during FECs can be used to find ΔG which is the free energy of binding to the native state from Jarzynski equality [105]:

$$\Delta G = -K_B T \ln \left[\left\langle \exp \left(-\frac{W}{K_B T} \right) \right\rangle \right] \quad (5)$$

W is the non-equilibrium work done to unfold the molecule which is basically the area under FECs.

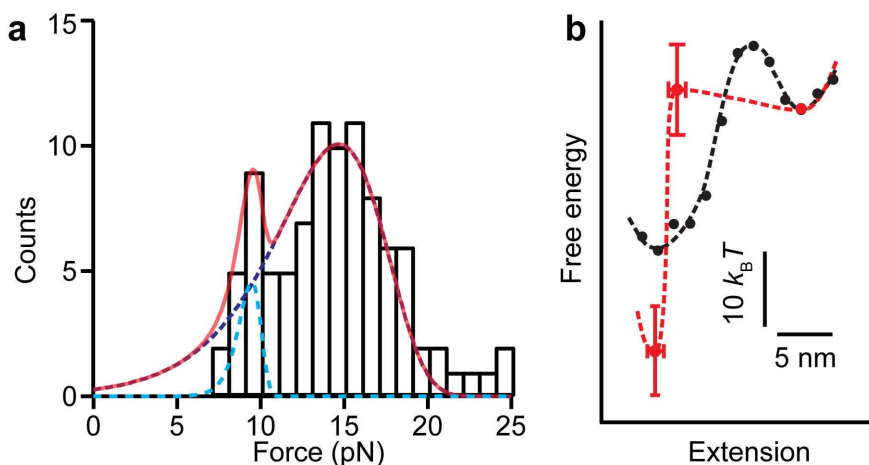


Figure 23: Effect of Fe-TMPyP binding on unfolding energy landscape. (a) The unfolding force distribution (black) for discrete transitions at 50 mM Fe-TMPyP had two peaks, near 9 and 15 pN (red: fit to equation 3). The low-force peak (cyan) matches the distribution for unfolding the native structure in the absence of ligand binding (grey; scale on right); the high-force peak (blue) corresponds to the unfolding of ligand-bound native structure. (b) Energy landscape for unfolding the native state without (black) and with (red) Fe-TMPyP bound. Figure taken from [27].

4.2.3 Fe-TMPyP can hinder native folding

As seen in Section 4.2.1, there are three different sets of populations. The population of FECs, which did not show discrete unfolding transition (Fig 24-a, black), could not fit to the WLC model. This is because this model works for proteins that truly unfold. The residual to a simple WLC fit shows that the model is not a good one for fitting the data, and something more is going on—there is a small 'shoulder' extension which is shorter than it should be for a simple WLC at low forces (Figure 24, red dashed line). Notably, the FEC of the handle

only data can be fit to the WLC model and completely covers all nucleotides of the handle (Figure24-b). Averaged FECs show the bigger picture of this behavior. We found that there is a shoulder-like feature at very low force (4-7 pN). Such features were previously observed and fit for the rapid and unstable structure of α -Synuclein [168]. Then, the shoulder was fit to a new model in which force-dependent average extension of the fluctuating structures was added to the extension of the handles and protein [168]:

$$x(F) = x_H(F) + x_{PU}(F) + \sum_{i=1}^2 N_i [P_u^i(F) \Delta x_i(F)] \quad (6)$$

In this equation:

$x_H(F)$ is the extension of the handles

$x_{PU}(F)$ is the extension of the unstructured portion of the protein

$\Delta x_i(F)$ is the extension of a given structural fluctuation at a given force F

$P_u(F)$ is the probability of unfolding the structure at that force

N_i represents the structure type, 1 means monomer and 2 means dimer PrP

The index i is a way to show different possible structures with characterized ΔL_c . N_i is also 1 for monomer and 2 for dimer. Here, the fluctuating structure is matched with the misfolded states M_1 and M_2 observed in our previous experiment without tetrapyrrole [69]. The parameters that we used to fit the fluctuating structure were taken from previous measurement. It means that we did not need to use any free parameters for fitting. Even when we used floating parameters and tested results with different assessment tests—such as a sum-of-squares lack-of-fit test, the reduced χ^2 , and the Wald-Wolfowitz runs test—no significant improvement was observed.

We know that PrP is not folding natively here, but we also know that PrP is capable of forming several misfolded states that are shorter than the native state (M_1 and M_2) [69]. Normally, we did not see these misfolded states in monomeric PrP at low force due to their unstable structures and more stable the native state. But, perhaps we can see them now because the native fold has been blocked by the ligand. To test, we can plug the numbers for these states that we measured earlier into our model above, and see how well it matches the data.

In addition, binding of Fe-TMPyP to the partially folded protein prevents the folding of the protein to the native state. This argument seems not to support the idea that Fe-TMPyP is supposed to help PrP in order to find the native structure. This means that Fe-TMPyP can in fact prevent PrP to form native structure. This is something that a 'chaperone' should not do!

Then you introduce the notion that maybe this effect is more important in terms of inhibiting interactions between molecules that cause aggregation into stable structures. This idea then leads into the next section..

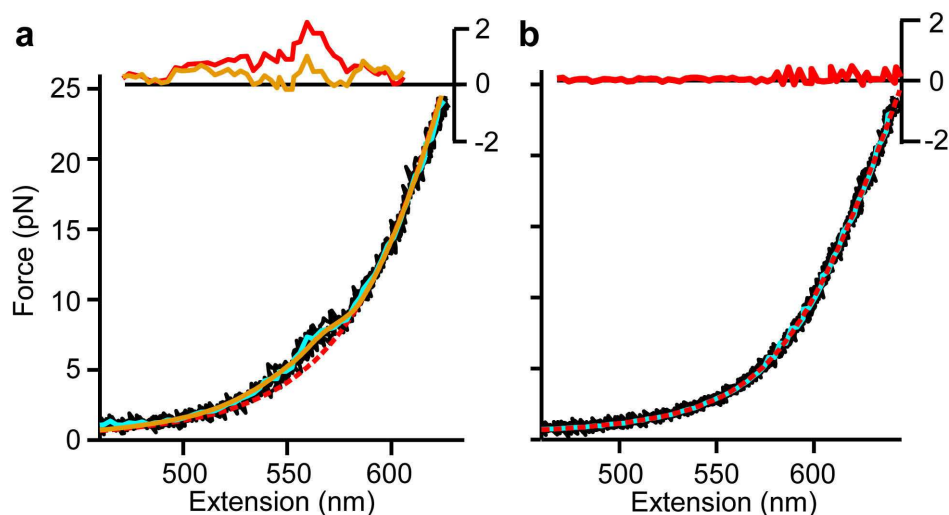


Figure 24: FECs without discrete transitions. (a) From B4–7 pN, these FECs are not well fit by the WLC model (red), leaving a systematic residual (inset). The average of these FECs (cyan) is well fit by a model (equation 2) with two misfolded states fluctuating in equilibrium (yellow). (b) FECs of Q6 the construct containing DNA handles only (black) and their average (cyan). It is fit very well to the expected simple WLC model, as evidenced by the lack of residual (inset), showing no shoulder feature. Figure taken from [27].

4.2.4 Effects on PrP dimers

We also looked at effects of binding of tetrapyrrole to a dimer protein. A dimer protein has been formed by interaction of the domains of two individual proteins. In our case, two ShPrP(90-231) linked and formed a dimer (Figure25-a, inset) [19], [169]. Previously, we have seen that without tetrapyrrole, a dimer always misfolds with ΔL_c value which did not match the native structure (Figure25-a, blue) [169]. This misfolded dimer structure called

M_D was more stable than a natively folded PrP because two native structures of each domain were never observed in pulling measurements. However, in the presence of tetrapyrrole, the stable misfolded state (M_D) appeared rarely. We mostly saw FECs with shoulder-like behavior without discrete transition (Figure25-b, black). The shoulder was similar to the one seen in monomeric PrP, at the same force, but the deviation from the WLC was about twice as big. Hence, dimeric FECs with shoulder-like feature also could be fit to equation (6) and the same parameters that we used for monomeric FECs with shoulder-like behavior (Figure25-b, yellow). In this case, for each monomer, we have misfolded states M_1 and M_2 because of the two domains of a dimer. Some FECs showed two discrete unfolding transitions with ΔL_c value for each domain that matches exactly with a monomer PrP. As a result, tetrapyrrole helped the dimer by increasing its chances of refolding into the correct structure. In the presence of tetrapyrrole, we could actually see two PrP^C domains, something that was never seen without the ligand present.

The benefit of using tetrapyrrole appears in the dimer. Without tetrapyrrole, PrP-dimer always misfolded to M_D . In the presence of tetrapyrrole, the dimer sometimes shows natively folded states. Also, it showed binding to the partially folded state (i.e. the presence of shoulder). So, what it is doing here is that by binding to partially folded state for each monomer in a dimer, it is preventing PrP-dimer from misfolding to M_D . This might be important to prevent aggregation.

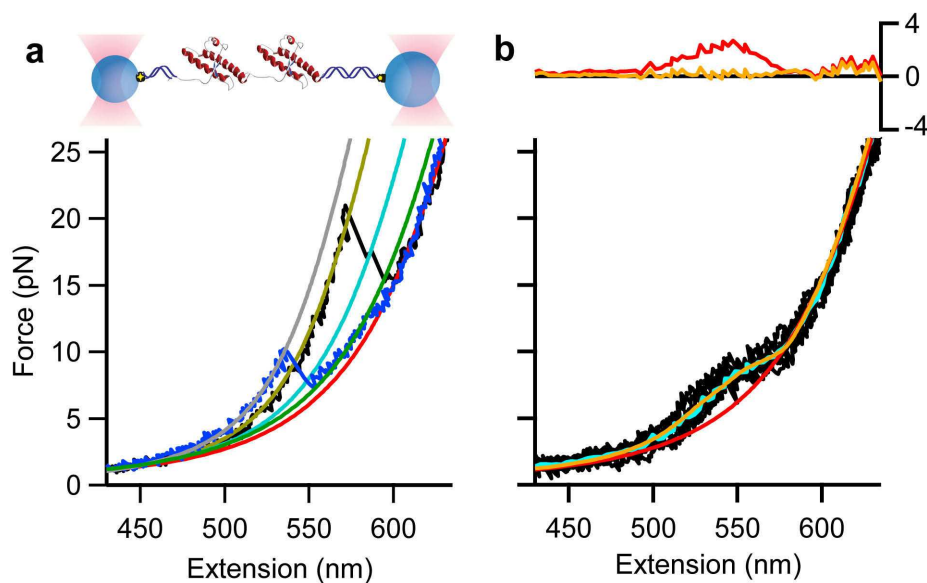


Figure 25: FECs of PrP dimer. (a) Inset: schematic of tandem dimer. FECs without Fe-TMPyP (grey) reveal a total DLc more than twice the value for isolated monomers, indicating that the dimer forms a stable, non-native state. With 50 mM Fe-TMPyP (black), some FECs unfolded in two steps, each having the same DLc as for unfolding PrPC, indicating that both domains were natively folded. Dotted lines: WLC fits (yellow, misfolded dimer; red, unfolded; cyan, natively folded domains). Total number of FECs: 164. (b) Most FECs with 50 mM Fe-TMPyP (black) showed no discrete transitions. The average (cyan) deviated markedly from a simple WLC model (red), but was well fit by the same model as for Fig.24 (yellow). Inset: fit residuals. Figure taken from [27].

4.2.5 In vitro aggregation

In addition to the single molecule study, aggregation assay was a good way to test the effects of tetrapyrrole on PrP. For this reason, the aggregation assay of PrP in the presence and absence of Fe-TMPyP was done in vitro condition (Figure26-a,b). The assay experiment was done using Thioflavin T (ThT) fluorescence to record the signal produced by the formation of ThT-positive aggregates under partial denaturing conditions [170]. A previous study was done using protein misfolded cyclic amplification (PMCA); but only the reduction of prion amplification by half with 11 μM Fe-TMPyP and final amount of aggregated prion has been shown [8].

In order to do the aggregation experiment, we used 200 μL of 0.5 mg/mL ShPrP protein in 50 mM sodium phosphate buffer pH 7.0 and 2 M GdnHCl. To do this experiment, the

protein was separated in clear-bottomed wells of 96-well plate which was covered by a thermal adhesive sealing film. After that, samples with the presence of 10 μM ThT were incubated at 37 degrees while being continuously shook at 500 rpm for 47 hours in the seeded condition and 358 hours for the unseeded condition. Fluorescence plate reader was used in order to do successive fluorescence measurements (excitation and emission were at 445 and 482 nm respectively; and the cutoff on a fluorescence plate reader was 475 nm). As explained before, the experiment was done in two seeded and unseeded conditions. For the seeded condition, the experiment was done with in the presence of 0.00025 % (w/v) pre-formed recombinant PrP fibrils.

Quenching is a term to represent any process which decreases the fluorescence intensity of a given substance. By doing this experiment, we realized that tetrapyrrole can quench the ThT fluorescence intensity. To have a better result of this reaction, we tried different concentrations of tetrapyrrole (2, 10 and 50 μM) to the unseeded aggregation construct. Fluorescence readings were recorded before and after adding tetrapyrrole. The fluorescence values dropped to 99.1%, 44.8% and 20.0% of the value for the control reactions after adding 2, 10, 50 μM tetrapyrrole respectively. After finishing the assay experiment, the final product was centrifuged to separate insoluble fibrils for immunoblotting technique. The immunoblotting technique was taken into account to test the amount of final aggregation and the amount of PrP that was incorporated into insoluble fibrils in the reactions.

In the next step, the output of fluorescence measurements was normalized to 1 by setting the final ThT values. Then, the result was fitted to equation (7).

$$Y(t) = \frac{Y_0 + (1 - Y_0)}{(1 + \exp(\frac{t_{1/2} - t}{\tau}))} \quad (7)$$

in this equation:

Y_0 is the initial fluorescence reading

$t_{1/2}$ is the time at which the ThT fluorescence is half of maximal

τ is the time that fluorescence needed to reach the final steady state

In our experiment, however, the kinetics of aggregation were considered. It is interesting that the time to reach half maximum of the ThT value ($t_{1/2}$) in unseeded conditions had little

change after adding 2 or 10 μM Fe-TMPyP. But, after adding a high dose of Fe-TMPyP (50 μM) the change was noticeable (Figure 26-c, blue). In contrast, there was not a significant change in lag phase duration which means that Fe-TMPyP affected the rate of fibril growth rather than seed formation. After adding 50 μM Fe-TMPyP, fluorescence values and Western blots of the supernatant showed a reduction in the total amount of insoluble aggregate. The results indicated the effects of 50 μM Fe-TMPyP in the aggregation process of ShPrP. We repeated the experiment in the seeded condition. By incubation of PrP monomers with pre-formed fibrils, the lag phase underwent a great reduction compared with the unseeded experiment (< 6.5 hours versus > 40 hours). In contrast, there was not a noticeable change in $t_{1/2}$ (Figure 26-c, black). As expected for this condition, the amount of insoluble PrP aggregation reduced by adding 50 μM Fe-TMPyP in both seeded and unseeded conditions (Figure 26-d).

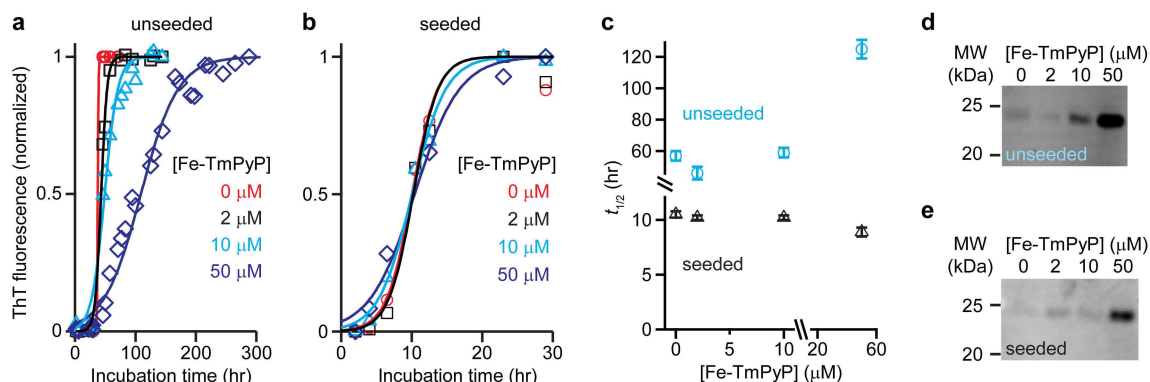


Figure 26: Effect of Fe-TMPyP on ensemble aggregation kinetics. (a) Time course of aggregation monitored by ThT fluorescence measured at different concentrations of Fe-TMPyP, without seeds present. Solid lines: fits to equation 5. (b) Same in the presence of seeds. (c) The time to reach half-maximal fluorescence was unaffected by Fe-TMPyP dose with seeds present, but was increased by a high dose in unseeded reactions. (d,e) The amount of soluble PrP not sequestered in fibrils increased significantly at high Fe-TMPyP doses for both (d) unseeded and (e) seeded reactions. Figure taken from [27].

4.3 Discussion

To conclude, Fe-TMPyP can bind to the folded ShPrP and can have thermodynamic effects on native folding by stabilizing the native structure of PrP. In addition, the mechanical effect and the kinetic effect of Fe-TMPyP makes the structure more rigid and raises the en-

ergy barrier to get to the unfolded state appreciably (the barrier to get out of the unfolded state remains the same). The other ability of Fe-TMPyP, which has not been detected so far, is binding Fe-TMPyP to an unfolded PrP molecule. The ligand allowed two unstable misfolded states M_1 and M_2 to persist longer because ligand blocked the native structure from folding. Generally, on-pathway intermediates have an important role on generating aggregation. For instance, if M_1 and M_2 are on-pathway intermediates, in the aggregation process, we might expect that the unfolded-state binding of Fe-TMPyP increases aggregation via reduced lag time. However, in off-pathway intermediates, binding of Fe-TMPyP to the protein does not have that much effects. In this case, the misfolded state tends to fold into the native structure as we saw in the absence of Fe-TMPyP [167]. The results show that Fe-TMPyP can bind to a single PrP molecule in two ways which are binding to the folded PrP monomer and binding to the unfolded PrP monomer. Fe-TMPyP can stabilize the native structure of single PrP molecules thermodynamically, kinetically, and mechanically by binding to the folded PrP. Specifically, it can alter the nature of the transition state by increasing the barrier height which makes passing the barrier harder in this case. This state can be justified by looking at the structure of PrP and the location of binding [8]. Moreover, Fe-TMPyP interacts with both strand 1 near the N-terminus of the PrP^C and with helix 3 near the C-terminus (Figure 22-a). We can conclude that, the compound acts like a clamp through both ends of PrP and it stabilizes the native structure. Hence, we have a reduction in $\Delta\chi^\ddagger$. The most interesting result is binding of tetrapyrrole to the dimer. Previous work on ShPrP without tetrapyrrole deduced the pathway for forming the M_D state, and it involved a high-force intermediate (labeled I_D3) that was the critical first step in misfolding. This step was seen in all FECs as the last part of the protein to unfold and the first to refold. Since the I_D3 with the ligand present generally was not seen, presumably the ligand prevents it from forming, thereby preventing M_D . The intermediate I_D3 formed by inter-domain interaction of dimer which is the C terminus of one monomer and N terminus of the other one. By Fe-TMPyP binding to the same inter-domain region, intermediate I_D3 is not formed unless in the purpose of forming M_D . Thus, there is a chance for dimers to refold into the native structure. Also, M_D was formed very rarely. Instead, M_1 and M_2 , which are off-pathway intermediates, are more likely to form. Hence, the chance of a stable misfolded state form-

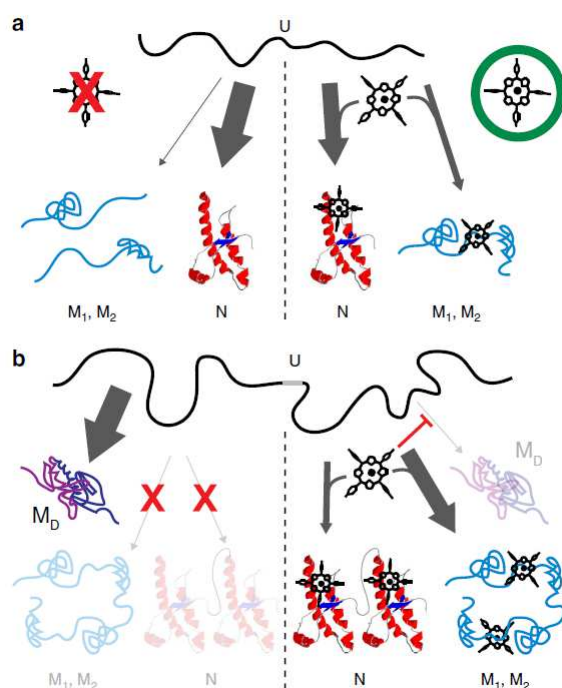


Figure 27: Cartoon of Fe-TMPyP effects on PrP folding. (a) Without Fe-TMPyP (left), PrP monomers fold natively; they can form misfolded states (for example, M1 and M2), but only transiently as they are unstable. With ligand (right), most of the time natively folded PrP is observed, but ligand binding to the unfolded protein can also allow misfolded states (M1 and M2) to form. (b) For dimers, without ligand (left) native folding is never observed, nor M1 and M2; instead, a stable misfolded dimeric structure forms. With ligand present (right), this stable misfolded structure is inhibited, and the structures observed in monomeric PrP are recovered (native fold or M1 and M2). Figure taken from [27].

ing decreases. Consequently, tetrapyrrole creates an opportunity for dimers to form native structure (Figure27).

Ensemble aggregation assay studies confirm the intermolecular contact blocking properties of Fe-TMPyP which was consistent with the single molecule studies. Fe-TMPyP binding with *PrP^C* can reduce the formation of prion via interaction with monomer *PrP^C* [8]. In contrast, this interaction is possible only in the presence of high doses of Fe-TMPyP (50 μ M) through growth rate of aggregation rather than the lag phase. In other words, Fe-TMPyP reduces the ability of seeds to bind to the cellular form of the PrP. As a result, Fe-TMPyP reduces the aggregation. However, Fe-TMPyP does not appear to affect seed formation. Because, the lag time, which reflects the time required for seeds to form, is ba-

sically the same in all cases. In an unseeded reaction, high concentration of Fe-TMPyP in the solution reduces the binding reaction with seeds and the cellular form of the PrP. However, in the seeded experiment, Fe-TMPyP effects are much less than what we observed in the unseeded incubation due to the high concentration of seed compared with Fe-TMPyP. The important point is that, in the seeded incubation, the reduction of amyloid PrP was observed in supernatant. It is important because the ligand is still reducing the total amount of amyloid being formed, even though the kinetics are unchanged. This is consistent with the reduction of prion amplification by PMCA.

Comparison results of pharmacological chaperones with those of cellular chaperones:

It is interesting to compare pharmacological chaperones with cellular chaperones. A molecular chaperone is a protein that interacts with, stabilizes or helps another protein to gain its functionally active conformation, without being present in its final structure [76], [171], [172]. In recent years, the mechanism of chaperone-assisted protein folding using single-molecule techniques started to be studied [173]. Trigger factor is a cellular chaperone which can stabilize folding of maltose binding protein (MBP) via stabilizing partially-folded intermediates rather than the native structure [79]. Another important effect of trigger factor is on the dimers of MBP which can reduce the inter-domain interactions. The reduction of inter-domain interactions is also possible with the Fe-TMPyP binding to dimers. SecB is another chaperone that has a similar effect on dimer MBP by preventing stable aggregation, but secB binds primarily to the unfolded or molten-globule states, suppressing native folding as well [174]. SMFS of a multi-domain protein, called luciferase and fluorescence studies of huntingtin protein revealed that prefoldin chaperone acts in a similar mechanism by preventing inter-domain interactions of luciferase and acting as a cellular chaperone in luciferase as well as suppressing the formation of toxic oligomers in huntingtin [175], [176].

Fe-TMPyP mimics some properties of cellular molecular chaperones by suppression of inter domain interaction of prion protein and by leading to a stable misfolded aggregation. But, its strong influence on the native state is different. So, stabilizing the native structure leads to a reduction in the rate of conversion of PrP^C to PrP^{Sc} in Fe-TMPyP. Also, blocking the inter-domain interactions tends to reduce the growth rate of oligomers. The second

property of Fe-TMPyP is more important because it has a similar activity to that of the cellular chaperone. By looking at molecules in the presence of different compounds, we can elucidate the mechanism of pharmacological chaperones which opens a new window to drug development.

5 Pentosan polysulphate (PPS) as an anti-prion compound

5.1 Motivation

Recent studies have shown that certain polysulphate polyanions can prevent the progression of transmissible spongiform encephalopathy [177]. Polyanions can bind to the PrP strongly with complex association and dissociation kinetics. One suggested mechanism suggests that certain polysulphate compounds can delay the TSE disease [178] by decreasing the cell-surface PrP^c [179]. Consequently, this reduction, inhibits conversion of PrP^c to PrP^{Sc} [154], [180]. The main question that arises from this is, how do polyanions work to decrease the rate of conversion?

Pentosan polysulphate is an example of polysulphate polyanions which has been successful in the treatment of at least one CJD patient [3]. Interestingly, PPS can act as an anti-scrapie compound in both *in vitro* and *in vivo* conditions [177]. In some cases, anti-scrapie protection in rodents was detected by short treatments months before peripheral scrapie infection happens [181], [182]. Studies suggested that PPS can inhibit the formation of PrP^{Sc} . This feature of PPS provides a likely explanation for its prophylactic efficacy [154], [180]. *In vitro* studies still can help us to learn a lot about PPS binding; but, there is not so much *in vitro* work that has been done. SPR of PPS binding has been measured, but no analysis of binding strength, or kinetics, or stoichiometry has been done. So, I tried to use SPR analysis as well as ITC measurements in order to help understand future measurements.

5.2 Bulk measurements

5.2.1 SPR analysis

Ligand binding interactions with proteins can be studied using SPR spectroscopy. SPR gives us a chance to measure real-time quantitative binding affinities [183]. In addition, measuring kinetics for proteins interacting with ligand molecules is possible with SPR spectroscopy. The positive aspect of this measurement is that, only small quantities of materials are needed. In order to do the measurement, one binding component should be kept immobilized on a sensor chip while a solution containing the other binding component is injected over the chip. SPR is an instrument for measuring the reflective index near a sensor surface. As the

flowing material binds to the immobilized compound, the accumulation of protein on the surface increases the reflective index [183], [184]. The instrument records the changes in reflective index in real time. The final result is plotted as response or resonance units (RUs) vs time [184].

To analyze the SPR result of the original paper, some basic contents such as association and dissociation constants and their associated rates of increase are needed [177]. The reaction is characterized by the on-rate constant k_{on} and the off-rate constant k_{off} , which have units of $M^{-1}s^{-1}$ and s^{-1} , respectively. The propensity of a compound to bind into another compound under equilibrium conditions can be described by the dissociation constant (K_d). The dissociation constant (K_d) can be measured using equilibrium binding analysis, or calculated from k_{on} and k_{off} .

A continuous surface plasmon resonance (SPR) experiment has been set up to find the binding of soluble PrP to the immobilized ligand on a biosensor chip [177]. In this experiment different amounts of the mature-length of recombinant PrP (recPrP) have been tested. The results indicated a 660 s association phase and a very slow dissociation phase, both present high binding affinities (Figure 28). The SPR sensorgrams of recPrP binding to immobilized PPS showed complex association and dissociation kinetics that the data could not fit with a simple curve fitting equations [177]. The result was obvious even when I tried to fit the data with an exponential and double exponential model which is presented in the next section. A reason for this complexity can be justified with the polyanions function which tends to participate in a wide range of interaction during the measurement [177].

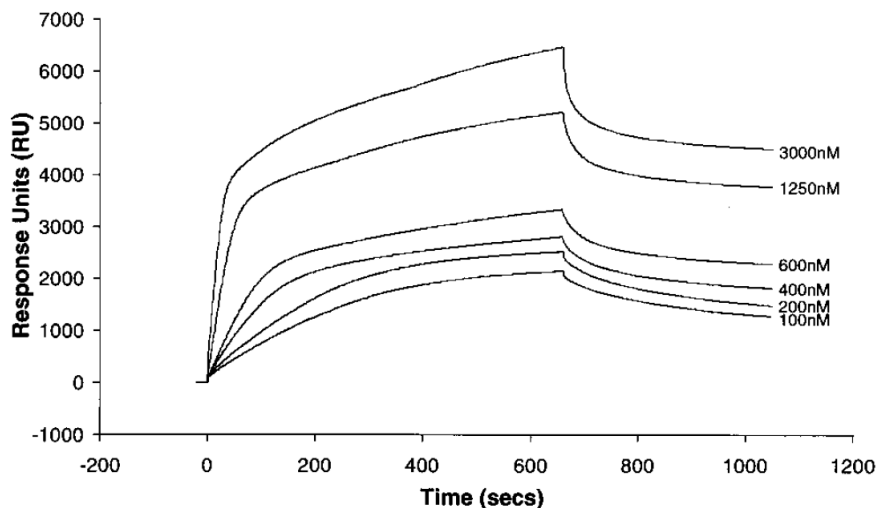


Figure 28: SPR sensorgrams of purified recPrP binding to immobilized PPS. A range of recPrP concentrations were injected over an immobilized PPS chip. Association phase, 0 ± 660 s ; dissociation phase, 660 s onwards (470 response units, RU, of PPS immobilized, recPrP injected at 5 $\mu\text{l}/\text{min}$). Figure adapted from [177]

In equilibrium measurement a series of flowing materials with different concentrations are injected into the immobilized compound. I used Igor Pro to analyze the data in the earlier paper [177]. Data points were recovered and then were transferred to an Igor experiment environment. The SPR signal amplitude during the binding phase of the measurement can be described by $\Delta R(t)_{bind} \propto \exp(1 - \gamma t)$ where γ , the rate of increase, is equal to $k_{on}C + k_{off}$ (C is the ligand concentration) [185], [186]. In the original SPR experiment, the immobilized compound was PPS and the flowing material was ShPrP which was injected with different concentrations [177]. In order to obtain the rate of increase, all SPR signals reported in the original paper, with different protein concentrations were analyzed (Figure 29 shows some recovered SPR signal with the fitted curve) [177].

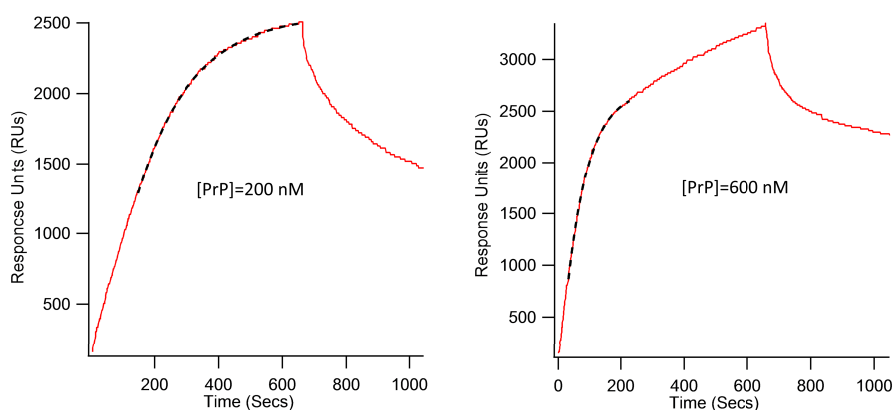


Figure 29: Recovered SPR sensorgrams of purified recPrP binding to immobilized PPS. A range of recPrP concentrations was injected over an immobilized PPS chip. Data points from [177] were recovered. Then, in order to find γ in all conditions the curves were regenerated using Igor. The black dashed line shows the fitted by a single-exponential function to the binding site [185], [187]. Data in panel 29 is taken from [177].

After that a linear fit to the ligand concentration dependence of γ (according to $\gamma = k_{on}C + k_{off}$) was used to determined the dissociation constant ($K_d = k_{off}/k_{on}$) [186]. Finally, after all of this analysis, the affinity constant was calculated to be 146 nM (Figure 30).

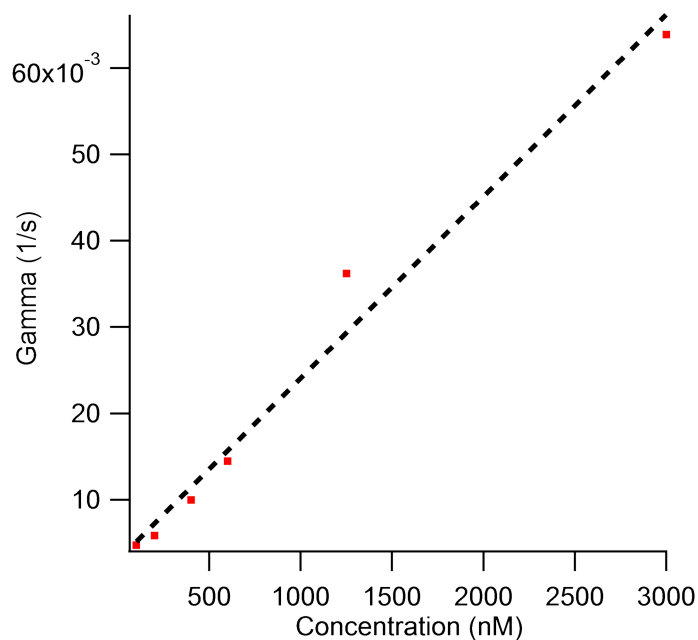


Figure 30: linear fit to the ligand concentration dependence of γ . In order to find the binding affinity from SPR measurements. Data in panel 29 is taken from [177].

5.2.2 ITC measurement

The thermodynamics of interactions between protein and small molecule, enzyme and inhibitor, protein and protein, protein and DNA and Etc can be studied using direct measurements of the heat released to the surrounding environment (exothermic process) or the heat taken up from the surrounding environment (endothermic process), when molecules interact [188], [189]. Isothermal titration calorimetry (ITC) is a universal detector that can measure the change in heat or enthalpy of chemical reactions. ITC measurement gives us an opportunity to answer to two main questions: how tightly do small molecules bind to a specific interaction site of another molecule? How fast dose the reaction between two molecules take place [189]? Measuring heat using ITC, is a way to understand about the amount of a reaction that has taken place, n (in moles, mmoles, μ moles,...) and the enthalpy change for the reaction, ΔH (in kcal/mol or KJ/mol), binding stoichiometry as well as the dissociation constant K_d [189]. In addition, the rate at which the heat is exchanged is equal to the rate of reaction $\delta n/\delta t$ and the enthalpy change, ΔH [189].

The ITC instrument is made of two cells (reference cell and sample cell) and one syringe to fill with ligand solution. The reference cell is usually filled with miliQ water and the sample cell is filled with protein solution. During the experiment small amounts of ligand solution are injected to the sample cell over a period of time while the heat of reaction is measured [188].

The measurement is initialized with the ligand solution in the syringe and the protein solution in the sample cell with the same buffer. For the first injection, a few micro-molar of ligand solution is injected to the sample. As a result, all injected ligands bind to the target macromolecule. The heat of reaction results in a generating signal. Then, the signal returns to the baseline before the next injection. The second injection is made and all injected ligands bind to the target molecules. Again, waiting time is needed for the signal to go back to the baseline. While the injections continue, the target molecule becomes saturated with ligand. As a result, less binding occurs and the heat changes start to decrease. Finally, no improvement of signal is observed when the target molecule is completely saturated [188].

I performed the ITC experiment with PPS compound and WT-ShPrP which was prepared

according to the procedure explained in section 3.2.1. The cell was filled with 0.1 mM ShPrP. The PPS concentration in Syringe was 1 mM. The buffer for both ligand and PrP was 10 mM sodium acetate pH 4.5. The experiment was done at 25 °C over a 60 min period of time. The same experiment was repeated injecting ligand in buffer in order to find the heat of reaction signal between ligand and buffer which then needed to be subtracted from the signal of ligand into PrP. After that, the result was analyzed using Origin 7 software. In order to fit data with one site model (for PrP and compound with 1:1 stoichiometry), we needed to subtract the signal from the ligand into buffer titration data (Figure 21). The final results show $K_d = 5 \mu M = 2.68 \mu M$.

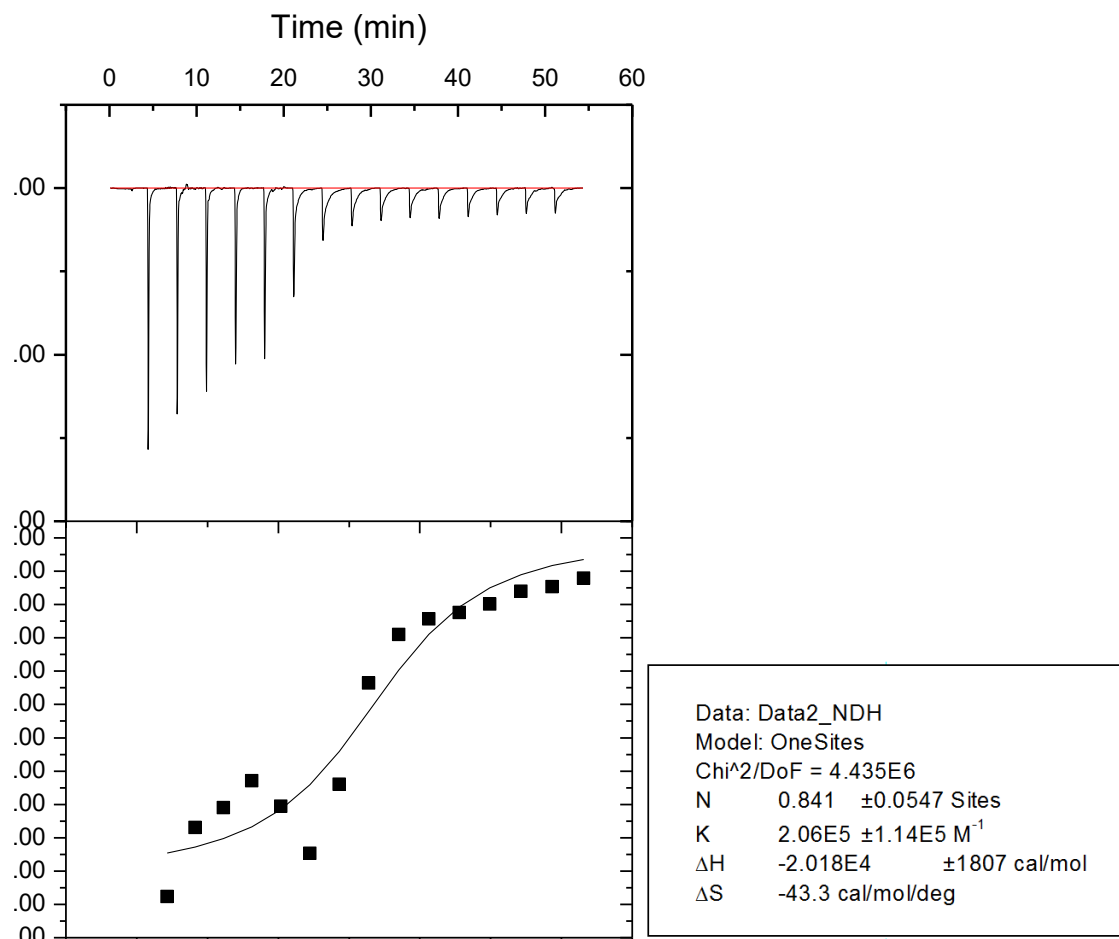


Figure 31: One site model fitted to the PPS titration into ShPrP. PrP concentration = 0.1 mM, PPS concentration = 1 mM, in pH 4.5 buffer. The background signal of PPS into buffer was removed using PPS titration into buffer.

Another way of analyzing the data is to pick the last two or three signals in PrP titrated with PPS data in order to use them as the background signal (Figure 32). The reason that we could do this is that when PrP is saturated with ligand by the end of experiment, the heat of reaction near baseline is related to the binding of PPS and buffer only. so we can consider

these signals as the background noise. The final results show $K_d = 50 \text{ nM} - 133 \text{ nM}$ in this case. The error in this case is bigger than the actual value because of the heat of the reaction of the ligand with the buffer. So, we got different results depending on what we choose as the baseline to subtract. Regardless, both analyses still give the answer that is broadly similar to the SPR numbers. We get a result of between $K_d = 0.05 \text{ } \mu\text{M}$ to $K_d = 5 \text{ } \mu\text{M}$, consistent with the SPR data given the large error.

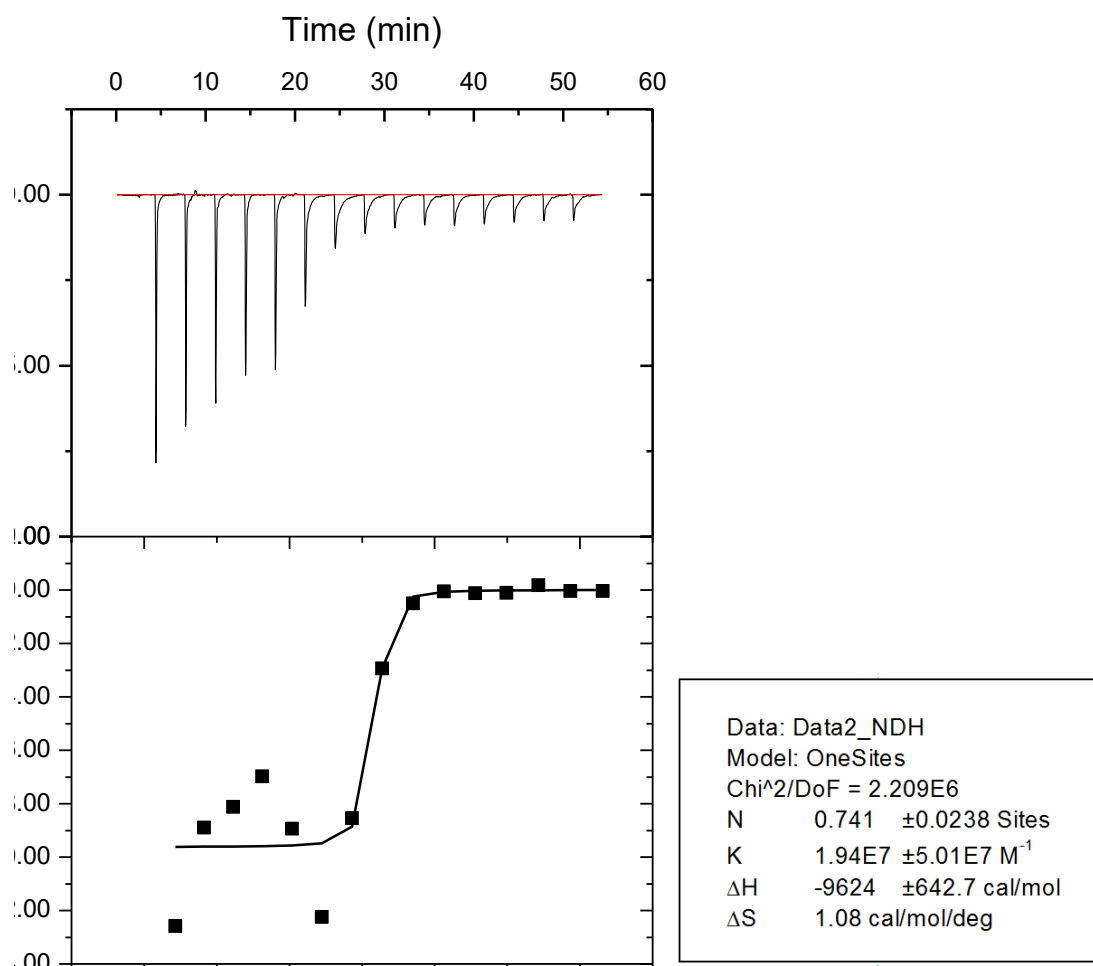


Figure 32: One site model fitted to the PPS titration into ShPrP. PrP concentration = 0.1 mM, PPS concentration = 1 mM, in pH 4.5 buffer. The background signal of PPS into buffer was removed using last three signals of PPS titration in PrP.

The important point that needs to be emphasized here is that we learned that the stoichiometry is basically 1:1—this answer does not really depend on how the baseline is defined, which makes it robust. To clarify which result is closer to the actual K_d further experiments are required. However, the 50 nM result is closer to the SPR result from the original paper [177].

6 Future work

In this work, we considered two subjects of protein studies: one deals with samples preparation of MoPrP (chapter 3) and the other deals with anti-prion ligands and their effects on PrP folding at the single molecule level (chapters 4 and 5).

Previous studies have been done on ShPrP with optical tweezers in our group. As the first subject, in order to understand the differences between the folding dynamics of mouse and hamster PrP, we started to measure MoPrP at the single-molecule level. Measurements have been done on MoPrP prepared using two different linking chemistries. We also investigated internal Cys labeling instead of terminus labeling using DNA handles. The experiment was performed with a fluorescent dye.

As the second subject, we studied the interaction between iron-tetrapyrrole ligand and ShPrP as well as the binding of PPS to ShPrP. We also investigated how iron-tetrapyrrole affects ShPrP folding at the single-molecule level. Finally, we studied the thermodynamics of interactions between protein and PPS in our lab. This information is needed for the force-extension measurements of ShPrP with PPS compound.

Two lines of research from this work can be considered:

- SMFS measurements of mouse PrP folding to compare to hamster, in order to determine what differences might account for subjects such as different disease susceptibility and species barriers for transmission. Measurements would be done in the same manner as performed on hamster PrP by pulling a single molecule with optical tweezers. The experiments can be done in different circumstances: equilibrium measurements and non-equilibrium measurements. Existence of intermediates, differences in kinetics and energetics and pathways for native and non-native folding, etc. would be investigated using single-molecule method.
- SMFS measurements of PPS effects on PrP folding. Key point here is whether the effects are similar to TMPyP, or whether it does different things. Are there echoes of how cellular chaperones work, once again? Study would be done in a similar way to TMPyP work, looking at both monomers (to understand effects on native folding

dynamics) and dimers (to see how PPS changes interactions that cause aggregation). SMFS studies have allowed the exploration of molecular folding and misfolding as well the kinetics and thermodynamics of their mechanical response to applied force. In order to investigate the effects of PPS on ShPrP folding using optical tweezers, basic information about the affinity constant of the PPS-PrP reaction is needed. After figuring out the dissociation constant for PPS and PrP interaction, investigating the effects of PPS on ShPrP via optical tweezers is suggested. Study would be done in the similar way to TMPyP work, looking at both monomers (to understand effects on native folding dynamics) and dimers (to see how PPS changes interactions that cause aggregation). In addition, some questions about the PPS-PrP combination can be answered through optical tweezers experiments. For example, how does the binding of PPS to the unstructured region of PrP affect the folding and misfolding of ShPrP [8]? How does PPS change the energy landscape parameters and as a result has an anti-prion effects on ShPrP? The key point here is to understand whether the effects are similar to TMPyP, or it has different effects on ShPrP folding.

Bibliography

- [1] Fabrizio Chiti and Christopher M Dobson. Protein misfolding, functional amyloid, and human disease. *Annu. Rev. Biochem.*, 75:333–366, 2006.
- [2] D Riesner, K Kellings, U Wiese, M Wulfert, C Mirenda, and SB Prusiner. Prions and nucleic acids: search for” residual” nucleic acids and screening for mutations in the prp-gene. *Developments in biological standardization*, 80:173–181, 1992.
- [3] Neil R Cashman and Byron Caughey. Prion diseases—close to effective therapy? *Nature Reviews Drug Discovery*, 3(10):874–884, 2004.
- [4] Stanley B Prusiner. Prions. *Proceedings of the National Academy of Sciences*, 95(23):13363–13383, 1998.
- [5] Glenn C Telling, Piero Parchi, Stephen J DeArmond, Pietro Cortelli, et al. Evidence for the conformation of the pathologic isoform of the prion protein enciphering and propagating prion diversity. *Science*, 274(5295):2079, 1996.
- [6] Byron Caughey, Gerald S Baron, Bruce Chesebro, and Martin Jeffrey. Getting a grip on prions: oligomers, amyloids and pathological membrane interactions. *Annual review of biochemistry*, 78:177, 2009.
- [7] David W Colby and Stanley B Prusiner. Prions. *Cold Spring Harbor perspectives in biology*, 3(1):a006833, 2011.
- [8] Andrew J Nicoll, Clare R Trevitt, M Howard Tattum, Emmanuel Risse, Emma Quarterman, Amaurys Avila Ibarra, Connor Wright, Graham S Jackson, Richard B Sessions, Mark Farrow, et al. Pharmacological chaperone for the structured domain of human prion protein. *Proceedings of the National Academy of Sciences*, 107(41):17610–17615, 2010.
- [9] Neil Stahl, David R Borchelt, Karen Hsiao, and Stanley B Prusiner. Scrapie prion protein contains a phosphatidylinositol glycolipid. *Cell*, 51(2):229–240, 1987.
- [10] Stanley B Prusiner. Scrapie prions. *Annual Reviews in Microbiology*, 43(1):345–374, 1989.
- [11] Bruno Oesch, David Westaway, Monika Wälchli, Michael P McKinley, Stephen BH Kent, Ruedi Aebersold, Ronald A Barry, Paul Tempst, David B Teplow, Leroy E Hood, et al. A cellular gene encodes scrapie prp 27-30 protein. *Cell*, 40(4):735–746, 1985.

- [12] Bruce Chesebro, Richard Race, Kathy Wehrly, Jane Nishio, Marshall Bloom, David Lechner, Sven Bergstrom, Ken Robbins, Leonard Mayer, Jerry M Keith, et al. Identification of scrapie prion protein-specific mrna in scrapie-infected and uninfected brain. 1985.
- [13] K Basler, B Oesch, M Scott, D Westaway, M Wälchli, DF Groth, MP McKinley, SB Prusiner, and C Weissmann. Scrapie and cellular prp isoforms are encoded by the same chromosomal gene. *Cell*, 46(3):417–428, 1986.
- [14] Laszlo LP Hosszu, Nicola J Baxter, Graham S Jackson, Aisling Power, Anthony R Clarke, Jonathan P Waltho, C Jeremy Craven, and John Collinge. Structural mobility of the human prion protein probed by backbone hydrogen exchange. *Nature Structural & Molecular Biology*, 6(8):740–743, 1999.
- [15] Ralph Zahn, Aizhuo Liu, Thorsten Lührs, Roland Riek, Christine von Schroetter, Francisco López Garc’a, Martin Billeter, Luigi Calzolari, Gerhard Wider, and Kurt Wüthrich. Nmr solution structure of the human prion protein. *Proceedings of the National Academy of Sciences*, 97(1):145–150, 2000.
- [16] Ilia V Baskakov, Giuseppe Legname, Michael A Baldwin, Stanley B Prusiner, and Fred E Cohen. Pathway complexity of prion protein assembly into amyloid. *Journal of Biological Chemistry*, 277(24):21140–21148, 2002.
- [17] Trent C Bjorndahl, Guo-Ping Zhou, Xuehui Liu, Rolando Perez-Pineiro, Valentyna Semenchenko, Fozia Saleem, Sandipta Acharya, Adina Bujold, Constance A Sobsey, and David S Wishart. Detailed biophysical characterization of the acid-induced prp to prp β conversion process. *Biochemistry*, 50(7):1162–1173, 2011.
- [18] Nöelle Bons, Nadine Mestre-Frances, Patrick Belli, Françoise Cathala, D Carleton Gajdusek, and Paul Brown. Natural and experimental oral infection of nonhuman primates by bovine spongiform encephalopathy agents. *Proceedings of the National Academy of Sciences*, 96(7):4046–4051, 1999.
- [19] Hao Yu, Derek R. Dee, and Michael T. Woodside. Single-molecule approaches to prion protein misfolding. *Prion*, 7(2):140–146, 2013.
- [20] Cédric Govaerts, Holger Wille, Stanley B Prusiner, and Fred E Cohen. Evidence for assembly of prions with left-handed β -helices into trimers. *Proceedings of the National Academy of Sciences of the United States of America*, 101(22):8342–8347, 2004.
- [21] Mari L DeMarco and Valerie Daggett. From conversion to aggregation: protofibril formation of the prion protein. *Proceedings of the National Academy of Sciences of the United States of America*, 101(8):2293–2298, 2004.
- [22] PA McBride, MI Wilson, P Eikelenboom, A Tunstall, and ME Bruce. Heparan sulfate proteoglycan is associated with amyloid plaques and neuroanatomically targeted prp pathology throughout the incubation period of scrapie-infected mice. *Experimental neurology*, 149(2):447–454, 1998.
- [23] Patricia A Merz, Robert A Somerville, Henryk M Wisniewski, Laura Manuelidis, and Elias E Manuelidis. Scrapie-associated fibrils in creutzfeldt–jakob disease. 1983.

- [24] Fabian Sokolowski, Andreas Johannes Modler, Ralf Masuch, Dietrich Zirwer, Michael Baier, Gudrun Lutsch, David Alan Moss, Klaus Gast, and Dieter Nauermann. Formation of critical oligomers is a key event during conformational transition of recombinant syrian hamster prion protein. *Journal of Biological Chemistry*, 278(42):40481–40492, 2003.
- [25] Shweta Jain and Jayant B Udgaonkar. Evidence for stepwise formation of amyloid fibrils by the mouse prion protein. *Journal of molecular biology*, 382(5):1228–1241, 2008.
- [26] Alessandro Borgia, Philip M Williams, and Jane Clarke. Single-molecule studies of protein folding. *Annu. Rev. Biochem.*, 77:101–125, 2008.
- [27] Amar Nath Gupta, Krishna Neupane, Negar Rezajooei, Leonardo Cortez, Valerie Sim, and Michael Woodside. Pharmacological chaperone reshapes the energy landscape for folding and aggregation of the prion protein. *Nature Communication*, 2016.
- [28] James D Watson, Francis HC Crick, et al. Molecular structure of nucleic acids. *Nature*, 171(4356):737–738, 1953.
- [29] Steven S Plotkin and José N Onuchic. Understanding protein folding with energy landscape theory part i: basic concepts. *Quarterly reviews of biophysics*, 35(02):111–167, 2002.
- [30] Christopher M Dobson. Protein folding and misfolding. *Nature*, 426(6968):884–890, 2003.
- [31] Ken A Dill, S Banu Ozkan, M Scott Shell, and Thomas R Weikl. The protein folding problem. *Annual review of biophysics*, 37:289, 2008.
- [32] Mikael Oliveberg and Peter G Wolynes. The experimental survey of protein-folding energy landscapes. *Quarterly reviews of biophysics*, 38(03):245–288, 2005.
- [33] D Thirumalai and Changbong Hyeon. Rna and protein folding: common themes and variations. *Biochemistry*, 44(13):4957–4970, 2005.
- [34] Christopher M Dobson, Andrej Sali, and Martin Karplus. Protein folding: a perspective from theory and experiment. *Angewandte Chemie International Edition*, 37(7):868–893, 1998.
- [35] Peter G Wolynes, Jose N Onuchic, D Thirumalai, et al. Navigating the folding routes. *SCIENCE-NEW YORK THEN WASHINGTON-*, pages 1619–1619, 1995.
- [36] Michael T Woodside and Steven M Block. Reconstructing folding energy landscapes by single-molecule force spectroscopy. *Annual review of biophysics*, 43:19, 2014.
- [37] Bernd Bukau and Arthur L Horwich. The hsp70 and hsp60 chaperone machines. *Cell*, 92(3):351–366, 1998.
- [38] R John Ellis. Macromolecular crowding: an important but neglected aspect of the intracellular environment. *Current opinion in structural biology*, 11(1):114–119, 2001.
- [39] F Ulrich Hartl and Manajit Hayer-Hartl. Molecular chaperones in the cytosol: from nascent chain to folded protein. *Science*, 295(5561):1852–1858, 2002.

- [40] Per Westermark. Aspects on human amyloid forms and their fibril polypeptides. *Febs Journal*, 272(23):5942–5949, 2005.
- [41] Stanley B Prusiner, Cedric Govaerts, Fred E Cohen, and Holger Wille. Evidence for assembly of prions with left-handed β -helices into trimers. *Proceedings of the National Academy of Sciences of the United States of America*, (22):8342–8347, 2004.
- [42] Hironobu Naiki, Norikazu Hashimoto, Satoru Suzuki, Hideki Kimura, Kazuya Nakakuki, and Fumitake Gejyo. Establishment of a kinetic model of dialysis-related amyloid fibril extension in vitro. *Amyloid*, 4(4):223–232, 1997.
- [43] Tricia R Serio, Anil G Cashikar, Anthony S Kowal, George J Sawicki, Jahan J Moslehi, Louise Serpell, Morton F Arnsdorf, and Susan L Lindquist. Nucleated conformational conversion and the replication of conformational information by a prion determinant. *Science*, 289(5483):1317–1321, 2000.
- [44] Jesper Søndergaard Pedersen, Gunna Christensen, and Daniel Erik Otzen. Modulation of s6 fibrillation by unfolding rates and gatekeeper residues. *Journal of molecular biology*, 341(2):575–588, 2004.
- [45] Diego U Ferreira, Elizabeth A Komives, and Peter G Wolynes. Frustration in biomolecules. *Quarterly reviews of biophysics*, 47(04):285–363, 2014.
- [46] Thomas R Jahn and Sheena E Radford. Folding versus aggregation: polypeptide conformations on competing pathways. *Archives of biochemistry and biophysics*, 469(1):100–117, 2008.
- [47] Derek R Dee and Michael T Woodside. Comparing the energy landscapes for native folding and aggregation of prp. *Prion*, (just-accepted):00–00, 2016.
- [48] Michael T Woodside, Cuauhtémoc Garc´a-Garc´a, and Steven M Block. Folding and unfolding single rna molecules under tension. *Current opinion in chemical biology*, 12(6):640–646, 2008.
- [49] Armin Hoffmann, Krishna Neupane, and Michael T Woodside. Single-molecule assays for investigating protein misfolding and aggregation. *Physical Chemistry Chemical Physics*, 15(21):7934–7948, 2013.
- [50] Jan Liphardt, Bibiana Onoa, Steven B Smith, Ignacio Tinoco, and Carlos Bustamante. Reversible unfolding of single rna molecules by mechanical force. *Science*, 292(5517):733–737, 2001.
- [51] Julio M Fernandez and Hongbin Li. Force-clamp spectroscopy monitors the folding trajectory of a single protein. *Science*, 303(5664):1674–1678, 2004.
- [52] Bibiana Onoa, Sophie Dumont, Jan Liphardt, Steven B Smith, Ignacio Tinoco, and Carlos Bustamante. Identifying kinetic barriers to mechanical unfolding of the t. thermophila ribozyme. *Science*, 299(5614):1892–1895, 2003.
- [53] Michael T Woodside, William M Behnke-Parks, Kevan Larizadeh, Kevin Travers, Daniel Herschlag, and Steven M Block. Nanomechanical measurements of the sequence-dependent folding landscapes of single nucleic acid hairpins. *Proceedings of the National Academy of Sciences*, 103(16):6190–6195, 2006.

- [54] William J Greenleaf, Michael T Woodside, and Steven M Block. High-resolution, single-molecule measurements of biomolecular motion. *Annual review of biophysics and biomolecular structure*, 36:171, 2007.
- [55] Hoi Sung Chung, John M Louis, and William A Eaton. Experimental determination of upper bound for transition path times in protein folding from single-molecule photon-by-photon trajectories. *Proceedings of the National Academy of Sciences*, 106(29):11837–11844, 2009.
- [56] Hoi Sung Chung, Kevin McHale, John M Louis, and William A Eaton. Single-molecule fluorescence experiments determine protein folding transition path times. *Science*, 335(6071):981–984, 2012.
- [57] Jeff Gelles, Bruce J Schnapp, and Michael P Sheetz. Tracking kinesin-driven movements with nanometre-scale precision. *Nature*, 331(6155):450–453, 1988.
- [58] Michael P Sheetz, Stephen Turney, Hong Qian, and Elliot L Elson. Nanometre-level analysis demonstrates that lipid flow does not drive membrane glycoprotein movements. *Nature*, 340(6231):284–288, 1989.
- [59] Ronald S Rock, Sarah E Rice, Amber L Wells, Thomas J Purcell, James A Spudich, and H Lee Sweeney. Myosin vi is a processive motor with a large step size. *Proceedings of the National Academy of Sciences*, 98(24):13655–13659, 2001.
- [60] WE Moerner and David P Fromm. Methods of single-molecule fluorescence spectroscopy and microscopy. *Review of Scientific Instruments*, 74(8):3597–3619, 2003.
- [61] Shimon Weiss. Measuring conformational dynamics of biomolecules by single molecule fluorescence spectroscopy. *Nature structural biology*, 7(9):724–729, 2000.
- [62] Masato Enari, Eckhard Flechsig, and Charles Weissmann. Scrapie prion protein accumulation by scrapie-infected neuroblastoma cells abrogated by exposure to a prion protein antibody. *Proceedings of the National Academy of Sciences*, 98(16):9295–9299, 2001.
- [63] Véronique Perrier, Jérôme Solassol, Carole Crozet, Yveline Frobert, Chantal Mourton-Gilles, Jacques Grassi, and Sylvain Lehmann. Anti-prp antibodies block prpsc replication in prion-infected cell cultures by accelerating prpc degradation. *Journal of neurochemistry*, 89(2):454–463, 2004.
- [64] Frank L Heppner, Christine Musahl, Isabelle Arrighi, Michael A Klein, Thomas Rüllicke, Bruno Oesch, Rolf M Zinkernagel, Ulrich Kalinke, and Adriano Aguzzi. Prevention of scrapie pathogenesis by transgenic expression of anti-prion protein antibodies. *Science*, 294(5540):178–182, 2001.
- [65] Byron Caughey, Richard E Race, and Bruce Chesebro. Detection of prion protein mrna in normal and scrapie-infected tissues and cell lines. *Journal of general virology*, 69(3):711–716, 1988.
- [66] PE Bendheim, HR Brown, RD Rudelli, LJ Scala, NL Goller, GY Wen, RJ Kascsak, NR Cashman, and DC Bolton. Nearly ubiquitous tissue distribution of the scrapie agent precursor protein. *Neurology*, 42(1):149–149, 1992.

- [67] Laura Solfrosi, Jose R Criado, Dorian B McGavern, Sebastian Wirz, Manuel Sánchez-Alavez, Shuei Sugama, Lorraine A DeGiorgio, Bruce T Volpe, Erika Wiseman, Gil Abalos, et al. Cross-linking cellular prion protein triggers neuronal apoptosis in vivo. *Science*, 303(5663):1514–1516, 2004.
- [68] Motohiro Horiuchi and Byron Caughey. Specific binding of normal prion protein to the scrapie form via a localized domain initiates its conversion to the protease-resistant state. *The EMBO journal*, 18(12):3193–3203, 1999.
- [69] Hao Yu, Xia Liu, Krishna Neupane, Amar Nath Gupta, Angela M Brigley, Allison Solanki, Iveta Sosova, and Michael T Woodside. Direct observation of multiple misfolding pathways in a single prion protein molecule. *Proceedings of the National Academy of Sciences*, 109(14):5283–5288, 2012.
- [70] Eustache Paramithiotis, Marc Pinard, Trebor Lawton, Sylvie LaBoissiere, Valerie L Leathers, Wen-Quan Zou, Lisa A Estey, Julie Lamontagne, Marty T Lehto, Leslie H Kondejewski, et al. A prion protein epitope selective for the pathologically misfolded conformation. *Nature medicine*, 9(7):893–899, 2003.
- [71] Dale Schenk, Robin Barbour, Whitney Dunn, Grace Gordon, Henry Grajeda, Teresa Guido, Kang Hu, Jiping Huang, Kelly Johnson-Wood, Karen Khan, et al. Immunization with amyloid- β attenuates alzheimer-disease-like pathology in the pdapp mouse. *Nature*, 400(6740):173–177, 1999.
- [72] Junji Hosokawa-Muto, Yuji O Kamatari, Hironori K Nakamura, and Kazuo Kuwata. Variety of antiprion compounds discovered through an in silico screen based on cellular-form prion protein structure: Correlation between antiprion activity and binding affinity. *Antimicrobial agents and chemotherapy*, 53(2):765–771, 2009.
- [73] Yuji O Kamatari, Yosuke Hayano, Kei-ichi Yamaguchi, Junji Hosokawa-Muto, and Kazuo Kuwata. Characterizing antiprion compounds based on their binding properties to prion proteins: implications as medical chaperones. *Protein Science*, 22(1):22–34, 2013.
- [74] Kazuo Kuwata, Noriyuki Nishida, Tomoharu Matsumoto, Yuji O Kamatari, Junji Hosokawa-Muto, Kota Kodama, Hironori K Nakamura, Kiminori Kimura, Makoto Kawasaki, Yuka Takakura, et al. Hot spots in prion protein for pathogenic conversion. *Proceedings of the National Academy of Sciences*, 104(29):11921–11926, 2007.
- [75] Tsutomu Kimura, Junji Hosokawa-Muto, Yuji O Kamatari, and Kazuo Kuwata. Synthesis of gn8 derivatives and evaluation of their antiprion activity in tse-infected cells. *Bioorganic & medicinal chemistry letters*, 21(5):1502–1507, 2011.
- [76] F Ulrich Hartl, Andreas Bracher, and Manajit Hayer-Hartl. Molecular chaperones in protein folding and proteostasis. *Nature*, 475(7356):324–332, 2011.
- [77] Tommer Ravid and Mark Hochstrasser. Diversity of degradation signals in the ubiquitin–proteasome system. *Nature Reviews Molecular Cell Biology*, 9(9):679–689, 2008.
- [78] Saurabh Gupta, Atmakuri Ramakrishna Rao, Pritish Kumar Varadwaj, Sachinandan De, and Trilochan Mohapatra. Extrapolation of inter domain communications and substrate binding cavity of camel hsp70 1a: A molecular modeling and dynamics simulation study. *PloS one*, 10(8):e0136630, 2015.

- [79] Alireza Mashaghi, Gunter Kramer, Philipp Bechtluft, Beate Zachmann-Brand, Arnold JM Driessen, Bernd Bukau, and Sander J Tans. Reshaping of the conformational search of a protein by the chaperone trigger factor. *Nature*, 500(7460):98–101, 2013.
- [80] Kazuo Kuwata, Yuji O Kamatari, Kazuyuki Akasaka, and Thomas L James. Slow conformational dynamics in the hamster prion protein. *Biochemistry*, 43(15):4439–4446, 2004.
- [81] Nathan J Cobb, Frank D Sönnichsen, Hassane Mchaourab, and Witold K Surewicz. Molecular architecture of human prion protein amyloid: A parallel, in-register β -structure. *Proceedings of the National Academy of Sciences*, 104(48):18946–18951, 2007.
- [82] Nathan J Cobb and Witold K Surewicz. Prion diseases and their biochemical mechanisms†. *Biochemistry*, 48(12):2574–2585, 2009.
- [83] NV Todd, J Morrow, K Doh-Ura, S Dealler, S O’Hare, P Farling, M Duddy, and NG Rainov. Cerebroventricular infusion of pentosan polysulphate in human variant creutzfeldt–jakob disease. *Journal of Infection*, 50(5):394–396, 2005.
- [84] KC Neuman and Steven M Block. Optical trapping. *Rev Sci Instrum*, 75(9):2787–809, 2004.
- [85] KC Neuman, GF Liou, G F Liou, K Bergman, and SM Block. Characterization of photodamage to escherichia coli in optical traps. *Rev Sci Instrum*, 77(5):2856–63, 1999.
- [86] Koen Visscher, Steven P Gross, and Steven M Block. Construction of multiple-beam optical traps with nanometer-resolution position sensing. *IEEE Journal of Selected Topics in Quantum Electronics*, 2(4):1066–1076, 1996.
- [87] Jane Clarke, Robert Best, Alessandro Borgia, and Michael Woodside. *Force spectroscopy of protein folding using optical tweezers*. unpublished book.
- [88] Keir C Neuman and Attila Nagy. Single-molecule force spectroscopy: optical tweezers, magnetic tweezers and atomic force microscopy. *Nature methods*, 5(6):491, 2008.
- [89] Dustin B Ritchie and Michael T Woodside. Probing the structural dynamics of proteins and nucleic acids with optical tweezers. *Current opinion in structural biology*, 34:43–51, 2015.
- [90] Carlos Bustamante, Yann R Chemla, Nancy R Forde, and David Izhaky. Mechanical processes in biochemistry. *Annual review of biochemistry*, 73(1):705–748, 2004.
- [91] Michael T Woodside and Megan T Valentine. Single-molecule manipulation using optical traps. In *Handbook of Single-Molecule Biophysics*, pages 341–370. Springer, 2009.
- [92] Lora Nugent-Glandorf and Thomas T Perkins. Measuring 0.1-nm motion in 1 ms in an optical microscope with differential back-focal-plane detection. *Optics letters*, 29(22):2611–2613, 2004.

- [93] Joshua W Shaevitz, Elio A Abbondanzieri, Robert Landick, and Steven M Block. Backtracking by single rna polymerase molecules observed at near-base-pair resolution. *Nature*, 426(6967):684–687, 2003.
- [94] Arthur Ashkin, JM Dziedzic, JE Bjorkholm, and Steven Chu. Observation of a single-beam gradient force optical trap for dielectric particles. *Optics letters*, 11(5):288–290, 1986.
- [95] Yasuhiro Harada and Toshimitsu Asakura. Radiation forces on a dielectric sphere in the rayleigh scattering regime. *Optics communications*, 124(5):529–541, 1996.
- [96] Ciro Cecconi, Elizabeth A Shank, Frederick W Dahlquist, Susan Marqusee, and Carlos Bustamante. Protein-dna chimeras for single molecule mechanical folding studies with the optical tweezers. *European Biophysics Journal*, 37(6):729–738, 2008.
- [97] Greg T Hermanson. *Bioconjugate techniques*. Academic press, 2013.
- [98] Zhongbo Yu, Deepak Koirala, Yunxi Cui, Leah F Easterling, Yuan Zhao, and Hanbin Mao. Click chemistry assisted single-molecule fingerprinting reveals a 3d biomolecular folding funnel. *Journal of the American Chemical Society*, 134(30):12338–12341, 2012.
- [99] Bharat Jagannathan, Phillip J Elms, Carlos Bustamante, and Susan Marqusee. Direct observation of a force-induced switch in the anisotropic mechanical unfolding pathway of a protein. *Proceedings of the National Academy of Sciences*, 109(44):17820–17825, 2012.
- [100] William J Greenleaf, Michael T Woodside, and Steven M Block. High-resolution, single-molecule measurements of biomolecular motion. *Annual review of biophysics and biomolecular structure*, 36:171, 2007.
- [101] William J Greenleaf, Michael T Woodside, Elio A Abbondanzieri, and Steven M Block. Passive all-optical force clamp for high-resolution laser trapping. *Physical review letters*, 95(20):208102, 2005.
- [102] Xinming Zhang, Lu Ma, and Yongli Zhang. High-resolution optical tweezers for single-molecule manipulation. *Yale J Biol Med*, 86(3):367–383, 2013.
- [103] Johannes Stigler, Fabian Ziegler, Anja Gieseke, J Christof M Gebhardt, and Matthias Rief. The complex folding network of single calmodulin molecules. *Science*, 334(6055):512–516, 2011.
- [104] Armin Hoffmann and Michael T Woodside. Signal-pair correlation analysis of single-molecule trajectories. *Angewandte Chemie International Edition*, 50(52):12643–12646, 2011.
- [105] Christopher Jarzynski. Nonequilibrium equality for free energy differences. *Physical Review Letters*, 78(14):2690, 1997.
- [106] Olga K Dudko, Gerhard Hummer, and Attila Szabo. Theory, analysis, and interpretation of single-molecule force spectroscopy experiments. *Proceedings of the National Academy of Sciences*, 105(41):15755–15760, 2008.

- [107] Lucas P Watkins and Haw Yang. Detection of intensity change points in time-resolved single-molecule measurements. *The Journal of Physical Chemistry B*, 109(1):617–628, 2005.
- [108] Mario Blanco and Nils G Walter. Analysis of complex single-molecule fret time trajectories. *Methods in enzymology*, 472:153–178, 2010.
- [109] John F Marko and Eric D Siggia. Stretching dna. *Macromolecules*, 28(26):8759–8770, 1995.
- [110] Michelle D Wang, Hong Yin, Robert Landick, Jeff Gelles, and Steven M Block. Stretching dna with optical tweezers. *Biophysical journal*, 72(3):1335, 1997.
- [111] Thomas L James, He Liu, Nikolai B Ulyanov, Shauna Farr-Jones, Hong Zhang, David G Donne, Kiyotoshi Kaneko, Darlene Groth, Ingrid Mehlhorn, Stanley B Prusiner, et al. Solution structure of a 142-residue recombinant prion protein corresponding to the infectious fragment of the scrapie isoform. *Proceedings of the National Academy of Sciences*, 94(19):10086–10091, 1997.
- [112] Christian B. Anfinsen. Principles that govern the folding of protein chains. *Science*, 181(4096):223–230, 1973.
- [113] Michael T Woodside, Peter C Anthony, William M Behnke-Parks, Kevan Larizadeh, Daniel Herschlag, and Steven M Block. Direct measurement of the full, sequence-dependent folding landscape of a nucleic acid. *Science*, 314(5801):1001–1004, 2006.
- [114] J Christof M Gebhardt, Thomas Bornschlöggl, and Matthias Rief. Full distance-resolved folding energy landscape of one single protein molecule. *Proceedings of the National Academy of Sciences*, 107(5):2013–2018, 2010.
- [115] Michael Hinczewski, J Christof M Gebhardt, Matthias Rief, and D Thirumalai. From mechanical folding trajectories to intrinsic energy landscapes of biopolymers. *Proceedings of the National Academy of Sciences*, 110(12):4500–4505, 2013.
- [116] P Jansson. Deconvolution of images and spectra, 1300 boylston street, chestnut hill, ma 02167, 1997.
- [117] Gerhard Hummer and Attila Szabo. Free energy reconstruction from nonequilibrium single-molecule pulling experiments. *Proceedings of the National Academy of Sciences*, 98(7):3658–3661, 2001.
- [118] Sanghyun Park and Klaus Schulten. Calculating potentials of mean force from steered molecular dynamics simulations. *The Journal of chemical physics*, 120(13):5946–5961, 2004.
- [119] David DL Minh. Free-energy reconstruction from experiments performed under different biasing programs. *Physical Review E*, 74(6):061120, 2006.
- [120] Jan Liphardt, Sophie Dumont, Steven B Smith, Ignacio Tinoco, and Carlos Bustamante. Equilibrium information from nonequilibrium measurements in an experimental test of jarzynski’s equality. *Science*, 296(5574):1832–1835, 2002.
- [121] Nolan C Harris, Yang Song, and Ching-Hwa Kiang. Experimental free energy surface reconstruction from single-molecule force spectroscopy using jarzynski’s equality. *Physical review letters*, 99(6):068101, 2007.

- [122] Amar Nath Gupta, Abhilash Vincent, Krishna Neupane, Hao Yu, Feng Wang, and Michael T Woodside. Experimental validation of free-energy-landscape reconstruction from non-equilibrium single-molecule force spectroscopy measurements. *Nature Physics*, 7(8):631–634, 2011.
- [123] Olga K Dudko, Gerhard Hummer, and Attila Szabo. Theory, analysis, and interpretation of single-molecule force spectroscopy experiments. *Proceedings of the National Academy of Sciences*, 105(41):15755–15760, 2008.
- [124] Olga K Dudko, Gerhard Hummer, and Attila Szabo. Intrinsic rates and activation free energies from single-molecule pulling experiments. *Physical review letters*, 96(10):108101, 2006.
- [125] Hendrik Anthony Kramers. Brownian motion in a field of force and the diffusion model of chemical reactions. *Physica*, 7(4):284–304, 1940.
- [126] Michael B Coulthart and Neil R Cashman. Variant creutzfeldt–jakob disease: a summary of current scientific knowledge in relation to public health. *Canadian Medical Association Journal*, 165(1):51–58, 2001.
- [127] Marek Fischer, Thomas Rüllicke, Alex Raeber, Andreas Sailer, Markus Moser, Bruno Oesch, Sebastian Brandner, Adriano Aguzzi, and Charles Weissmann. Prion protein (prp) with amino-proximal deletions restoring susceptibility of prp knockout mice to scrapie. *The EMBO journal*, 15(6):1255, 1996.
- [128] Timothy D Kurt and Christina J Sigurdson. Cross-species transmission of cwd prions. *Prion*, 10(1):83–91, 2016.
- [129] J Zuegg and JE Gready. Molecular dynamics simulations of human prion protein: importance of correct treatment of electrostatic interactions. *Biochemistry*, 38(42):13862–13876, 1999.
- [130] K Wuthrich. Nmr structure of the mouse prion protein domain prp (121231). *Nature*, 382:180182, 1996.
- [131] Pravas Kumar Baral, Mridula Swayampakula, Adriano Aguzzi, and Michael NG James. X-ray structural and molecular dynamical studies of the globular domains of cow, deer, elk and syrian hamster prion proteins. *Journal of structural biology*, 192(1):37–47, 2015.
- [132] Hao Yu, Xia Liu, Krishna Neupane, Amar Nath Gupta, Angela M Brigley, Allison Solanki, Iveta Sosova, and Michael T Woodside. Direct observation of multiple misfolding pathways in a single prion protein molecule. *Proceedings of the National Academy of Sciences*, 109(14):5283–5288, 2012.
- [133] David M Patterson, Lidia A Nazarova, and Jennifer A Prescher. Finding the right (bioorthogonal) chemistry. *ACS chemical biology*, 9(3):592–605, 2014.
- [134] Marjoke F Debets, Christianus WJ van der Doelen, Floris PJT Rutjes, and Floris L van Delft. Azide: A unique dipole for metal-free bioorthogonal ligations. *Chem-BioChem*, 11(9):1168–1184, 2010.
- [135] Hartmuth C Kolb, MG Finn, and K Barry Sharpless. Click chemistry: diverse chemical function from a few good reactions. *Angewandte Chemie International Edition*, 40(11):2004–2021, 2001.

- [136] Jason E Hein and Valery V Fokin. Copper-catalyzed azide–alkyne cycloaddition (cuAAC) and beyond: new reactivity of copper (I) acetylides. *Chemical Society Reviews*, 39(4):1302–1315, 2010.
- [137] Rolf Huisgen. 1, 3-dipolar cycloadditions. past and future. *Angewandte Chemie International Edition in English*, 2(10):565–598, 1963.
- [138] Vsevolod V Rostovtsev, Luke G Green, Valery V Fokin, and K Barry Sharpless. A stepwise Huisgen cycloaddition process: copper (I)-catalyzed regioselective “ligation” of azides and terminal alkynes. *Angewandte Chemie*, 114(14):2708–2711, 2002.
- [139] Christian W Tornøe, Caspar Christensen, and Morten Meldal. Peptidotriazoles on solid phase:[1, 2, 3]-triazoles by regiospecific copper (I)-catalyzed 1, 3-dipolar cycloadditions of terminal alkynes to azides. *The Journal of organic chemistry*, 67(9):3057–3064, 2002.
- [140] Philipp ME Gramlich, Christian T Wirges, Antonio Manetto, and Thomas Carell. Postsynthetic DNA modification through the copper-catalyzed azide–alkyne cycloaddition reaction. *Angewandte Chemie International Edition*, 47(44):8350–8358, 2008.
- [141] Adrian Salic and Timothy J Mitchison. A chemical method for fast and sensitive detection of DNA synthesis in vivo. *Proceedings of the National Academy of Sciences*, 105(7):2415–2420, 2008.
- [142] Daniela C Dieterich, Jennifer J Lee, A James Link, Johannes Graumann, David A Tirrell, and Erin M Schuman. Labeling, detection and identification of newly synthesized proteomes with bioorthogonal non-canonical amino-acid tagging. *Nature protocols*, 2(3):532–540, 2007.
- [143] Melissa L Blackman, Maksim Royzen, and Joseph M Fox. Tetrazine ligation: fast bioconjugation based on inverse-electron-demand Diels–Alder reactivity. *Journal of the American Chemical Society*, 130(41):13518–13519, 2008.
- [144] G Gorin, PA Martić, and G Doughty. Kinetics of the reaction of n-ethylmaleimide with cysteine and some congeners. *Archives of biochemistry and biophysics*, 115(3):593–597, 1966.
- [145] James R Heitz, Constance D Anderson, and Bruce M Anderson. Inactivation of yeast alcohol dehydrogenase by n-alkylmaleimides. *Archives of biochemistry and biophysics*, 127:627–636, 1968.
- [146] Ramajeyam Selvaraj and Joseph M Fox. trans-cyclooctene—a stable, voracious dienophile for bioorthogonal labeling. *Current opinion in chemical biology*, 17(5):753–760, 2013.
- [147] Robert D Bach. Ring strain energy in the cyclooctyl system. the effect of strain energy on [3+ 2] cycloaddition reactions with azides. *Journal of the American Chemical Society*, 131(14):5233–5243, 2009.
- [148] Raffaella Rossin, Sandra M van den Bosch, Wolter ten Hoeve, Marco Carvelli, Ron M Versteegen, Johan Lub, and Marc S Robillard. Highly reactive trans-cyclooctene tags with improved stability for Diels–Alder chemistry in living systems. *Bioconjugate chemistry*, 24(7):1210–1217, 2013.

- [149] Neal K Devaraj, Greg M Thurber, Edmund J Keliher, Brett Marinelli, and Ralph Weissleder. Reactive polymer enables efficient in vivo bioorthogonal chemistry. *Proceedings of the National Academy of Sciences*, 109(13):4762–4767, 2012.
- [150] Raffaella Rossin, Pascal Renart Verkerk, Sandra M van den Bosch, Roland Vulders, Iris Verel, Johan Lub, and Marc S Robillard. In vivo chemistry for pretargeted tumor imaging in live mice. *Angewandte Chemie International Edition*, 49(19):3375–3378, 2010.
- [151] Jennifer A Prescher and Carolyn R Bertozzi. Chemistry in living systems. *Nature chemical biology*, 1(1):13–21, 2005.
- [152] Byron Caughey, Lynne D Raymond, Gregory J Raymond, Laura Maxson, Jay Silveira, and Gerald S Baron. Inhibition of protease-resistant prion protein accumulation in vitro by curcumin. *Journal of virology*, 77(9):5499–5502, 2003.
- [153] Sigal Caspi, Michele Halimi, Anat Yanai, Shmuel Ben Sasson, Albert Taraboulos, and Ruth Gabizon. The anti-prion activity of congo red putative mechanism. *Journal of Biological Chemistry*, 273(6):3484–3489, 1998.
- [154] Byron Caughey and GREGORY J Raymond. Sulfated polyanion inhibition of scrapie-associated prp accumulation in cultured cells. *Journal of virology*, 67(2):643–650, 1993.
- [155] David A Kocisko, Andrew Vaillant, Kil Sun Lee, Kevin M Arnold, Nadine Bertholet, Richard E Race, Emily A Olsen, Jean-Marc Juteau, and Byron Caughey. Potent antiscrapie activities of degenerate phosphorothioate oligonucleotides. *Antimicrobial agents and chemotherapy*, 50(3):1034–1044, 2006.
- [156] Sina Ghaemmaghami, Barnaby CH May, Adam R Renslo, and Stanley B Prusiner. Discovery of 2-aminothiazoles as potent antiprion compounds. *Journal of virology*, 84(7):3408–3412, 2010.
- [157] Gianluigi Forloni, Selina Iussich, Tazeen Awan, Laura Colombo, Nadia Angeretti, Laura Girola, Ilaria Bertani, Giorgio Poli, Maria Caramelli, Maria Grazia Bruzzone, et al. Tetracyclines affect prion infectivity. *Proceedings of the National Academy of Sciences*, 99(16):10849–10854, 2002.
- [158] Fabrizio Tagliavini, Gianluigi Forloni, Laura Colombo, Giacomina Rossi, Laura Girola, Barbara Canciani, Nadia Angeretti, Lidia Giampaolo, Elisa Peressini, Tazeen Awan, et al. Tetracycline affects abnormal properties of synthetic prp peptides and prp sc in vitro. *Journal of molecular biology*, 300(5):1309–1322, 2000.
- [159] Carsten Korth, Barnaby CH May, Fred E Cohen, and Stanley B Prusiner. Acridine and phenothiazine derivatives as pharmacotherapeutics for prion disease. *Proceedings of the National Academy of Sciences*, 98(17):9836–9841, 2001.
- [160] Erika Chung, Frances Prelli, Stephen Dealler, Woo Sirl Lee, Young-Tae Chang, and Thomas Wisniewski. Styryl-based and tricyclic compounds as potential anti-prion agents. *PLoS One*, 6(9):e24844, 2011.
- [161] Ikuko Murakami-Kubo, Katsumi Doh-ura, Kensuke Ishikawa, Satoshi Kawatake, Kensuke Sasaki, Jun-ichi Kira, Shigeru Ohta, and Toru Iwaki. Quinoline derivatives are therapeutic candidates for transmissible spongiform encephalopathies. *Journal of virology*, 78(3):1281–1288, 2004.

- [162] Brian Y Feng, Brandon H Toyama, Holger Wille, David W Colby, Sean R Collins, Barnaby CH May, Stanley B Prusiner, Jonathan Weissman, and Brian K Shoichet. Small-molecule aggregates inhibit amyloid polymerization. *Nature chemical biology*, 4(3):197–199, 2008.
- [163] Winslow S Caughey, Suzette A Priola, David A Kocisko, Lynne D Raymond, Anne Ward, and Byron Caughey. Cyclic tetrapyrrole sulfonation, metals, and oligomerization in antiprion activity. *Antimicrobial agents and chemotherapy*, 51(11):3887–3894, 2007.
- [164] Winslow S Caughey, Lynne D Raymond, Motohiro Horiuchi, and Byron Caughey. Inhibition of protease-resistant prion protein formation by porphyrins and phthalocyanines. *Proceedings of the National Academy of Sciences*, 95(21):12117–12122, 1998.
- [165] David A Kocisko, Winslow S Caughey, Richard E Race, Grant Roper, Byron Caughey, and John D Morrey. A porphyrin increases survival time of mice after intracerebral prion infection. *Antimicrobial agents and chemotherapy*, 50(2):759–761, 2006.
- [166] Suzette A Priola, Anne Raines, and Winslow S Caughey. Porphyrin and phthalocyanine antiscrapie compounds. *Science*, 287(5457):1503–1506, 2000.
- [167] Hao Yu, Amar Nath Gupta, Xia Liu, Krishna Neupane, Angela M Brigley, Iveta Sosova, and Michael T Woodside. Energy landscape analysis of native folding of the prion protein yields the diffusion constant, transition path time, and rates. *Proceedings of the National Academy of Sciences*, 109(36):14452–14457, 2012.
- [168] Allison Solanki, Krishna Neupane, and Michael T Woodside. Single-molecule force spectroscopy of rapidly fluctuating, marginally stable structures in the intrinsically disordered protein α -synuclein. *Physical review letters*, 112(15):158103, 2014.
- [169] Hao Yu, Derek R Dee, Xia Liu, Angela M Brigley, Iveta Sosova, and Michael T Woodside. Protein misfolding occurs by slow diffusion across multiple barriers in a rough energy landscape. *Proceedings of the National Academy of Sciences*, 112(27):8308–8313, 2015.
- [170] Leonardo M Cortez, Jitendra Kumar, Ludovic Renault, Howard S Young, and Valerie L Sim. Mouse prion protein polymorphism phe-108/val-189 affects the kinetics of fibril formation and the response to seeding evidence for a two-step nucleation polymerization mechanism. *Journal of Biological Chemistry*, 288(7):4772–4781, 2013.
- [171] F Ulrich Hartl. Molecular chaperones in cellular protein folding. 1996.
- [172] F Ulrich Hartl and Manajit Hayer-Hartl. Converging concepts of protein folding in vitro and in vivo. *Nature structural & molecular biology*, 16(6):574–581, 2009.
- [173] Alireza Mashaghi, Gunter Kramer, Don C Lamb, Matthias P Mayer, and Sander J Tans. Chaperone action at the single-molecule level. *Chemical reviews*, 114(1):660–676, 2013.

- [174] Philipp Bechtluft, Ruud GH Van Leeuwen, Matthew Tyreman, Danuta Tomkiewicz, Nico Nouwen, Harald L Tepper, Arnold JM Driessen, and Sander J Tans. Direct observation of chaperone-induced changes in a protein folding pathway. *Science*, 318(5855):1458–1461, 2007.
- [175] Zackary N Scholl, Weitao Yang, and Piotr E Marszalek. Chaperones rescue luciferase folding by separating its domains. *Journal of Biological Chemistry*, 289(41):28607–28618, 2014.
- [176] Erika Tashiro, Tamotsu Zako, Hideki Muto, Yoshinori Ito, Karin Sörgjerd, Naofumi Terada, Akira Abe, Makoto Miyazawa, Akira Kitamura, Hirotake Kitaura, et al. Prefoldin protects neuronal cells from polyglutamine toxicity by preventing aggregation formation. *Journal of Biological Chemistry*, 288(27):19958–19972, 2013.
- [177] Debbie B Brtmacombe, Alan D Bennett, Fred S Wusteman, Christopher J Bostock, et al. Characterization and polyanion-binding properties of purified recombinant prion protein. *Biochemical Journal*, 342(3):605–613, 1999.
- [178] Christine Farquhar, Alan Dickinson, and Moira Bruce. Prophylactic potential of pentosan polysulphate in transmissible spongiform encephalopathies. *The Lancet*, 353(9147):117, 1999.
- [179] Show-Ling Shyng, Sylvain Lehmann, Krista L Moulder, and David A Harris. Sulfated glycans stimulate endocytosis of the cellular isoform of the prion protein, prpc, in cultured cells. *Journal of Biological Chemistry*, 270(50):30221–30229, 1995.
- [180] Ruth Gabizon, Zeev Meiner, Michele Halimi, and Shmuel A Ben-Sasson. Heparin-like molecules bind differentially to prion-proteins and change their intracellular metabolic fate. *Journal of cellular physiology*, 157(2):319–325, 1993.
- [181] Bernhard Ehlers and Heino Diringer. Dextran sulphate 500 delays and prevents mouse scrapie by impairment of agent replication in spleen. *Journal of General Virology*, 65(8):1325–1330, 1984.
- [182] Richard H Kimberlin and CA Walker. Suppression of scrapie infection in mice by heteropolyanion 23, dextran sulfate, and some other polyanions. *Antimicrobial agents and chemotherapy*, 30(3):409–413, 1986.
- [183] Simon G Patching. Surface plasmon resonance spectroscopy for characterisation of membrane protein–ligand interactions and its potential for drug discovery. *Biochimica et Biophysica Acta (BBA)-Biomembranes*, 1838(1):43–55, 2014.
- [184] P Anton Van Der Merwe. Surface plasmon resonance, 2001.
- [185] Shiming Lin, Adam Shih-Yuan Lee, Chih-Chen Lin, and Chih-Kung Lee. Determination of binding constant and stoichiometry for antibody-antigen interaction with surface plasmon resonance. *Current Proteomics*, 3(4):271–282, 2006.
- [186] Derek R Dee, Amar Nath Gupta, Max Anikovskiy, Iveta Sosova, Elena Grandi, Laura Rivera, Abhilash Vincent, Angela M Brigley, Nils O Petersen, and Michael T Woodside. Phthalocyanine tetrasulfonates bind to multiple sites on natively-folded prion protein. *Biochimica et Biophysica Acta (BBA)-Proteins and Proteomics*, 1824(6):826–832, 2012.

- [187] Satoshi Kawatake, Yuki Nishimura, Suehiro Sakaguchi, Toru Iwaki, and Katsumi Doh-Ura. Surface plasmon resonance analysis for the screening of anti-prion compounds. *Biological and Pharmaceutical Bulletin*, 29(5):927–932, 2006.
- [188] Stoyan Milev. Isothermal titration calorimetry: Principles and experimental design. *General Electric*, 9, 2013.
- [189] Matthew W Freyer and Edwin A Lewis. Isothermal titration calorimetry: experimental design, data analysis, and probing macromolecule/ligand binding and kinetic interactions. *Methods in cell biology*, 84:79–113, 2008.